

**" Sixth Workshop on Non-Linear Dynamics and  
Earthquake Prediction"**

**15 - 27 October 2001**

**Holyland Earthquake Records in  
Dead-Sea Sediments**

*A. Agnon*

**Institute of Earth Sciences  
The Hebrew University  
Jerusalem**



## Long-term earthquake clustering: A 50,000-year paleoseismic record in the Dead Sea Graben

Shmuel Marco,<sup>1</sup> Mordechai Stein, and Amotz Agnon

Institute of Earth Sciences, Hebrew University, Jerusalem, Israel

Hagai Ron

Institute for Petroleum Research and Geophysics, Holon, Israel

**Abstract.** The temporal distribution of earthquakes in the Dead Sea Graben is studied through a 50,000-year paleoseismic record recovered in laminated sediments of the Late Pleistocene Lake Lisan (paleo-Dead Sea). The Lisan represents more than 10 times the 4000 years of historical earthquake records. It is the longest and most complete paleoseismic record along the Dead Sea Transform and possibly the longest continuous record on Earth. It includes unique exposures of seismite beds (earthquake-induced structures) associated with slip events on syndepositional faults. The seismites are layers consisting of mixtures of fragmented and pulverized laminae. The places where the seismites abut syndepositional faults are interpreted as evidence for their formation at the sediment-water interface during slip events on these faults. Thicker sediment accumulation above the seismites in the downthrown blocks indicates that a seismite formed at the water-sediment interface on both sides of the fault scarps. Modern analogs and the association with surface ruptures suggest that each seismite formed during a  $M_L \geq 5.5$  earthquake. The  $^{230}\text{Th}$ - $^{234}\text{U}$  ages of a columnar section, obtained by thermal ionization mass spectrometry, give a mean recurrence time of ~1600 years of  $M_L \geq 5.5$  earthquakes in the Dead Sea Graben. The earthquakes cluster in ~10,000-year periods separated by quiet periods of similar length. This distribution implies that a long-term behavior of the Dead Sea Transform should be represented by a mean recurrence of at least 20,000 year record. This observation has ramifications for seismic hazard assessment based on shorter records.

### Introduction

The knowledge of past long-term behavior of seismogenic faults is a key to understanding earthquake physics and related hazard assessment. Studies of paleoseismic records are often hindered by difficulties in identifying the correct earthquake indicators, finding a sufficiently large time window, obtaining continuous records, and dating the events either relatively or absolutely.

The mean recurrence period of strong earthquakes is significant because it is a measure of the strength of the fault and of the rate of stress buildup [Scholz, 1990]. However, it gives no information on the pattern of event distribution through time. It has long been realized that slip on faults is cyclic, but its detailed temporal distribution and the patterns of its periodicity are still unclear, partly because the instrumental and preinstrumental records are usually either incomplete or too short. In the cases of short records, earthquake clustering may cause a serious deviation in the estimated recurrence period. Clustering has been inferred where there is a marked contrast between seismic rates of the last several centuries and rates over thousands of years or longer [Grant and Sieh, 1994; Swan, 1988]. Clustering might bias

estimates of seismic efficiency (the ratio of seismic to geologic slip) that may provide information on the mechanical properties of the faults. Garfunkel *et al.* [1981] estimate the seismic slip rate in the Dead Sea Transform in historical times at 15-50% of the Pliocene-Pleistocene geologic slip rate. A 90-year instrumental record yields seismic efficiency as low as 7% in the Dead Sea Transform [Salamon, 1993].

We report a 50,000-year, continuous, dateable paleoseismic record in the Late Pleistocene lacustrine Lisan Formation on the Dead Sea shore [Marco *et al.*, 1994]. The Lisan represents a time span more than tenfold the 4000 years of historical earthquake record [Ben-Menahem, 1991]. It is the longest and most complete paleoseismic record along the Dead Sea Transform and possibly the longest known record on Earth. The record includes seismites, a term introduced by Seilacher [1969], and used here for earthquake-induced structures in sediments, as proposed by Vittori *et al.* [1991]. We document their stratigraphic position, estimate their recurrence time, and analyze the temporal distribution of strong earthquakes. The data presented here provide direct evidence for long-term clustering of strong earthquakes in the Dead Sea Graben.

### The Lisan Formation

Sediments of Lake Lisan are exposed along a 220-km length of the Dead Sea Transform, from Lake Kinneret (Sea of Galilee) in the north to the Arava Valley in the south (Figure 1). The deposits of this lake, the Lisan Formation, unconformably

<sup>1</sup>Also at Geological Survey, Jerusalem, Israel.

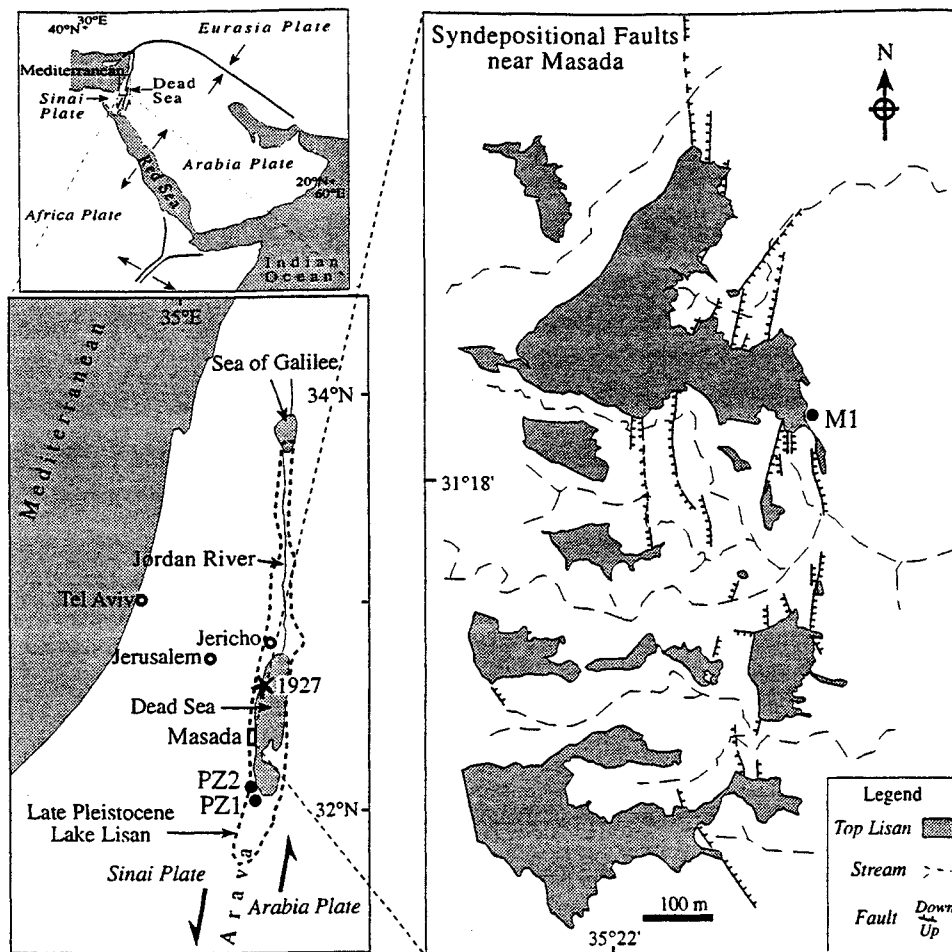


**Figure 1.** (right) The N-S striking fault zone near Masada includes syndepositional faults, which do not offset the top of the Lisan Formation. Solid circle marks the site of columnar section M1. (top) Plate tectonic setting of the Middle East. (bottom left) Sites of columnar sections PZ1 and PZ2 in the Peratzim Valley (solid circles); paleoshoreline of Lake Lisan (dashed). Star marks the epicenter of the 1927 earthquake [Shapira et al., 1992].

overlie earlier units. The Lisan Formation consists of alternating laminae of white aragonite and dark detritus. The white laminae are composed of aragonite; the detrital material contains fine-grained calcite, dolomite, aragonite, quartz, and clays [Begin et al., 1974]. Both types of laminae are up to a few millimeters thick. The paired laminae were interpreted as seasonal precipitates (varves): the aragonite is authigenic, possibly annual summer precipitate of Lake Lisan, whereas the dark laminae are detrital flood inputs into the lake during winter storms [Bentor and Vroman, 1960; Katz et al., 1977]. The extremely dry climate preserved the aragonite, which otherwise readily reacts with water and transforms to calcite [Katz and Kolodny, 1989]. The exceptional preservation of the varves that serve as sensitive stratigraphic markers, their similarity to the modern deposits of the Dead Sea, the continuous stratigraphic record, and the extensive outcrops along an active plate boundary (Figure 2), all make the Lisan Formation an ideal candidate for paleoseismic studies [El-Isa and Mustafa, 1986; Seilacher, 1984].

The Lisan sediments onlap all the canyons that flow to the Dead Sea and therefore postdate the period of the major landscaping. The  $^{14}\text{C}$  dating and archeological artifacts [Copeland and Vita-Finzi, 1978; Neev and Emery, 1967; Vita-Finzi, 1964] indicate that the Lisan stage came to an end no earlier than 18 ka and perhaps somewhat later. U series dating

of aragonite from the Lisan Formation by  $\alpha$  counting yielded ages of 71 to 18 ka with the stratigraphy [Kaufman, 1971; Kaufman et al., 1992]. The top 1.5-3.5 m of the Lisan Formation in the Dead Sea area is characterized by abundance



**Figure 2.** Typical view of Lisan Formation. The hard, gypsum-rich top of the formation forms a flat plain unaffected by syndepositional faults. Vertical exposures are about 40 m.

of gypsum and scarcity of aragonite. The above mentioned ages were all measured below this part of the section. Recently, thermal ionization mass spectrometry (TIMS) was applied to determine the U and Th isotopic compositions of aragonite samples from the Lisan Formation [Schramm *et al.*, 1995; Stein *et al.*, 1992]. U series dating by TIMS was successfully applied to aragonitic corals [Chen *et al.*, 1986; Edwards *et al.*, 1987]. Reproducible ages with uncertainty of less than 1% were obtained by TIMS for corals having very low concentrations of  $^{232}\text{Th}$  and the  $^{234}\text{U}/^{238}\text{U}$  activity ratios in equilibrium with seawater of  $1.15 \pm 0.01$  [Stein *et al.*, 1993]. The advantage of the TIMS measurements over the conventional  $\alpha$  counting is the significantly smaller sample that is required for analysis (facilitating the acquisition of highly pure aragonite samples) and the significantly higher precision in age determination. The problem with lake sediments, such as Lisan aragonite is twofold: (1) there is no a priori constraint on the U isotope composition of the water and (2) the amount of  $^{232}\text{Th}$  is significantly higher than in coral aragonite; therefore "common"  $^{238}\text{U}$  and  $^{230}\text{Th}$  may be incorporated within the samples and, consequently, may affect the measured age. All these problems were thoroughly studied by A. Schramm *et al.* (manuscript in preparation, 1995). They found that pure aragonite samples (>99% aragonite) yield constant  $^{234}\text{U}/^{238}\text{U}$  activity ratio of  $1.50 \pm 0.02$ , which is indistinguishable from the value of present-day Dead Sea water [Schramm *et al.*, 1995; Stein *et al.*, 1992]. This result provides an important constraint for the assessment of  $^{230}\text{Th}$ - $^{234}\text{U}$  ages in the Lisan aragonite. The analytical error on pure aragonite Lisan samples (>99% aragonite) is less than 1%, yet the ages might be slightly too old due to presence of detrital  $^{238}\text{U}$ ,  $^{234}\text{U}$ , and  $^{230}\text{Th}$  associated with  $^{232}\text{Th}$ .

The ages of section PZ1 (Figure 3) show that the lowest exposed layers are 71 ka old. Linear regression yields an average sedimentation rate of 0.86 mm/yr ( $R=0.981$ ). A similar rate can be derived from the ages determined by Kaufman *et al.* [1992].

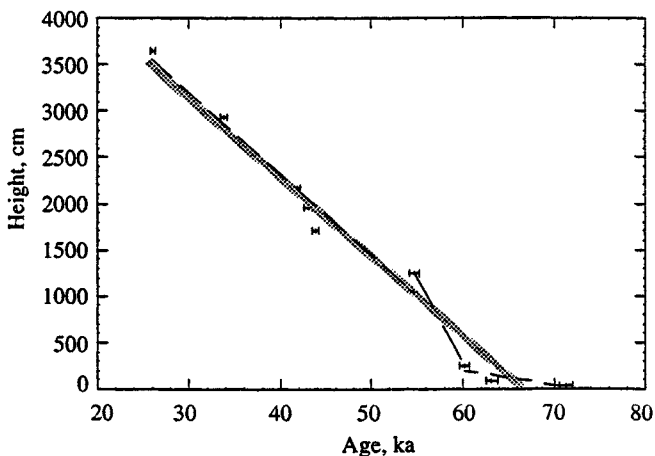


**Figure 3.** U series ages of nine horizons in section PZ1. Data are from Schramm *et al.* [1995] and A. Schramm *et al.* (manuscript in preparation, 1995). Error bars show 1% analytical uncertainty. Linear regressions of three segments (dashed) give sedimentation rates of 0.16 mm/yr in the lower 250 cm, 1.84 mm/yr from 250 cm to 1250 cm, and 0.88 mm/yr above 1250 cm. A single regression of the entire section (gray line) gives a mean sedimentation rate of 0.86 mm/yr.

The sediments in the study areas of the Peratzim Valley and Masada are characteristic horizontal lake bottomsets. Interfingering of varves and clastics in the range of sand to cobble conglomerate are common in alluvial fans at the margins of the graben valley, where they form typical foresets, in places overlain by topsets. The absence of intraformational erosion channels, hiatuses, or unconformities indicates that the deposition of the Lisan Formation bottomsets had been continuous. Fossil beach terraces at 180 m below sea level, paleontological considerations, and sediment chemistry led Begin *et al.* [1974] to conclude that the center of Lake Lisan was quite deep, reaching 200 m or even 600 m [Katz *et al.*, 1977]. The lake level lowered rapidly at the end of a long period of dry climate.

The lowering of water level of the modern Dead Sea was accompanied by incision of canyons into the Lisan Formation, creating vertical exposures of more than 40 m.

### Seismological Studies in the Region

Our current knowledge of the seismicity of the Dead Sea Transform is based on the following, mostly short-term records.

#### Current Seismicity

The Dead Sea Transform system produces most of the large earthquakes in the region (see the *Seismological Bulletins* of the Institute for Petroleum Research and Geophysics (IPRG) and Salamon [1993]). Microearthquakes ( $1.0 \leq M_L \leq 5$ ) tend to concentrate near tensional features such as the Dead Sea Graben [Shapira and Feldman, 1987; van Eck and Hofstetter, 1990]. This observation is common to other large strike-slip faults [e.g., Lovell *et al.*, 1987; Segall and Pollard, 1980]. Focal mechanisms of large events in the Dead Sea Transform generally show strike-slip or normal solutions [Salamon, 1993; van Eck and Hofstetter, 1990]. During the period 1919-1963 the frequency-magnitude relation,  $\log N = a - bM$ , where  $N$  is the average number of earthquakes per year with magnitude  $M$  [Gutenberg and Richter, 1954], from the Dead Sea to north of Lebanon, was such that  $a=3.25$  and  $b=0.8$  (Table 1). Different segments appear to have similar  $b$  values of 0.8 [Shapira and Feldman, 1987]. A compilation of seismicity for the last century yields a  $b$  value of 1 [Salamon, 1993]. Focal plane solutions of large events along the Dead Sea Transform confirm the plate tectonic model: the large events align with the trace of the transform and sinistral motion predominates. Microseismicity occurs over a broad area and shows a mixture of strike-slip and normal faulting [Ben-Menahem, 1991; Salamon, 1993; van Eck and Hofstetter, 1990]. The last destructive earthquake ( $M_L=6.2$ ) struck the Dead Sea area in 1927. Its epicenter was about 25 km south of Jericho [Shapira *et al.*, 1992].

#### Archeoseismicity

A compilation of 4000 years of historical seismological record [Ben-Menahem, 1991] infers that the mean return period of strong earthquakes along the 430-km-long Arava-Dead Sea-Jordan river segment was 1500 years. The estimated frequency-magnitude relation is  $\log N = 3.10 - 0.86M$ .

#### Paleoseismicity

El-Isa and Mustafa [1986] interpreted convolute folds in the Lisan as earthquake deformations in a previous study on the

**Table 1.** Frequency of Seismic Events From Previous Studies

Time Window	Frequency	Method	Reference
1927-1974	2/100 years of $M \geq 6$	instrumental	<i>Ben-Menahem et al.</i> [1976]
1919-1963	$\log N = 3.25-0.8M$	instrumental	<i>Arieh</i> [1967]
1733 y in Late Pleistocene	$\log N = 5.24-0.68M$	paleoseismicity	<i>El-Isa and Mustafa</i> [1986]
last 4000 years	$\log N = 3.10-0.86M$	historical reports	<i>Ben-Menahem</i> [1991]
last 2000 years	2/2000 years	trenches	<i>Reches and Hoexter</i> [1981]
50- 17 ka	1/1000-1/3000 years	trenches	<i>Amit et al.</i> [1994]
1900-1990	$b=1$	instrumental	<i>Salamon</i> [1993]
Late Pleistocene (?) -Recent	~thousands of years	seismic reflection	<i>Niemi and Ben-Avraham</i> [1994]

Lisan Formation on the east shores of the Dead Sea. El Isa and Mustafa concluded that during a period of 1733 years in the Late Pleistocene the average recurrence period was  $340 \pm 20$  years for  $M_L \geq 6.5$ , with a frequency-magnitude relation  $\log N = 5.24 - 0.68M$ .

In a trench study across the Jericho fault *Reches and Hoexter* [1981] identified two major earthquakes during the last 2000 years. Another trench study of Late Pleistocene alluvial fans in the southern Arava rift (about 180 km south of the Dead Sea) revealed multiple-event faults. *Amit et al.* [1994] and *Enzel et al.* [1994] estimate recurrence periods of 1000 to 3000 years for the period between 50 ka and 17 ka. *Gardosh et al.* [1990] estimate post-Lisan normal faults along the western shores of the Dead Sea to accommodate a subsidence rate of 0.85 mm/yr

## Syn depositional Faults and "Mixed Layers"

### Observations

*Marco and Agnon* [1995] discovered fault planes with vertical displacements up to 2 meters in the Lisan outcrop of the Masada area. Undisturbed layers that overlie the faults indicate that the faults are syn depositional. Deformed layers terminate at the faults (Figure 4). We call them "mixed layers" because they consist of mixtures of fragments of the two typical varve components of the Lisan Formation. In contrast to the common facies of laminated varves, the mixed layers exhibit unusual thickness, structure, and fabric. They are typically several centimeters to a few tens of centimeters thick (locally up to 1 m). They consist of nonlayered mixtures of fine-grained matrix and tabular fragments of varves of various sizes (several millimeters to centimeters). In places, fragment-supported texture shows a gradual upward transition to a matrix-supported texture (Figure 4). We used X ray diffraction to analyze the composition of three pairs of samples, taken from different localities. A pair consists of one sample of a mixed layer and one of its immediately underlying varves. The analyses show that the bulk composition of the varves varies between localities but the mixed layer composition is identical to that of underlying varves. No imbrication or other transport indicators were found. The mixed layers frequently overlie folded varve layers. These folds are asymmetrical and recumbent and in places exhibit box shapes. The typical wavelength is about 30 cm. The upper contact of the mixed layers is invariably sharp, but the lower contact is often irregular, intruded by fragments and mushroom-shaped diapirs from the underlying layers (Figure 5). Parts of the mixed layers exhibit sharp lower contacts. In several occurrences we found fissures that extend downward from mixed layers (Figure 6). These fissures are several centimeters wide, filled with material

from the mixed layer. No vertical displacement is observed across the fissures. Each mixed layer is restricted to a single stratigraphic horizon enclosed by undeformed beds. Mixed layers have been traced continuously over an area as large as the outcrop, i.e., hundreds of meters to a few kilometers.

Near the fault planes the mixed layers commonly contain cobble-sized laminated intraclasts that fell from the degrading scarp. The mixed layers are thicker in the downthrown block near the faults, filling 10-30 cm deep troughs. About 20-30 m away, the mixed layers thin out by a factor of 5 to 10 and maintain a uniform thickness throughout the outcrop area. Detailed sections across the syn depositional faults near Masada show thicker varve accumulation above the mixed layers in the downthrown block (Figure 4). The strike of the fault zone near Masada is parallel to the N-S trend of the Dead Sea Transform in the area (Figure 1). Strikes of individual fault planes are parallel to the strike of faults exposed in the main escarpment [*Agnon*, 1983]. The normal slip is consistent with the graben structure of the Dead Sea basin.

### Interpretation

The mixed layers are interpreted as originally laminated layers that were fluidized, brecciated, partly resuspended, and then resettled. The crucial question is whether the mixed layers are seismites (earthquake deformations of the original varve) or they are produced by other processes, such as flood storms, and slope failures.

**Flash floods.** Flash floods may trigger turbidity currents at lake bottom [e.g., *Hsu*, 1989]. However, the mixed layers are not turbidites because (1) they contain large varve fragments (Figure 4) which are extremely friable and would be expected to disintegrate completely during lateral transport in a turbulent flow, (2) the texture and fabric of each mixed layer are laterally uniform, which is an unlikely feature of turbidites, (3) in places the fragments at the bottom of the mixed layers can be restored to their original place, indicating little or no horizontal transport, and (4) no imbrication or other transport indicators are observed.

Evidence for flood events is exposed in incised alluvial fans near the outlets of canyons. These are wedges of coarse clastics in the range of sand to cobble conglomerate that interfinger with the lacustrine varves. The disturbances caused by these floods to the underlying varves do not extend beyond the coarse clastic intercalations. The mixed layers do not contain exotic clasts and are not associated with these wedges which do not disturb the laminated bottomsets and do not form mixed layers. Recent floods spread out in the Dead Sea forming a layer that floats above the dense lake water. The density of Lake Lisan was lower than the Dead Sea but higher

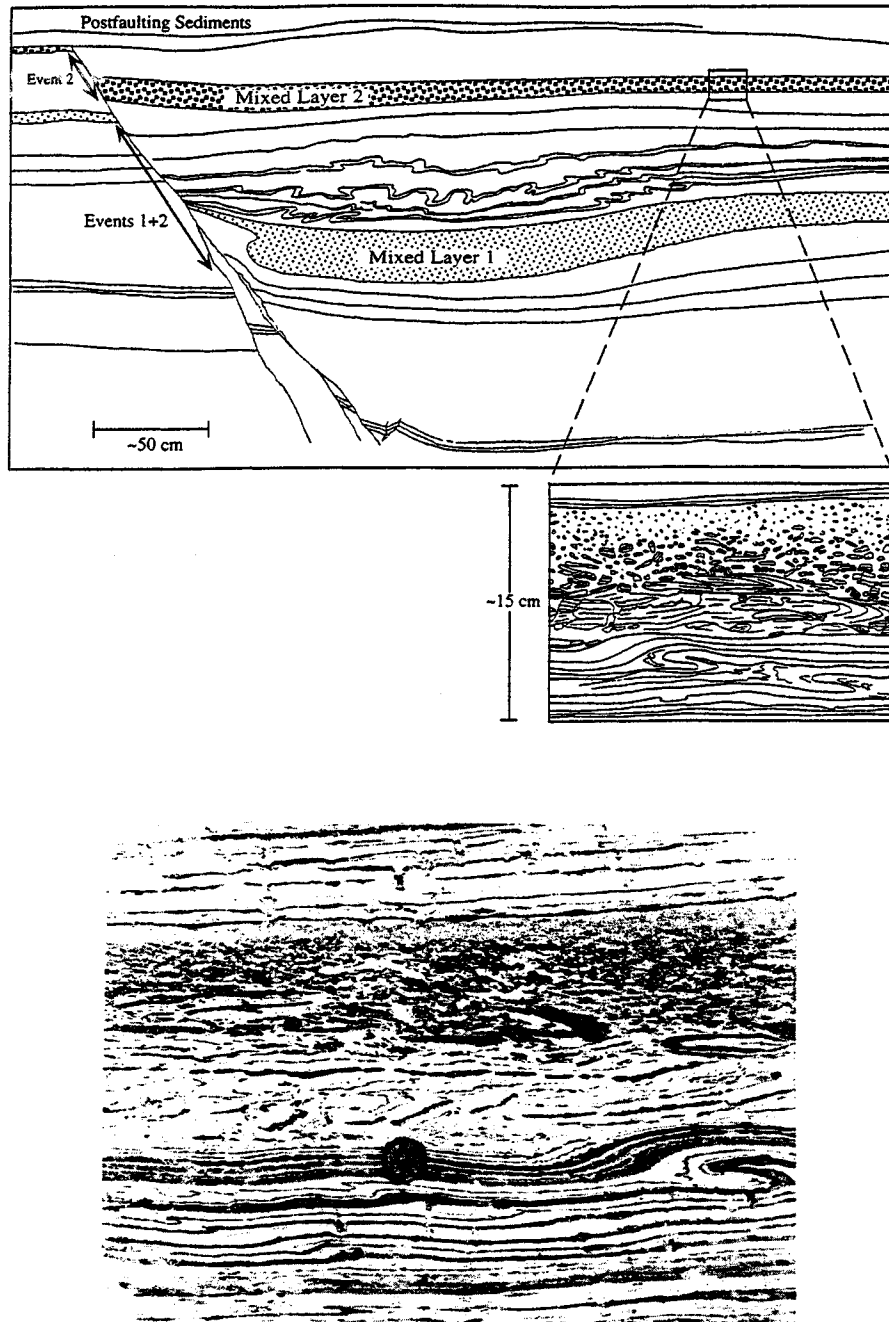


**Figure 4.** A syndepositional normal fault in the Lisan Formation near Masada unconformably overlain by undisturbed layers. Two mixed layers terminate at the fault in every block. They are thicker in the downthrown block, filling 10-30 cm deep troughs. The lower mixed layer in the downthrown block is also bent and overlain by folded varve layers that show local downdip transport. This folding formed by local slumping of varved layers into the trough. Lithologic markers show that the mixed layers correlate across the fault. They formed during two events when the fault slipped abruptly and ruptured the surface, creating a subaqueous scarp. Because of this scarp, sediment accumulation above the mixed layers in the downthrown block is thicker than in the footwall. A typical mixed layer (inset) shows a gradual upward transition from folded varves, through fragment-supported texture, to matrix-supported texture at the top. Such mixed layers are interpreted as earthquake deformations (partly traced from a photograph and partly drawn in the field). Photograph shows a mixed layer enclosed in a laminated sequence.

than seawater [Katz *et al.*, 1977] rendering flood-triggered turbidity currents impossible [Hsu, 1989].

**Storm waves.** By calculating the stress variation that is caused by the passage of surface waves one can estimate their effect at the bottom. Ten-meter-high storm waves with frequency of 0.1 Hz induce cyclic loading that is capable of

triggering failure in low-strength sediments at a water depth that is comparable to the wave height [Allen, 1982]. Lake Lisan's highest water level was -180 m, and the depth of the center was at least 200 m [Begin *et al.*, 1974] and possibly 600 m [Katz *et al.*, 1977]. The studied outcrops are well below the depth affected by waves (except for the uppermost,

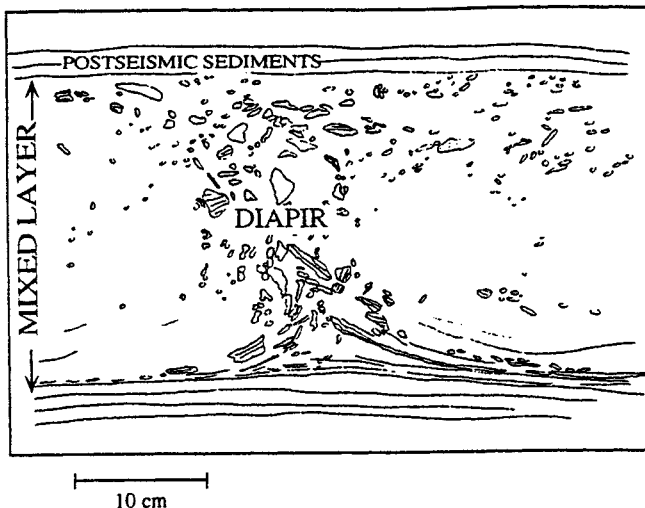


Figure 5. A trace of a photograph showing a diapir of varve fragments intruding the lower contact of a mixed layer. The intrusion must have occurred after the formation but before the consolidation of the mixed layer. It may have been triggered by an aftershock.

gypsum-rich layers, which were deposited as lake level was dropping). It is concluded that storms could not trigger the formation of mixed layers.

**Slope failures.** The considerations applied above to exclude turbidity currents and the horizontal position of the layers argue against gravity-triggered slope failure.

Seismically triggered sublacustrine slope failures accompanying historical earthquakes occurred mainly in alluvial fans and delta sediments, composed mostly of sand and gravel [Keefer, 1984]. The slope reported for these subaqueous landslides was at most localities steeper than  $10^\circ$  [Keefer, 1984], but an unusually low angle of  $0.25^\circ$  is reported in a single case [Field et al., 1982]. Seismic reflection profiles in the Dead Sea revealed slumped sediments in the Jordan River fan [Niemi and Ben-Avraham, 1994], showing the plausibility of earthquake-triggered slumps in other fans as well. The absence of alluvial fan components in the mixed layers, in addition to the preservation of the delicate varve fragments, indicates that turbulent mass flows from slope failures did not reach the flat bottom of the lake, where mixed layers formed.

**Earthquakes.** The conclusion of the discussion above is that flash floods, storm waves, and gravitational slope failures cannot explain the mixed layers. The following arguments point to earthquakes as the most plausible mechanism for the formation of mixed layers.

The mixed layers are flat-lying, restricted to single stratigraphic horizons. The extremely friable varve fragments and the absence of exotic components show negligible transport. Near Masada, the mixed layers abut syndepositional faults. The association of mixed layers with faults and with fissures filled by the mixed material point to their contemporaneous formation. Thicker varve accumulation above the mixed layers in the downthrown block (Figure 4) is indicative of a fault scarp that formed simultaneously with a mixed layer. The latter formed at the water-sediment interface on both sides of the scarp whenever a rupture occurred.

The diapirs of varve fragments (Figure 5) could have intruded into the mixed layers only before the layers consolidated, but they also postdate the shake that produced

the mixed layers. Aftershocks that hit the area before the consolidation of the mixed layers provide a plausible trigger to those diapirs.

Deformed layers of soft sediment somewhat similar to the mixed layers have been described around the world and identified as seismites [e.g., Davenport and Ringrose, 1987; Doig, 1991; Guiraud and Plaziat, 1993; Vittori et al., 1991], and references therein. The association of such soft sediment deformation with strong earthquakes is also backed by observations of recent events [Allen, 1986; Sims, 1975]. For example, resuspension of sediments was directly observed in lakes less than 10 km from the epicenter of the 1935 Témiskaming, Canada,  $M6.3$  earthquake. Piston cores recovered a 20-cm-thick chaotic layer, composed of tabular fragments of a previously formed silt layer [Doig, 1991]. What makes the mixed layers here special is their geometrical relationship to surface ruptures that formed them. Their widespread distribution beyond the fault zone offers an opportunity to study their occurrence pattern in columnar sections. Hence we suggest that each mixed layer formed during an earthquake just before the first undisturbed overlying lamina was deposited (Figure 7). The top of a mixed layer is the stratigraphic level at which the earthquake occurred. The time interval between earthquakes is represented by the distance between the tops of the mixed layers. The thickness of the mixed layers probably reflects the local intensity of the shaking (peak particle velocity, duration of motion, ground acceleration) as well as local sediment properties (composition, compaction, cohesion, particle size, and shape) and subtle lake bottom topography.

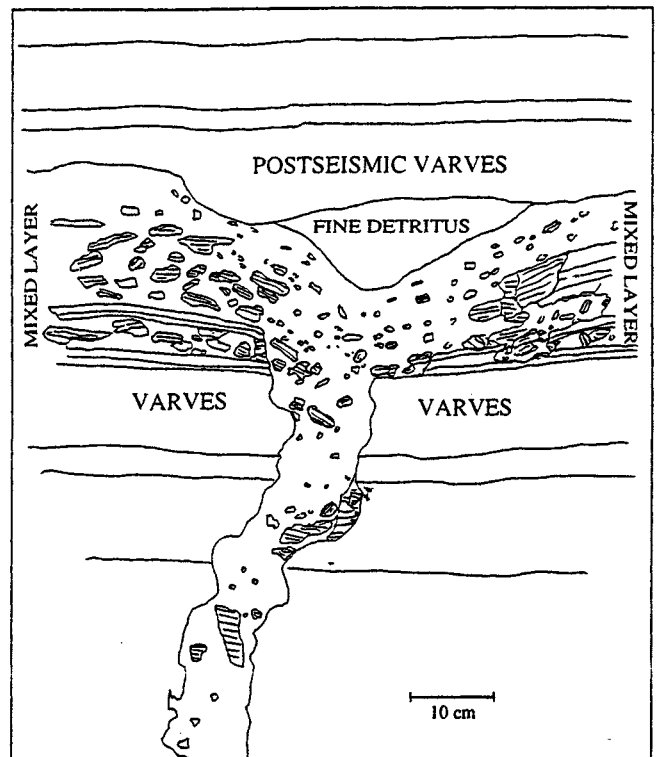
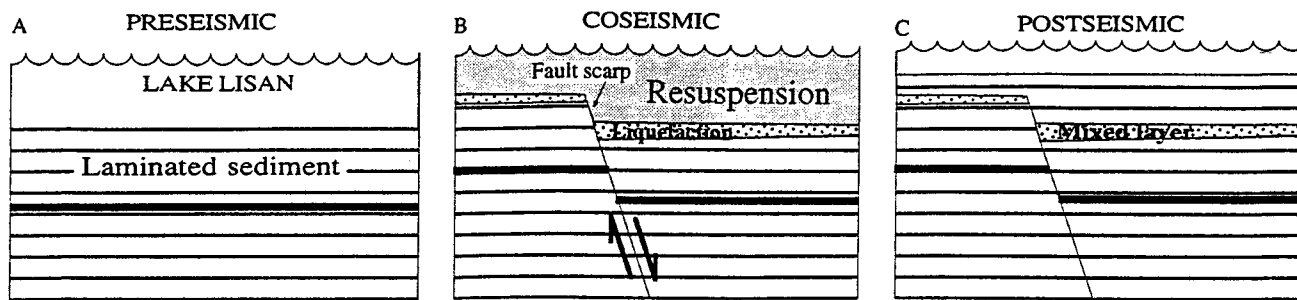


Figure 6. A fissure extends downward from a mixed layer. It is filled with the mixed material and is therefore contemporaneous. A lens of fine-grained detrital material fills a small depression at the top of the mixed layer. It is attributed to the compaction of the mixed material prior to the deposition of the overlying bed (traced from a photograph).



**Figure 7.** Interpretation of the fault-mixed layer association shown in Figure 3: (a) Laminated sediments are deposited at the bottom of Lake Lisan. (b) A fault ruptures the surface creating a subaqueous scarp. The coseismic movements deform, fluidize, and resuspend the sediment. A mixed layer forms on both sides of the fault scarp when the suspended sediments resettle. The mixed layer in the downthrown block is thicker. (c) Sedimentation continues; thicker sequence accumulates on the downthrown block. A second cycle of stages in Figures 7a-7c forms the configuration observed in Figure 4.

Previous studies in the Lisan Peninsula identified convolute folds as earthquake deformations [El-Isa and Mustafa, 1986; Seilacher, 1984], although no association with faults was reported. Our observations indicate that in places, folds are local slumps, limited by small-scale topography (e.g., Figure 4). Folded layers of alternating aragonite-detritus laminae are common throughout the Lisan Formation. At many localities the folded layers form half lenses (concave-bottomed), several millimeters to 1-1.5 m thick. In contrast to the widespread mixed layers, the folded layers extend over several centimeters to tens of meters. Their lower contacts are either flat or moderately arcuate décollement planes. The original thickness of the folded packages of varves varies between a few millimeters up to a few tens of centimeters; the thickest are 50-60 cm. The folds are commonly recumbent, asymmetric, or box-shaped. They recline in opposing directions, usually down-dip. Previous studies [Karcz and Mimran, 1978; Mimran and Karcz, 1983] described the folds and revealed that in places the aragonite needles exhibit preferred orientation but very little breakage. We conclude that local slump structures were triggered either by the sediment self load or by weak seismicity which did not affect a large area. The formation of widespread mixed layers required significantly stronger shaking than that associated with the local slumps.

Provided that each mixed layer formed during an earthquake, we can now examine their temporal distribution.

### Columnar Sections: Observations

In order to study the temporal distribution of earthquakes during Lisan time, we documented three detailed columnar sections of the Lisan Formation: PZ1 and PZ2 in the Peratzim Valley and M1 near Masada (Figure 1). The lowest age in section PZ1 (71 ka) is consistent with the base of the formation elsewhere [Kaufman *et al.*, 1992]. In PZ2 the contact with the underlying formation is exposed, whereas in PZ1 it was found by digging 1 m. Near Masada (M1) the base is not exposed.

A total of 29 mixed layers were found along the 38.85 m of Section PZ1 and 34 layers in 41.32 m of Section PZ2, about 2 km apart. Twenty-eight mixed layers are found in 32.84 meters of section M1.

Section PZ2 is closer to the graben-bounding escarpment and contains several sand and conglomerate intercalations which do not reach section PZ1. Figure 8 shows an example of

the correlation of lithologic units, in particular, mixed layers. The data available at present do not permit such a detailed correlation with the Masada outcrop. We are currently dating samples from the Masada section to enable the correlation with the Peratzim Valley sections. The correlation of individual mixed layers may be difficult because their continuity is affected by attenuation or amplification due to bedrock topography and composition. Salt diapirs that are common in the Dead Sea basin [Neev and Emery, 1967] possibly attenuate seismic wave propagation. This may obstruct the continuity of the mixed layers. An example of such effect has been reported in the Ionian Islands [Stiros, 1994]. The effect of topography of the bedrock below the soft sediments was demonstrated in the San Francisco 1906 earthquake, where buried valleys amplified ground movements and displacements [O'Rourke *et al.*, 1992].

The locations of the mixed layers, their thicknesses, and the distance from each top to the previous one (the interval) are presented in Table 2. We assume that the earthquake record is complete, although it is possible that the formation of a thick mixed layer may have obliterated a former one or more. It also seems possible that two or more temporally close events are represented by a single mixed layer. The diapirs that intrude mixed layers (Figure 5) possibly record this scenario.

## Discussion

### Temporal Distribution

The mean intervals between the upper contacts of the mixed layers are 101 cm in section M1, 130 cm in PZ1, and 109 cm in section PZ2. The standard deviations are 100 cm in section M1, 199 cm in section PZ1, and 123 cm in PZ2. The coefficient of variation (the ratio of the standard deviation to the mean) is 1 in section M1, 1.53 in section PZ1, and 1.13 in section PZ2. The mean time interval between successive upper contacts in section PZ1 is 1.6 kyr with a standard deviation of 2.86 kyr, giving a ratio of 1.75 (Table 3). The ratio standard deviation/mean was suggested to quantify the degrees of periodicity or clustering in the temporal distribution [Ben-Zion and Rice, 1995; Kagan and Jackson, 1991]. The numerical simulations of Ben-Zion and Rice suggest that this ratio decreases with earthquake size and with the level of geometrical regularity of the fault system.

The ages determined in section PZ1 allow the transformation of thickness to temporal intervals by dividing

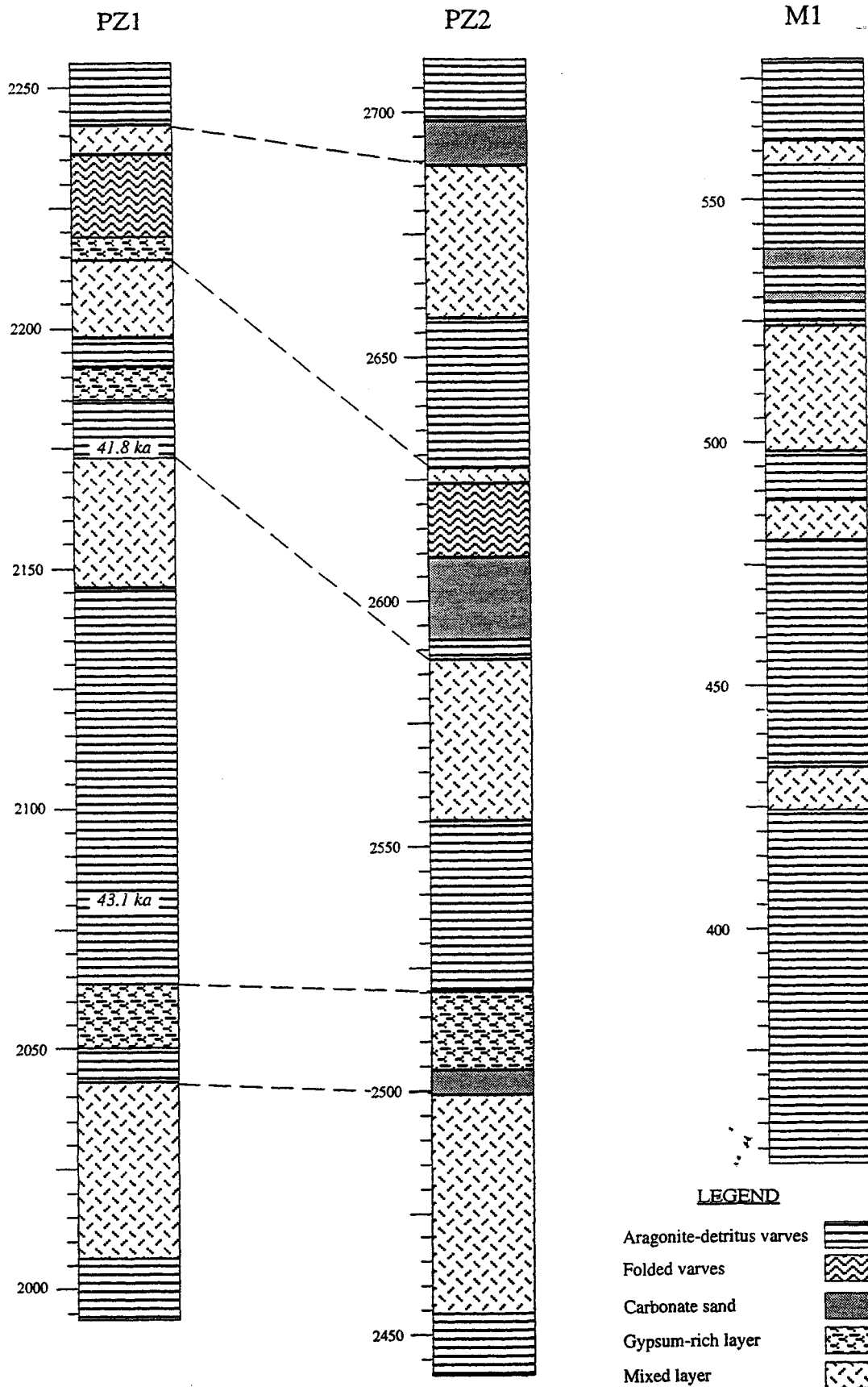


**Figure 8.** An example of segments of sections PZ1 and PZ2 in the Peratzim Valley and M1 near Masada. The level is measured in centimeters from the base of the Lisan Formation. Detailed correlation is hindered by facies variations. We suggest a tentative correlation between PZ1 and PZ2, which will be tested by radiometric dating.

**Table 2.** The locations of the Mixed Layers in Columnar Sections PZ1 and PZ2 in the Peratzim Valley and M1 near Masada (Figure 1)

Top cm	Age, ka	Bottom, cm	Thickness, cm	Interval, cm
<i>Section PZ1</i>				
3862	24.4	3850	12	150
3712	26.1	3707	5	18
3694	26.3	3687	7	139
3555	27.8	3543	12	81
3474	28.6	3472	2	5
3469	28.7	3454	15	22
3447	28.9	3440	7	143
3304	30.5	3289	15	99
3205	31.6	3195	10	196
3009	33.7	2994	15	394
2615	38	2595	20	373
2242	42.1	2236	6	28
2214	42.4	2198	16	41
2173	42.8	2146	27	130
2043	44.2	2006	37	133
1910	45.7	1900	10	29
1881	46	1873	8	36
1845	46.4	1829	16	143
1702	48	1690	12	38
1664	48.4	1647	17	225
1439	50.8	1436	3	19
1420	51	1417	3	26
1394	51.3	1379	15	34
1360	51.7	1346	14	40
1320	52.1	1272	48	105
1215	55.4	1195	20	41
1174	55.7	1164	10	14
1160	55.7	1110	50	1026
134	71	125	9	34
Average			15	130
S.D.			12	199
<i>Section PZ2</i>				
3701		3698	3	15
3686		3683	3	23
3663		3657	6	106
3557		3554	3	50
3507		3489	18	24
3483		3477	6	15
3468		3463	5	26
3442		3437	5	83
3359		3350	9	15
3344		3334	10	47
3297		3294	3	21
3276		3270	6	53
3223		3220	3	203
3020		3017	3	12
3008		3006	2	29
2979		2975	4	80
2899		2895	4	210
2689		2658	31	62
2627		2624	3	39
2588		2555	33	89
2499		2454	45	244
2255		2248	7	140
2115		2110	5	389
1726		1721	5	99
1627		1617	10	273
1354		1341	13	33
1321		1305	16	174
1147		1128	19	58
1089		1075	14	37
1052		1049	3	34

**Table 2.** (continued)

Top cm	Age, ka	Bottom, cm	Thickness, cm	Interval, cm
1018		1012	6	63
955		935	20	59
896		866	30	491
405		400	5	405
Average			11	109
S.D.			10	123
<i>Section M1</i>				
2826		2824	2	89
2737		2736	1	94
2643		2641	2	46
2597		2595	2	44
2553		2549	4	45
2508		2505	3	164
2344		2342	2	45
2299		2296	3	47
2252		2250	2	49
2203		2200	3	55
2148		2145	3	162
1986		1984	2	59
1927		1925	2	48
1879		1878	1	457
1422		1417	5	140
1282		1274	8	72
1210		1207	3	100
1110		1108	2	193
917		915	2	365
552		547	5	38
514		488	26	36
478		470	8	55
423		414	9	143
280		275	5	93
187		185	2	38
149		147	2	13
136		118	18	20
116		111	5	116
Average			5	101
S.D.			5	100

The top and bottom of each layer are measured in centimeters from the base of the section. The interval is measured from the top of the mixed layer to the top of the former one below. Section PZ1 includes the absolute ages interpolated from the linear regression (Figure 3).

the intervals with the mean sedimentation rate. Sedimentation rates are calculated in two ways (Figure 3): by linear regression of all data and of three segments of the section. The age of the top of each mixed layer is then interpolated, and the time intervals are averaged. The mean recurrence interval in section PZ1 is about 1600 years, in agreement with other estimates for the last 4000 years [Ben-Menahem, 1991; Garfunkel et al., 1981; Reches and Hoexter, 1981]. Ages of sections PZ2 and M1 are not available yet; we tentatively assume similar sedimentation rates because of the similar stratigraphy. Most of the lithologic units of sections PZ1 and PZ2 correlate (Figure 8). The general division of the Lisan into lower detritus-rich and upper aragonite-rich units separated by a thin gypsum-rich unit is common to all three sections. We tentatively adopt *Begin's* [1974] correlation based on these units. Correlation with contemporaneous events recorded by

**Table 3.** Mean Interval Between the Upper Contacts of the Mixed Layers (M), Standard Deviation (S), and Ratio S/M

Section	Unit	M	S	S/M
PZ1 (three segments)	kyr	1.63	2.86	1.75
PZ1 (single regression)	kyr	1.49	2.26	1.51
PZ1	cm	130	199	1.53
PZ2	cm	109	123	1.13
M1	cm	101	100	0.99

The intervals are kiloyears in PZ1, where U series ages have been measured, and centimeters in all three sections. The mean sedimentation rate in PZ1 was calculated twice (Figure 3): by a single linear regression and by dividing the section into three segments. The mean intervals for both ways of calculations are presented.

Amit *et al.* [1994] in the southern Arava, some 180 km south of our study area, is not established.

Figure 9 displays the population of the time intervals between the mixed layers (the interseismic interval) illustrating the rarity of long intervals. This is also evident in Figure 10 that shows that the mixed layers in all three sections are clustered. The detailed stratigraphic correlation between the sections is not fully resolved because of slight facies changes (more ages are currently being measured in order to determine the precise correlation). However, the pattern of clustering is robust in all sections. In section PZ1 the earthquakes appear clustered during periods of 8-12 kyr, with relatively quiet periods of similar duration between the clusters (Figure 10). This pattern is independent of our choice of calculated sedimentation rate. Each cluster exhibits a different fine structure (i.e., the detailed distribution of events), limiting the predictability of the sequence. However, a period of the order of 20,000 years is likely to include a complete cycle of both a cluster and a quiet period. A mean recurrence time that is calculated for shorter periods may not represent the long-term seismic behavior.

### Magnitudes

The assignment of magnitudes to the mixed layers can promote seismotectonic analysis because magnitudes, moments, fault area, and slip are all related [e.g., Kanamori and Anderson, 1975; Wells and Coppersmith, 1994].

Liquefaction is a major cause of damage during large earthquakes [Youd and Perkins, 1987]. Direct observations as well as experiments indicate that liquefaction related to earthquakes is mainly associated with those of magnitude 6 and more [Allen, 1982]. The dominant cause of liquefaction of loose, water-saturated, clastic sediments is cyclic loading by earthquake surface waves that subject the sediment to repeated horizontal shaking [Allen, 1982].

The thicknesses of the mixed layers in each columnar section obey a log-linear frequency distribution (Figure 11), similar to the behavior of earthquake magnitudes [Gutenberg and Richter, 1954]. Yet, it is wrong to assign magnitudes to mixed layers because in addition to magnitude, the thickness of a mixed layer is influenced also by subtle bottom topography (Figure 4) as well as variables such as peak particle velocity, duration of motion, ground acceleration, and

local sediment properties. There is no correlation between the thickness of the mixed layers and the preceding interval (Figure 12). The large number of unknown variables, in addition to the weak correlation of acceleration with magnitude, hinders the assignment of earthquake magnitudes to the observed mixed layers. However, a general idea about magnitudes may be gained by comparison with observed liquefaction and fluidization elsewhere. The ground surface acceleration during earthquakes that are associated with liquefaction is of the order of 0.2g and the frequencies are mostly in the range 0.1-10 Hz [Richter, 1958]. For example, at a site undergoing liquefaction, simultaneous measurements of pore water pressure and ground accelerations during the Superstition Hills, California,  $M=6.6$  earthquake reveal that excess pore pressures were generated once horizontal acceleration reached 0.21g. In other earthquakes, excess pore pressure did not occur at 0.17g [Holzer *et al.*, 1989].

Intensity VII of the Modified Mercalli Intensity Scale is the lowest that includes "water turbid with mud" [Grünthal, 1993]. This intensity occurs where the peak ground acceleration is 0.1g to 0.15g and the average peak velocity is 8-12 cm/s. In

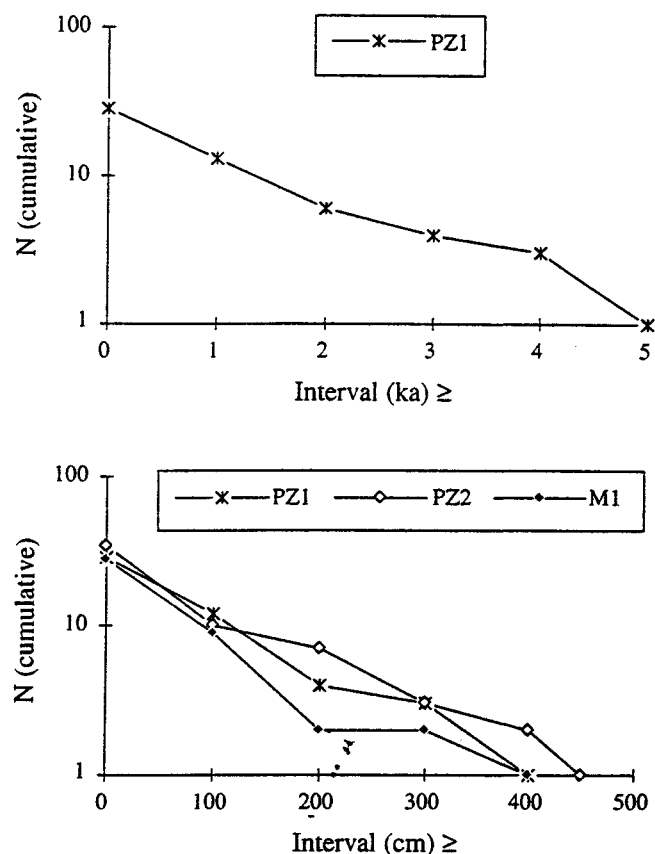


**Figure 9.** The frequency  $N$  of intervals is plotted as a function of their length. Long intervals are rare, and shorter intervals are progressively more common.  $N$ , shown on a log scale, is the number of individual intervals equal to or greater than the abscissa value. An interval is the vertical distance between upper contacts of two consecutive mixed layers in a columnar section. It can be transformed into a time interval by dividing by the sedimentation rate. (top) Population of time intervals in section PZ1 where ages have been determined and sedimentation rate is known. (bottom) Population of thickness intervals, exhibiting similar behavior in all three columnar sections.

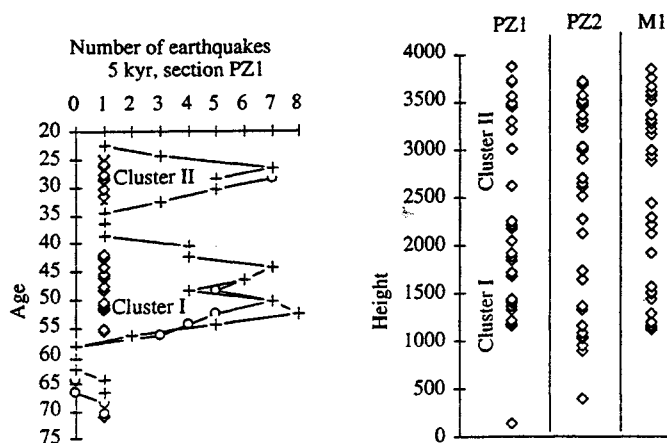


**Figure 10.** (left) The distribution of mixed layers (i.e., earthquakes) along section PZ1; open diamonds show the individual layers. Crosses and open circles are the number of earthquakes per 5 kyr sliding window, shifted by 2-kyr increments leaving 3-kyr overlap. The crosses show the distribution when the ages of the mixed layers are calculated by a single linear regression, whereas the circles show the distribution when the ages are calculated in three segments (Figure 3). The distribution shows two clusters of frequent events. A cycle about 20,000 years long includes a cluster period and a quiet intercluster period. The pattern of clustering is independent of our choice of calculated sedimentation rates. (right) The distribution of individual mixed layers along sections PZ1, PZ2, and M1. The top of the Lisan is used as a datum. All three sections show clusters of mixed layers separated by quiescent intervals.

the 1906 San Francisco earthquake, intensity VII was reported on the San Francisco peninsula within 3 km to about 15 km from the San Andreas fault [Bolt, 1988]. In the Bingöl, Turkey,  $M_s=6.7$  earthquake, intensity VII occurred up to 10 km from the fault [Seymen and Aydin, 1972]. Out of 58 observed sites that liquefied during earthquakes, 54 occurred during events of  $M \geq 6$  and maximum accelerations of 0.08g-0.25g [Kuribayashi and Tatsuoka, 1975; Youd, 1977]. Liquefaction of sand may occur at  $M$  as low as 5 [Audemard and de Santis, 1991] and 4.6 [Sims and Garvin, 1995], but a quantitative analysis [Allen, 1986] based on observations [Kuribayashi

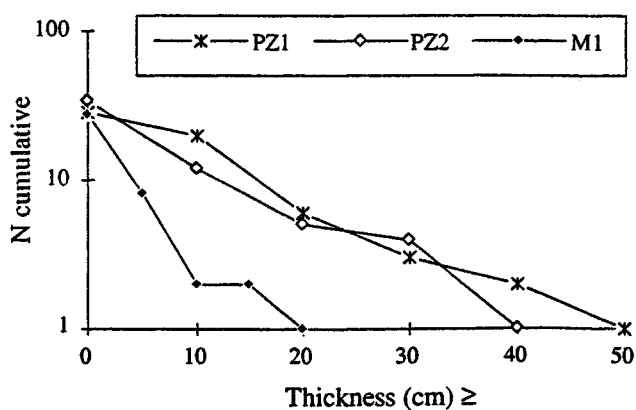


**Figure 11.** The frequency  $N$  of mixed layers is plotted as a function of their thicknesses. Thicker mixed layers are progressively rare, whereas thinner ones are more common.  $N$ , shown on a log scale, is the number of mixed layers whose thickness is equal to or greater than the abscissa value.

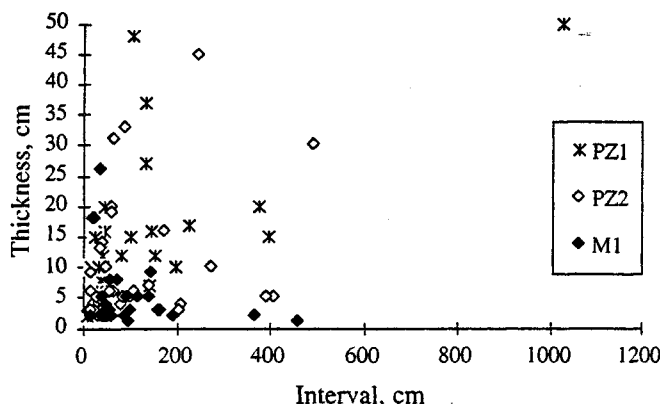


**Figure 12.** No correlation is found between the thickness of a mixed layer and the thickness of undisturbed layers below it (deposited in the interseismic interval).

and Tatsuoka, 1975; Youd, 1977] indicates that it is more characteristic of greater magnitudes. The clay content in the Lisan (20-35%) and the grain sizes of a few microns [Arkin and Michaeli, 1986; Begin et al., 1974] make it less prone to liquefaction than sand [Allen, 1982; Seed et al., 1983]. For epicentral distances exceeding 100 km,  $M_s 7.5$  appears to be a minimum threshold [Vittori et al., 1991]. By comparison, it seems reasonable that the mixed layers of the Lisan Formation also formed during earthquakes with magnitudes 5.5-7 in the vicinity of the Dead Sea. We cannot constrain the maximum magnitude, and it is also possible that the mixed layers record magnitudes above 7 that occurred within distances of the order of 100 km and more. The distinction between weak and near earthquakes and far but strong ones seems, as yet, impossible. The character of the mixed layers indicates that their formation involved fluidization which requires stronger shaking than liquefaction [Lowe, 1975]. Magnitude 5.5 is therefore a conservative lower bound. The surface ruptures near Masada provide an independent constraint for the magnitude since surface faults are rarely reported below magnitude 5.5 [Wells and Coppersmith, 1994].

Finding the "missing link" between any measurable feature of the mixed layers and earthquake magnitudes will contribute to a better constraint on the long-term frequency-magnitude relation, maximum possible magnitude, and the seismic efficiency of the Dead Sea Transform. Such a link may be sought by correlating mixed layers in the post-Lisan sediments with historically or instrumentally recorded earthquakes.

**Conclusions**

The fine alternating aragonite and detritus laminae of the Lisan Formation provide highly sensitive markers that allow recognition of millimeter-scale deformation. Widespread layers composed of mixtures of brecciated laminae are identified as seismites, earthquake-induced deformations of the sediment. Assuming that each mixed layer is a seismite that formed in a single,  $M_L \geq 5.5$  event, we conclude that the long-term mean recurrence period of strong ( $M_L \geq 5.5$ ) earthquakes in the Dead Sea graben is about 1.6 kyr with a large standard deviation of about 2.8 kyr. The earthquakes cluster at periods of ~10,000 years separated by quieter periods of similar length. This clustering suggests that a mean recurrence time

determined for less than 20,000 years might misrepresent the long-term behavior of the fault zone.

**Acknowledgments.** We are grateful to Gidi Baer, Yehuda Ben-Zion, Greg Beroza, Zvi Garfunkel, Ehud Gavze, Kenneth Hsü, Ia'akov Karcz, Ze'ev Reches, Amos Salamon, Gadi Shamir, and Avi Shapira for stimulating discussions and helpful suggestions. Reviews by Bob Yeats, Rivka Amit, Gadi Shamir, Greg Beroza, Yehuda Ben-Zion, and an anonymous referee greatly improved the manuscript. Annu Kyösyä, Revital Ken-Tor, Alexandra Schramm, and Meir Abelson are thanked for their assistance in field work. The research was partly supported by a grant from the Earth Sciences Research Administration in the Ministry of Energy, Israel, to A. Agnon and grant 89-232 to H. Ron from the U.S.-Israel Binational Science Foundation, Jerusalem, Israel.

## References

- Agnon, A., The evolution of sedimentary basins and the morphotectonics in the western fault escarpment of the Dead Sea (in Hebrew, English abstract), M.Sc. thesis, Hebrew Univ., Jerusalem, 1983.
- Allen, C. R., Seismological and paleoseismological techniques of research in active tectonics, in *Active Tectonics*, edited by R. E. Wallace, 148-154, National Academy Press, Washington, D.C., 1986.
- Allen, J. R. L., *Sedimentary Structures: Their Character and Physical Basis*, 663 pp., Elsevier, New York, 1982.
- Allen, J. R. L., Earthquake magnitude-frequency, epicentral distance, and soft-sediment deformation in sedimentary basins, *Sediment. Geol.*, **46**, 67-75, 1986.
- Amit, R., J. B. J. Harrison, Y. Enzel, and N. Porat, Paleoseismology in the southern Arava rift, Israel, *U.S. Geol. Surv. Open File Rep.*, **94-568**, 8-10, 1994.
- Arieh, E. J., Seismicity of Israel and adjacent areas, *Isr. Geol. Surv. Bull.*, **43**, 1-14, 1967.
- Arkin, Y., and L. Michaeli, The significance of shear strength in the deformation of laminated sediments in the Dead Sea area, *Isr. J. Earth Sci.*, **35**, 61-72, 1986.
- Audemard, F. A., and F. de Santis, Survey of liquefaction structures induced by recent moderate earthquakes, *Bull. Int. Assoc. Eng. Geol.*, **44**, 5-16, 1991.
- Begin, Z. B., A. Ehrlich, and Y. Nathan, Lake Lisan, the Pleistocene precursor of the Dead Sea, *Geol. Surv. Isr. Bull.*, **63**, 30, 1974.
- Ben-Menahem, A., Four thousand years of seismicity along the Dead Sea rift, *J. Geophys. Res.*, **96**, 20,195-20,216, 1991.
- Ben-Menahem, A., A. Nur, and M. Vered, Tectonics, seismicity and structure of the Afro-Eurasian junction- the breaking of an incoherent plate, *Phys. Earth Planet. Inter.*, **12**, 1-50, 1976.
- Ben-Zion, Y., and J. R. Rice, Slip patterns and earthquake populations along different classes of faults in elastic solids, *J. Geophys. Res.*, **100**, 12,959-12,983, 1995.
- Bentor, Y. K., and A. Vroman, The geological map of Israel, 1:100,000, Sheet 16, Mt. Sedom, Geol. Surv. of Israel, Jerusalem, 117, 1960.
- Bolt, B. A., *Earthquakes*, 282 pp., W. H. Freeman, New York, 1988.
- Chen, J. H., R. L. Edwards, and G. J. Wasserburg,  $^{238}\text{U}$ ,  $^{234}\text{U}$ , and  $^{232}\text{Th}$  in seawater, *Earth Planet. Sci. Lett.*, **80**, 241-251, 1986.
- Copeland, L., and C. Vita-Finzi, Archaeological dating of geological deposits in Jordan, *Levant*, **X**, 10-25, 1978.
- Davenport, C. A., and P. S. Ringrose, Deformation of Scottish Quaternary sediment sequence by strong earthquake motions, in *Deformation of Sediments and Sedimentary Rocks*, edited by M. E. Jones and R. M. Preston, *Geol. Soc. Spec. Publ. London*, **29**, 299-314, 1987.
- Doig, R., Effects of strong seismic shaking in lake sediments, and earthquake recurrence interval, Témiscaming, Quebec, *Can. J. Earth Sci.*, **28**, 1349-1352, 1991.
- Edwards, R. L., J. H. Chen, and G. J. Wasserburg,  $^{238}\text{U}$ - $^{234}\text{U}$ - $^{230}\text{Th}$ - $^{232}\text{Th}$  systematics and the precise measurement of time over the past 500,000 years, *Earth Planet. Sci. Lett.*, **81**, 175-192, 1987.
- El-Isa, Z. H., and H. Mustafa, Earthquake deformations in the Lisan deposits and seismotectonic implications, *Geophys. J. R. Astron. Soc.*, **86**, 413-424, 1986.
- Enzel, Y., R. Amit, J. Bruce, J. Harrison, and N. Porat, Morphologic dating of fault scarps and terrace risers in the southern Arava, Israel: Comparison to other age-dating techniques and implications for paleoseismicity, *Isr. J. Earth Sci.*, **43**, 91-103, 1994.
- Field, M. E., J. V. Gardner, A. E. Jennings, and B. D. Edwards, Earthquake-induced sediment failure on a 0.25° slope, Klamath River delta, California, *Geology*, **10**, 542-546, 1982.
- Gardosh, M., Z. Reches, and Z. Garfunkel, Holocene tectonic deformation along the western margins of the Dead Sea, *Tectonophysics*, **180**, 123-137, 1990.
- Garfunkel, Z., I. Zak, and R. Freund, Active faulting along the Dead Sea transform (rift), *Tectonophysics*, **80**, 1-26, 1981.
- Grant, L. B., and K. Sieh, Paleoseismic evidence of clustered earthquakes on the San Andreas fault in the Carrizo Plain, California, *J. Geophys. Res.*, **99**, 6819-6841, 1994.
- Grünthal, G., *European Macroseismic Scale 1992*, 79 pp., Centr. Eur. de Geodyn. et de Seismol., Luxembourg, 1993.
- Guiraud, M., and J. C. Plaziat, Seismites in the fluvial Bima sandstone: identification of paleoseisms and discussion of their magnitudes in a cretaceous synsedimentary strike-slip basin (Upper Benue, Nigeria), *Tectonophysics*, **225**, 493-522, 1993.
- Gutenberg, B., and C. F. Richter, *Seismicity of the Earth and Associated Phenomena*, 310 pp., Princeton Univ. Press, Princeton, N. J., 1954.
- Holzer, T. L., T. L. Youd, and T. C. Hanks, Dynamics of liquefaction during the 1987 Superstition Hills, California, earthquake, *Science*, **244**, 56-59, 1989.
- Hsü, K. J., *Physical Principles of Sedimentology*, 233 pp., Springer-Verlag, New York, 1989.
- Kagan, Y. Y., and D. D. Jackson, Long-term earthquake clustering, *Geophys. J. Int.*, **104**, 117-133, 1991.
- Kanamori, H., and D. L. Anderson, Theoretical basis of some empirical relations in seismology, *Bull. Seismol. Soc. Am.*, **65**, 1073-1095, 1975.
- Karcz, I., and Y. Mimran, Soft sediment deformation in calcareous marls of Lisan Formation, in *Tenth International Congress on Sedimentol.*, Int. Assoc. of Sedimentol., Jerusalem, 349-350, 1978.
- Katz, A., and N. Kolodny, Hypersaline brine diagenesis and evolution in the Dead Sea Lake Lisan system (Israel), *Geochim. Cosmochim. Acta*, **53**, 59-67, 1989.
- Katz, A., Y. Kolodny, and A. Nissenbaum, The geochemical evolution of the Pleistocene Lake Lisan-Dead Sea system, *Geochim. Cosmochim. Acta*, **41**, 1609-1626, 1977.
- Kaufman, A., U series dating of Dead Sea basin carbonates, *Geochim. Cosmochim. Acta*, **35**, 1269-1281, 1971.
- Kaufman, A., Y. Yechieli, and M. Gardosh, Reevaluation of the lake-sediment chronology in the Dead Sea Basin, Israel, based on new  $^{230}\text{Th}/^{234}\text{U}$  dates, *Quat. Res.*, **38**, 292-304, 1992.
- Keefe, D. K., Landslides caused by earthquakes, *Geol. Soc. Am. Bull.*, **95**, 406-421, 1984.
- Kuribayashi, E., and F. Tatsuoka, Brief review of liquefaction during earthquakes in Japan, *Soils Found.*, **15**, 81-92, 1975.
- Lovell, J., S. Crampin, R. Evans, and S. Balamir-Ucer, Microearthquakes in the TDP swarms, Turkey: Clustering in space and time, *Geophys. J. R. Astron. Soc.*, **91**, 313-330, 1987.
- Lowe, D. R., Water escape structures in coarse-grained sediments, *Sedimentology*, **23**, 285-308, 1975.
- Marco, S., and A. Agnon, Prehistoric earthquake deformations near Masada, Dead Sea graben, *Geology*, **23**, 695-698, 1995.
- Marco, S., A. Agnon, M. Stein, and H. Ron, A 50,000 year continuous record of earthquakes and surface ruptures in the Lisan Formation, the Dead Sea graben, *U.S. Geol. Surv. Open File Rep.*, **94-568**, 112-114, 1994.
- Mimran, Y., and I. Karcz, Study of fabrics in sedimentary folds of Lisan Formation, in *Israel Geological Society Annual Meeting*, p. 55, Isr. Geol. Soc., Jerusalem, Nazaret, 1983.
- Neev, D., and K. O. Emery, The Dead Sea, depositional processes and environments of evaporites, *Geol. Surv. Isr. Bull.*, **41**, 147 pp., 1967.
- Niemi, T. M., and Z. Ben-Avraham, Evidence for Jericho earthquakes from slumped sediments of the Jordan River delta in the Dead Sea, *Geology*, **22**, 395-398, 1994.
- O'Rourke, T. D., P. A. Beaujon, and C. R. Scawthorn, Large ground deformations and their effects on lifeline facilities: 1906 San Francisco earthquake, in *Case Studies of Liquefaction and Lifeline Performance During Past Earthquakes*, edited by T. D. O'Rourke and M. Hamada, 1-130, Natl. Cent. for Earthquake Eng. Res., Buffalo, N. Y., 1992.
- Reches, Z., and D. F. Hoexter, Holocene seismic and tectonic activity in the Dead Sea area, *Tectonophysics*, **80**, 235-254, 1981.
- Richter, C. F., *Elementary Seismology*, 768 pp., W. H. Freeman, New York, 1958.
- Salamon, A., Seismotectonic analysis of earthquakes in Israel and

- adjacent areas (in Hebrew with English abstract), Ph.D. thesis, Hebrew Univ., Jerusalem, 1993.
- Scholz, C. H., *The Mechanics of Earthquakes and Faulting*, 439 pp., Cambridge Univ. Press, New York, 1990.
- Schramm, A., M. Stein, and S. L. Goldstein, Constancy of  $^{234}\text{U}/^{238}\text{U}$  ratios in Late Pleistocene aragonitic sediments—Lake Lisan, paleo-Dead Sea, *Terra Nova*, 7, 325, Eur. Union. Geol. Meet. Suppl., 1995.
- Seed, H. B., I. M. Idriss, and I. Arrango, Evaluation of liquefaction potential using field performance data, *J. Geotech. Eng., Am. Soc. Civ. Eng.*, 109, 458-482, 1983.
- Segall, P., and D. D. Pollard, Mechanics of discontinuous faults, *J. Geophys. Res.*, 85, 4337-4350, 1980.
- Seilacher, A., Fault-graded beds interpreted as seismites, *Sedimentology*, 13, 155-159, 1969.
- Seilacher, A., Sedimentary structures tentatively attributed to seismic events, *Mar. Geol.*, 55, 1-12, 1984.
- Seymen, I., and A. Aydin, The Bingöl earthquake fault and its relation to the North Anatolian fault zone, *Bull. Miner. Res. Explor. Inst. Turkey*, 79, 1-8, 1972.
- Shapira, A., R. Avni, and A. Nur, A new estimate for the epicenter of the Jericho earthquake of 11 July 1927, *Isr. J. Earth Sci.*, 42, 93-96, 1992.
- Shapira, A., and L. Feldman, Microseismicity of three locations along the Jordan rift, *Tectonophysics*, 141, 89-94, 1987.
- Sims, J. D., Determining earthquake recurrence intervals from deformational structures in young lacustrine sediments, *Tectonophysics*, 29, 144-152, 1975.
- Sims, J. D., and C. D. Garvin, Recurrent liquefaction induced by the 1989 Loma Prieta earthquake and 1990 and 1991 aftershocks: Implications for paleoseismicity studies, *Bull. Seismol. Soc. Am.*, 85, 51-65, 1995.
- Stein, M., S. L. Goldstein, H. Ron, and S. Marco, Precise TIMS  $^{230}\text{Th}$  -  $^{234}\text{U}$  ages and magnetostratigraphy of Lake Lisan sediments (paleo-Dead Sea), *Eos Trans. AGU*, 73(14), Spring Meet. Suppl., 154, 1992.
- Stein, M., G. J. Wasserburg, P. Aharon, J. H. Chen, Z. R. Zhu, A. Bloom, and J. Chappell, TIMS U-series dating and stable isotopes of the last interglacial event in Papua New Guinea, *Geochim. Cosmochim. Acta*, 57, 2541-2554, 1993.
- Stiros, S., Anomalous attenuation of seismic waves in the Ionian Islands, Greece, *Eos Trans. AGU*, 75, 117-118, 1994.
- Swan, F. H., Temporal clustering of paleoseismic events on the Oued Fodda fault, Algeria, *Geology*, 16, 1092-1095, 1988.
- van Eck, T., and A. Hofstetter, Fault geometry and spatial clustering of microearthquakes along the Dead Sea-Jordan rift fault zone, *Tectonophysics*, 180, 15-27, 1990.
- Vita-Finzi, C., Observations on the Late Quaternary of Jordan, *Palestine Explor. Q., Jan.-June*, 19-33, 1964.
- Vittori, E., S. S. Labini, and L. Serva, Palaeoseismology: Review of the state-of-the-art, *Tectonophysics*, 193, 9-32, 1991.
- Wells, D. L., and K. J. Coppersmith, New empirical relationships among magnitudes, rupture length, rupture width, rupture area, and surface displacement, *Bull. Seismol. Soc. Am.*, 84, 974-1002, 1994.
- Youd, T. L., Discussion of "Brief review of liquefaction during earthquakes in Japan" by E. Kuribayashi and T. Tatsuoka, *Soils Found.*, 17, 82-85, 1977.
- Youd, T. L., and D. M. Perkins, Mapping of liquefaction severity index, *J. Geotech. Eng. Am. Soc. Civ. Eng.*, 113, 1374-1392, 1987.

A. Agnon, S. Marco, and M. Stein, Institute of Earth Sciences, Hebrew University, Jerusalem 91904, Israel. (e-mail: smarco@shum.cc.huji.ac.il)

H. Ron, Institute for Petroleum Research and Geophysics, P.O.Box 2286, Holon 58122, Israel.

(Received September 28, 1994, revised May 12, 1995; accepted May 23, 1995.)





## 817-YEAR-OLD WALLS OFFSET SINISTRALLY 2.1 m BY THE DEAD SEA TRANSFORM, ISRAEL

SHMUEL MARCO,<sup>1,2</sup> AMOTZ AGNON,<sup>2</sup> RONNIE ELLENBLUM,<sup>3</sup>  
AMIR EIDELMAN,<sup>2</sup> URI BASSON<sup>4</sup> and ADRIAN BOAS<sup>5</sup>

<sup>1</sup> Geological Survey of Israel, Jerusalem, Israel

<sup>2</sup> Institute of Earth Sciences, Hebrew University, Jerusalem, Israel

<sup>3</sup> Department of Geography, Hebrew University, Jerusalem, Israel

<sup>4</sup> Geosense Ltd, Tel Aviv, Israel

<sup>5</sup> Israel Antiquities Authority, Jerusalem, Israel

(Received 2 November 1995; accepted in revised form 10 October 1996)

**Abstract**—Archeological excavations in the Crusader Ateret Fortress near the Jordan River exposed E–W trending walls displaced sinistrally up to 2.1 m by the Dead Sea transform fault. A water duct, probably of Crusader age, is also offset sinistrally across the fault by about 1–2 m, but newer water ducts parallel to the former one show no displacement. The maximum width of the fault zone is about 10 m.

Post-Crusader structures show significantly less deformation, and together with the low seismic activity, suggest there has been negligible creep. It is therefore conceivable that in this particular fault segment, stress is occasionally relieved by strong destructive earthquakes associated with surface ruptures. Historical accounts include descriptions of post-Crusader earthquakes in the northern part of Israel in A.D. 1202, 1546, 1759, and 1837. These events caused destruction and casualties over large areas. We conclude that most of the displacement of the Ateret Fortress walls occurred during one of these strong earthquakes, probably that of 1202 A.D., and some additional offset occurred during subsequent events. The associated magnitude is estimated at 6.5–7.1.

The Ateret site is extremely valuable for paleoseismic studies in general, and assessment of seismic hazard to nearby population centers in particular, as there is an abundance of well-dated man-made structures and a small number of candidate earthquakes. © 1997 Elsevier Science Ltd

### INTRODUCTION

Accounts of earthquake-induced surface ruptures along the Dead Sea transform fault zone are rare (Amiran, 1951; Ambraseys and Melville, 1988; Ben-Menahem, 1991; Amiran *et al.*, 1994), and some of them might be unreliable (Karcz and Kafri, 1978; Ambraseys and Karcz, 1992). Here we report the first evidence for a historical sinistral surface rupture. It was discovered during archeological excavations that began in 1994 in the Ateret Crusader Fortress, where E–W trending walls are displaced sinistrally 2.1 m by a N–S fault, and younger Muslim structures are displaced by about 0.2 m.

The Ateret Fortress is located on the active Jordan Gorge Fault, a straight segment of the Dead Sea transform between the Sea of Galilee and the Hula Valley. It was established by the Crusaders in 1178 A.D. on the western bank of the Jordan River, just south of the Benot Ya'akov bridge (Fig. 1A). Its construction terminated 11 months later due to an Arab conquest.

The Dead Sea transform forms a boundary between the Sinai and the Arabia plates (Fig. 1B). South of the Sea of Galilee the transform offsets 105 km sinistrally a variety of pre-Miocene to Early Miocene geological features (Quennell, 1956; Freund *et al.*, 1968). Recent activity along the transform is manifested by deformation of Pleistocene rocks, and by historical and current seismicity.

The trace of the Dead Sea transform is discontinuous and contains bends (Fig. 1B). Pull-apart grabens form between overlapping left-stepping jogs, for example, Hula Valley, and push-up swells form at right-stepping jogs (e.g., Rosh Pina saddle (Garfunkel, 1981)). Previous studies in the area (Picard, 1963; Picard and Golani, 1965; Belitzky, 1987; Heimann and Ron, 1987; Harash and Bar, 1988; Goren-Inbar and Belitzky, 1989; Rotstein and Bartov, 1989; Heimann and Ron, 1993) show that the Pleistocene sediments and basalts in the Benot Ya'akov Bridge area are strongly deformed and the geometry of the faults has changed with time. The Jordan Gorge has been proposed as a 'morphotectonic junction' and 'the epicentre area of strong earthquakes' (Harash and Bar, 1988).

Historical accounts include descriptions of post-Crusader earthquake-induced damage in the northern part of Israel in A.D. 1202, 1546, 1759, and in 1837 (Amiran *et al.*, 1994). The events caused destruction and casualties in the cities of Tiberias (Fig. 1B) and Baalbek (on the Yammouneh fault, some 100 km north from Ateret) and their vicinities (Amiran *et al.*, 1994). Current seismicity in the study area is subdued relative to adjacent areas (the Kinneret and Hula segments) of the Dead Sea transform (IPRG, 1983–1995; Shapira and Feldman, 1987). Salamon (1993) suggested that the plate boundary in this region becomes diffuse because the displacement is divided among several branching faults and partly accommodated by underthrust belts (Kashai and Crocker, 1987; Walley, 1988; Chaimov and Barazangi, 1990). Sparse microseismicity is distributed across the plate margin. The largest event in the last 15-year record is an  $M_L$  4.3 earthquake in the Hula Valley just north of Ateret. Focal plane solutions show mainly sinistral motion with a minor normal component (van Eck and Hofstetter, 1990). A geodetic survey in the study area indicates that no detectable transform movement has taken place since the establishment of benchmarks in 1988 (I. Karcz, *pers. commun.* 1994).

## THE YOUNG FAULT AT THE ATERET SITE

### *Bedrock*

Pleistocene lake sediments, dipping 60°E, crop out in the area between the fortress and the Jordan River. They are underlain by the 0.8–0.9 Ma-old Yorda basalt flow (Heimann and Ron, 1993). A N–S-striking fault plane is exposed in the lake sediments east of the fortress and N-trending horizontal slickenside lineations in a basalt outcrop some 50 m south of the fortress, were considered to be an indication of a fault (S. Belitzky, *pers. commun.* 1994).

### *Crusader structures*

The Ateret Fortress covers an area of about 150×50 m with the long dimension trending north–south. A 4 m-thick defense wall that surrounds Ateret Hill is composed of a pair of

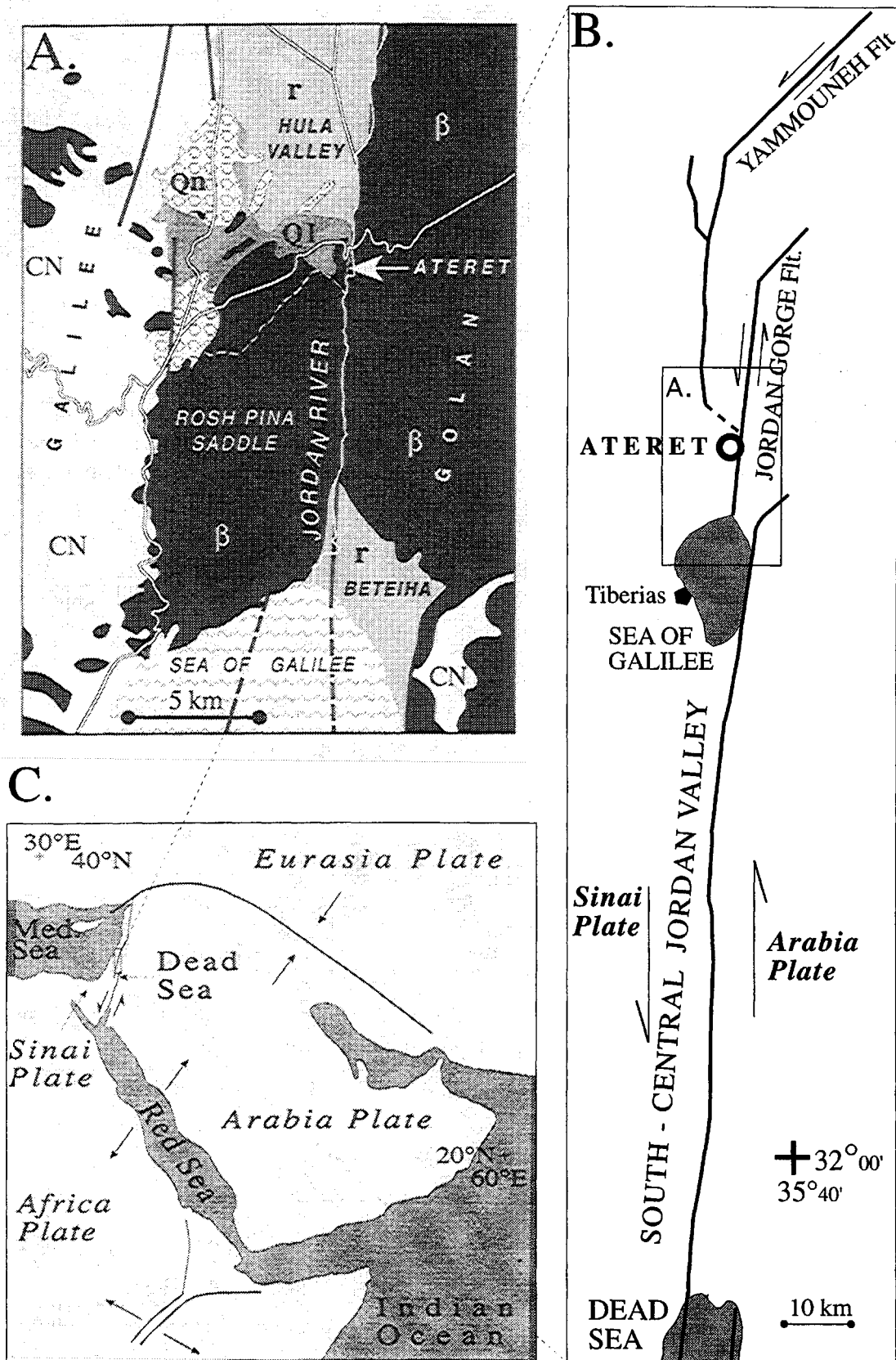


Fig. 1. Location maps: A. Geological map of the Ateret area, after Picard and Golani (1965). CN—Cretaceous to Neogene marine sediments;  $\beta$ —Miocene to Pleistocene basalt flows; Q1—Quaternary lacustrine sediments; Qn—Quaternary alluvium; r—recent alluvium. Solid black lines are faults. B. The Dead Sea transform and the Jordan Gorge fault segment. C. Tectonic plates of the Middle East.

parallel meticulously laid supports made with rectangular 0.5 m-thick thick limestone blocks, separated by a 2 m fill of cemented basaltic cobbles. At present, deformation is best exposed east of the excavated main gate in the southern wall (Figs 2 and 3) where left-lateral displacements amount to 2.1 m. The displacement is distributed over less than 10 m by rotations and small faults between the carved limestone blocks. All the displacements are purely horizontal (all the blocks retain their original level), and all rotations are about vertical axes. The fault lineament traverses the northern walls of the fortress where the walls are severely damaged.

### Post-Crusader structures

In the northern part of the fortress, additional walls from the Arabic period show lesser left-lateral displacements of the order of 0.2–0.3 m at points which coincide with the N–S lineament. A Muslim-style room is interpreted as a mosque due to the presence of a south-facing round niche identified as a “makhreb” or a praying apse. The mosque wall is bent and offset sinistrally, and a layer of building stones, that lies imbricated directly on the floor, suggests collapse.

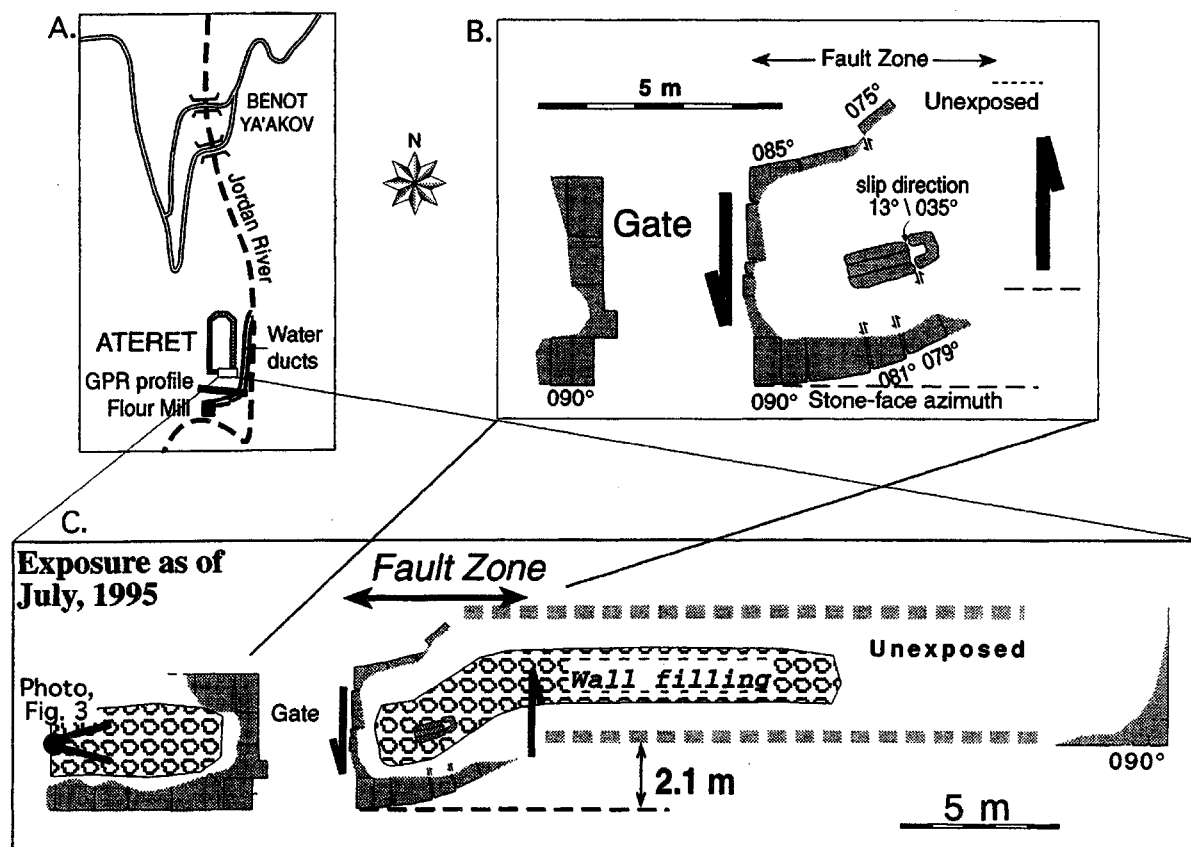


Fig. 2. Site map showing the man-made linear structures and their lateral offset. A. Location of the Ateret fortress, water-ducts, flour mill and the GPR profile. B. Detailed map of the fault zone showing displacement and rotation of masonry. C. Map of southern wall showing how the displacement was measured. The photograph in Fig. 3 was taken from the western side of the gate.

## WATER DUCTS

The Ateret water-powered flour mill, with some Crusader masonry remnants, is located some 100 m south of the fortress (Fig. 2). Two water ducts link the Ateret mill with the Jordan River, one of them is displaced about 1.5 m at a point that aligns with the N–S lineament along which the fortress is displaced. The offset duct is made of Crusader-style limestone blocks, and is tentatively assigned a Crusader age. In a newer water duct that runs parallel to the old one, no



Fig. 3. Deformation of the southern wall of the Ateret Fortress looking east. Arrow points at fault zone. Location is shown in Fig. 2.

offset was observed. Local farmers remember that the newer duct operated until the 1930s. The continuous ducts suggest that the fault is currently locked. The displacement of the discontinuous duct was therefore episodic, probably during the same event that displaced the fortress.

#### GROUND PENETRATING RADAR (GPR) SURVEY

GPR profiles that intersect the lineament (two north and one south of the fortress) show a discontinuity of the gently inclined shallow beds at the lineament (Fig. 4). This observation adds support to our argument that the deformation of the walls occurred by surface rupture.

#### MAGNITUDE ESTIMATE

In order to estimate the magnitude of the earthquake that was associated with the displacement of the fortress walls, we first use the relation  $M_0 = \mu Au$  (Brune, 1968) to estimate the seismic moment ( $M_0$ ). We examined a range of values of average slip ( $u$ ) on a fault plane whose area ( $A$ ) is between 300 and 1500 km<sup>2</sup> assuming a shear modulus ( $\mu$ ) of  $3.10^{11}$  dyne/cm<sup>2</sup>. We then assume a moment–magnitude relation  $\log M_0 = 1.5 M_L + 16$ , which was determined for earthquakes in Israel (Shapira and Hofstetter, 1993), to find the magnitude. Although Shapira and Hofstetter (1993) considered the local magnitude,  $M_L$ , other studies show that magnitudes calculated from moments approximately equal surface wave magnitudes,  $M_s$  (Wells and Coppersmith, 1994). This estimate is compared with another magnitude estimate which is based on earthquake statistics for the Middle East and considers the average slip and the length of faults (Ambraseys, 1988). The second estimate yields values that are less than 0.1 magnitude units higher in the relevant range of slip values. Figure 5 shows the range of possible magnitudes between  $M=6.0$  where the average slip is 10 cm on a  $15 \times 20$  km fault, and  $M=7.4$  for an average slip of 200 cm on a 100 km-long fault (Ambraseys, 1988). If the average slip on the fault is about half the maximum surface displacement (Wells and Coppersmith, 1994), and the southern wall at Ateret exhibits the maximum offset, we may assume a 1 m average slip. This suggests that the magnitude of the earthquake associated with the slip at Ateret may be constrained between 6.6 and 7.1. If the average displacement was 2 m, the magnitude was about 7.4.

#### WHICH EARTHQUAKE?

We assume that the displacements at Ateret reflect the entire movement on the transform fault. The local geology and topography indicate that the fortress lies on the main N–S trending fault in the area (Fig. 1). The post-Crusader earthquakes in the northern part of Israel occurred in A.D. 1202, 1546, 1759, and 1837 (Amiran *et al.*, 1994).

Ambraseys and Melville (1988) estimated the meiseoseismal zone of the 1202 A.D. (20 May) earthquake. Their estimated zone extends from 100 km south to 150 km north of Ateret. They assigned a magnitude of 7.6 to the event and calculated about 2.5 m of maximum displacement. Prior to the present findings, Ambraseys and Barazangi (1989) indicated possible surface faulting based on the “extremely elongated epicentral area” of the 1202 A.D. event. Damage from the 1546 A.D. (14 January) event extended from 150 km south to 75 km north of Ateret (Amiran *et al.*, 1994). Ambraseys and Karcz (1992) argue for a moderate magnitude ( $M_s \approx 6.0$ )

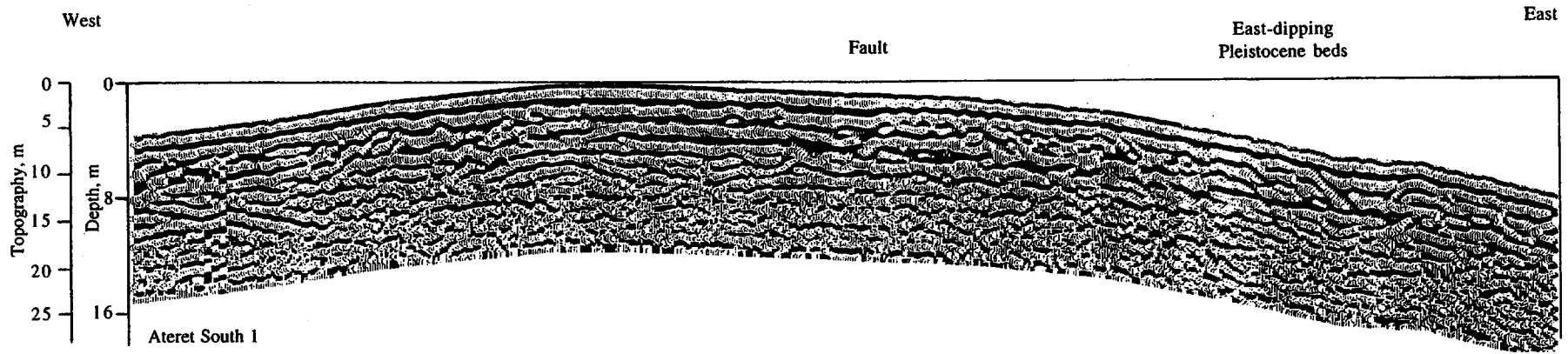


Fig. 4. A 150 m-long ground penetrating radar image south of the Ateret Fortress. The uppermost two reflections are the result of direct airwave, direct groundwater, and a possible very shallow reflector. The fault is marked where the horizontal reflectors terminate towards the east, on the fault lineament that offsets the fortress walls. The profile location is shown in Fig. 2.

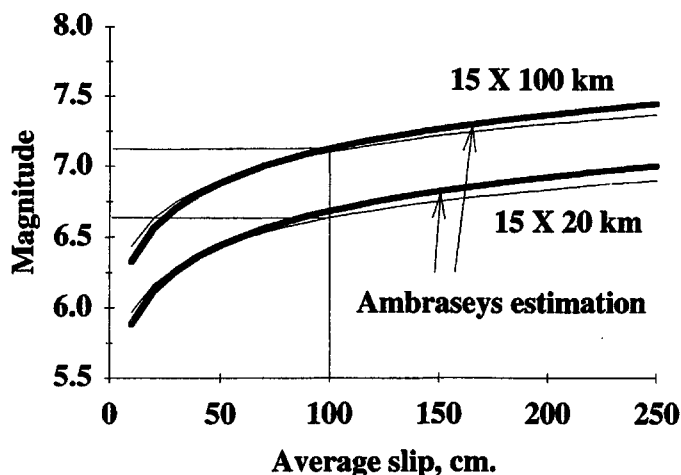


Fig. 5. Magnitude estimate. The upper pair of curves refers to a  $15 \times 100$  km fault, the lower pair refers to a  $15 \times 20$  km fault. Bold curves show the calculation by using Ambraseys' (1988) relation of fault length to magnitude. Faint curves show the magnitude based on the moment–magnitude relation of Shapira and Hofstetter (1993).

for this event with maximum damage in the Judean Hills. Ambraseys and Barazangi (1989) have assigned a double event for the 1759 A.D. (October 30) damage, with surface rupture in the Yammounh segment, north of the Jordan segment of the Dead Sea transform. Their inferred southern epicentre of an  $M \approx 6.6$  “foreshock” could be related to faulting at Ateret (Fig. 1). The last destructive earthquake in the study area was the  $M \approx 6.3$  1837 (January 1) Safed earthquake. The centre of the IX isoseismal of Vered and Striem (1977) coincides with the Ateret site. The last destructive earthquake that struck the Dead Sea transform was the  $M \approx 6.2$  1927 A.D. Jericho earthquake whose epicentre lies 150 km south of Ateret (Vered and Striem, 1977; Shapira *et al.*, 1992). It seems that the likely candidate for the major offset of the fortress wall is the 1202 A.D. earthquake. Later earthquakes hit the Muslim structures, perhaps adding to the offset of the Crusader structure.

Projecting the inferred extent of damage in the past to possible future earthquakes, we expect widespread damage to large population centres in Jordan, Syria, and Israel. If most of the observed slip represents a characteristic earthquake for the Jordan Gorge Fault, the region is at high risk in the near future: even at a long-term slip rate as low as 2.5 mm/y, a simple time-predictable model implies a slip deficit of  $\approx 2$  m (barring active slip on parallel strands east or west of the fortress). Precise dating of the displacement events, and documentation of possible previous events (or slip on parallel strands) are the subject of our ongoing investigation.

#### SUMMARY

- A strong earthquake displaced the 1178 A.D. Ateret Fortress walls by  $\sim 2$  m. The magnitude is estimated at 6.5–7.1.
- Either the same earthquake or another one displaced the lower water duct of the Ateret Mill, and predates the construction of the upper water duct.
- The 1202 event is a candidate for most or all of the observed displacement. Alternatively, the 1759 and 1837 A.D. events together can account for a significant fraction of the slip if these events were limited to the Jordan Gorge Fault.
- Large population centres in Jordan, Syria, and Israel are at peril if the observed slip

represents a characteristic earthquake for the Jordan Gorge Fault. Even at a long-term slip rate as low as 2.5 mm/y, a simple time-predictable model implies high risk in the near future.

*Acknowledgements*—We are grateful to all the people who worked in the excavation in the soaring heat of the summer in the Jordan Valley, to the Jewish National Fund, to Shmuel Belitzky for illuminating the local geology, to Vered Eidelman-Shatil who helped in drafting the figures, and to Ron Bogosh who improved the style of the manuscript.

#### REFERENCES

- Ambraseys N. N. (1988) Magnitude–fault length relationships for earthquakes in the Middle East. In: *Historical Seismograms and Earthquakes of the World* (Lee, W. K. H., Meyers, H. and Shimazaki, K. eds), pp. 309–310. Academic Press, San Diego.
- Ambraseys N. N. and Barazangi M. (1989) The 1759 earthquake in the Bekaa valley: Implications for earthquake hazard assessment in the eastern Mediterranean region. *J. Geophys. Res.* **94**, 4007–4013.
- Ambraseys N. N. and Karcz I. (1992) The earthquake of 1546 in the Holy Land. *Terra Nova* **4**, 253–262.
- Ambraseys N. N. and Melville C. P. (1988) An analysis of the eastern Mediterranean earthquake of 20 May 1202. In: *Historical Seismograms and Earthquakes of the World* (Lee, W. K. H., Meyers, H. and Shimazaki, K. eds), pp. 181–200. Academic Press, San Diego.
- Amiran D. (1951) A revised earthquake catalogue of Palestine. *Isr. Explor. J.* **1**, 223–246.
- Amiran D. H. K., Arie E. and Turcotte T. (1994) Earthquakes in Israel and adjacent areas: Macroseismic observations since 100 B.C.E. *Israel Explor. Jour.* **44**, 260–305.
- Belitzky S. (1987) Tectonics of the Korazim Saddle. M.Sc. Thesis. Hebrew University, Jerusalem (in Hebrew, English abstract).
- Ben-Manahem A. (1991) Four thousand years of seismicity along the Dead Sea rift. *J. Geophys. Res.* **96**, 20,195–20,216.
- Brune J. N. (1968) Seismic moment, seismicity, and rate of slip along major fault zones. *J. Geophys. Res.* **73**, 777–784.
- Chaimov T. A. and Barazangi M. (1990) Crustal shortening in the Palmyride fold belt, Syria, and implications for movement along the Dead Sea fault system. *Tectonics* **9**, 1369–1386.
- Freund R., Zak I. and Garfunkel Z. (1968) Age and rate of the sinistral movement along the Dead Sea Rift. *Nature* **220**, 253–255.
- Garfunkel Z. (1981) Internal structure of the Dead Sea leaky transform (rift) in relation to plate kinematics. *Tectonophysics* **80**, 81–108.
- Goren-Inbar N. and Belitzky S. (1989) Structural position of the Pleistocene Gesher Benot Ya'akov site in the Dead Sea Rift zone. *Quaternary Research* **31**, 371–376.
- Harash A. and Bar Y. (1988) Faults, landslides and seismic hazards along the Jordan River Gorge, northern Israel. *Eng. Geol.* **25**, 1–15.
- Heimann A. and Ron H. (1987) Young faults in the Hula pull-apart basin, central Dead Sea transform. *Tectonophysics* **141**, 117–124.
- Heimann A. and Ron H. (1993) Geometric changes of plate boundaries along part of the northern Dead Sea Transform: Geochronologic and paleomagnetic evidence. *Tectonics* **12**, 477–491.
- IPRG (1983–1995) Seismological Bulletins. Earthquakes in and around Israel. Institute for Petroleum Research and Geophysics, Israel.
- Karcz I. and Kafri U. (1978) Evaluation of supposed archaeoseismic damage in Israel. *J. Archaeol. Sci.* **5**, 237–253.
- Kashai E. L. and Crocker P. F. (1987) Structural geometry and evolution of the Dead Sea–Jordan rift system as deduced from new subsurface data. *Tectonophysics* **141**, 33–60.

- Picard L. (1963) The Quaternary in the Northern Jordan Valley. *Proceedings, Israel Academy of Sciences and Humanities* **1**(4), 1–34.
- Picard L. Y. and Golani U. (1965) Israel Geological Map, 1:250,000 (northern sheet).
- Quennell A. M. (1956) Tectonics of the Dead Sea rift. *Congreso Geologico Internacional, 20th session, Asociacion de Servicios Geologicos Africanos, Mexico*, 385–405.
- Rotstein Y. and Bartov Y. (1989) Seismic reflection across a continental transform: an example from a convergent segment of the Dead Sea rift. *J. Geophys. Res.* **94**, 2902–2912.
- Salamon A. (1993) Seismotectonic analysis of earthquakes in Israel and adjacent areas. Ph.D. Thesis. Hebrew University, Jerusalem (in Hebrew with English abstract).
- Shapira A., Avni R. and Nur A. (1992) A new estimate for the epicenter of the Jericho earthquake of 11 July 1927. *Isr. J. Earth Sci.* **42**, 93–96.
- Shapira A. and Feldman L. (1987) Microseismicity of three locations along the Jordan rift. *Tectonophysics* **141**, 89–94.
- Shapira A. and Hofstetter A. (1993) Source parameters and scaling relationships of earthquakes in Israel. *Tectonophysics* **217**, 217–226.
- van Eck T. and Hofstetter A. (1990) Fault geometry and spatial clustering of microearthquakes along the Dead Sea-Jordan rift fault zone. *Tectonophysics* **180**, 15–27.
- Vered M. and Striem H. L. (1977) A macroseismic study and the implications of structural damage of two recent major earthquakes in the Jordan rift. *Bull. Seism. Soc. Am.* **67**, 1607–1613.
- Walley C. D. (1988) A braided strike-slip model for the northern continuation of the Dead Sea Fault and its implications for Levantine tectonics. *Tectonophysics* **145**, 63–72.
- Wells D. L. and Coppersmith K. J. (1994) New empirical relationships among magnitudes, rupture length, rupture width, rupture area, and surface displacement. *Bull. Seismol. Soc. Am.* **84**, 974–1002.

# Prehistoric earthquake deformations near Masada, Dead Sea graben

Shmuel Marco Institute of Earth Sciences, Hebrew University, Jerusalem 91904, Israel, and Geological Survey of Israel, 30 Malkhe Israel, Jerusalem 95501, Israel

Amotz Agnon Institute of Earth Sciences, Hebrew University, Jerusalem 91904, Israel

## ABSTRACT

Earthquake-induced fluidizations and suspensions of lake sediments, associated with syndepositional faults, form a paleoseismic record in the Dead Sea graben. The association of fluidized beds with surface faulting supports the recognition of mixed layers as reliable earthquake indicators and provides a tool for the study of very long term (>70 ka) seismicity along the Dead Sea transform. The faults compose a fault zone that offsets laminated sediments of the late Pleistocene Lake Lisan. They exhibit displacements of as much as 2 m. Layers of massive mixtures of laminated fragments are interpreted as disturbed beds, each formed by an earthquake. The undisturbed laminated layers between these mixed layers represent the interseismic interval. A typical vertical slip of about 0.5 m per event is separated by several hundred years of quiescence. The fault zone lies within the Dead Sea graben, 2 km east of Masada, where archaeology and historical accounts indicate repeated strong earthquake damage. The distribution of strikes in the fault zone resembles that of the faults exposed in and around the graben, including the seismogenic ones. The excellent exposures over hundreds of metres allow an unprecedented temporal and spatial resolution of slip events on faults.

## INTRODUCTION

Paleoseismic records in active regions are valuable in estimating past activity and associated seismic hazard. An ideal record consists of reliable, clear, and datable earthquake indicators that span a long time. We show that the laminated sediments of Lake

Lisan (paleo-Dead Sea) provide an excellent opportunity to study the paleoseismicity along the Dead Sea transform.

The Lisan Formation was deposited continuously along a 220-km-long tectonic depression that is part of the Dead Sea transform (Fig. 1). U-series ages range from 72 to

18 ka; the sedimentation rate has averaged 0.8–0.9 mm/yr (Kaufman et al., 1992; Marco et al., 1994). Most of the Lisan Formation in the study area is composed of alternating laminae of aragonite and detritus; the latter consists of fine-grained calcite, dolomite, quartz, and clay. Because of the absence of bioturbation in Lake Lisan, fine and clearly visible ~1-mm-thick laminae were preserved. The paired laminae resemble present deposits of the Dead Sea; they are interpreted as annual varves. Winter floods supplied detritus and carbonate, and evaporation during summer deposited aragonite (Begin et al., 1974; Katz et al., 1977). The Lisan deposits postdate the major landscaping of the current topography. In places, they are overlain by the Dead Sea highstand deposits that exhibit similar features. The retreat of the modern Dead Sea enables ongoing incision of canyons into the Lisan, creating vertical exposures of more than 40 m.

Post-Lisan faulting, historical earthquakes, and current seismic activity near the

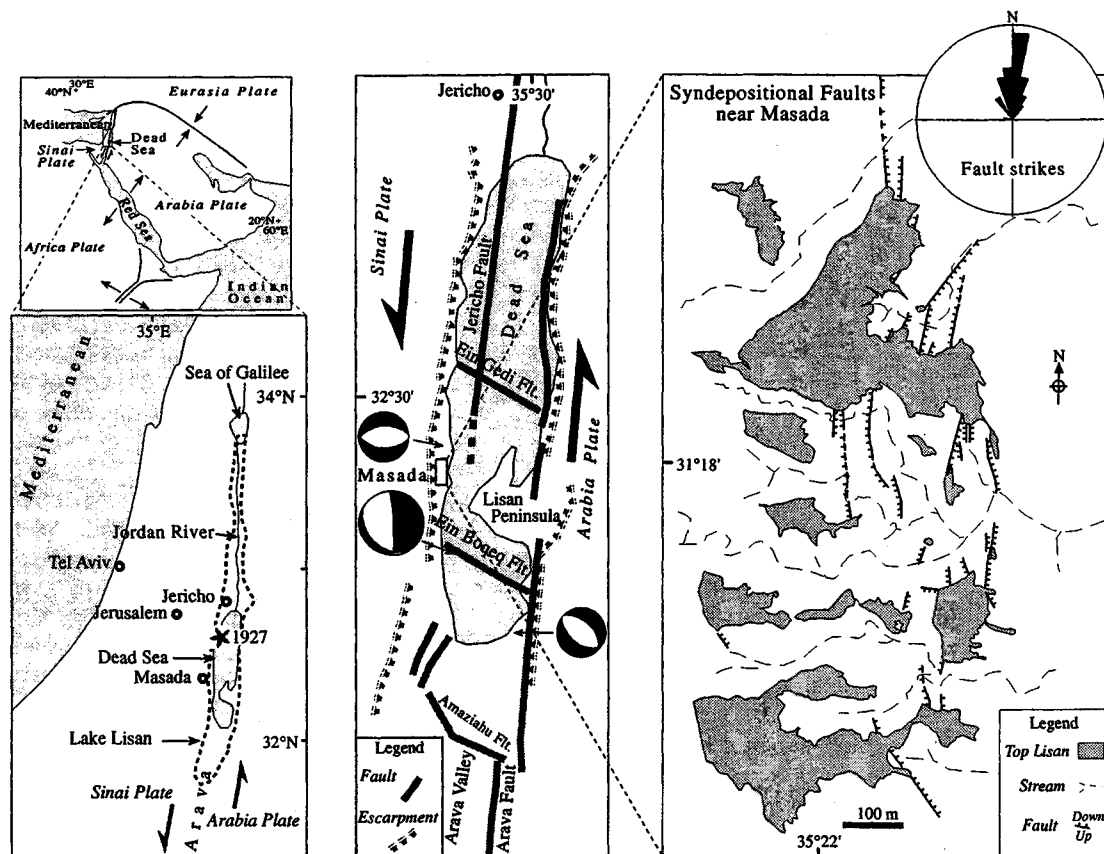
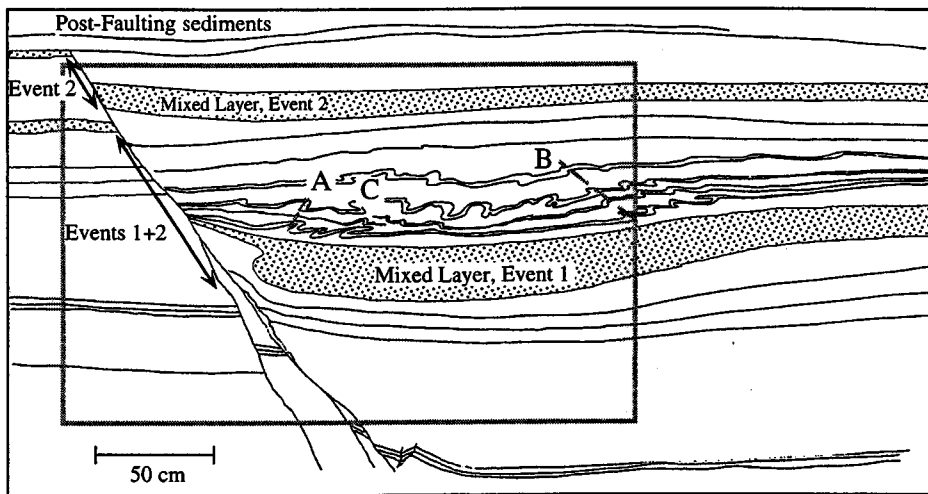


Figure 1. Right: Syndepositional fault zone near Masada. General north trend parallels Dead Sea transform in area and principal morphotectonic features to east and west of fault zone. Most fault planes similarly strike north, and a few strike northeast or southeast. Dips are 40°–70° eastward as well as westward. Rose diagram shows strike distribution weighted by fault length; largest petal is 28%. Upper left: Plate-tectonic setting of Middle East. Lower left: Extent of Lake Lisan. Star denotes epicenter of 1927 M 6.2 damaging earthquake (Shapira et al., 1993). Center: Active faults in Dead Sea region (Garfunkel et al., 1981; ten Brink and Ben-Avraham, 1989). In addition to left-lateral motion on north-striking faults, focal mechanisms of  $M_L$  2–4 earthquakes (van Eck and Hofstetter, 1990) show normal faulting on planes parallel to syndepositional faults near Masada.



**Figure 2.** Syndepositional normal fault in Lisan Formation near Masada unconformably overlain by undisturbed layers. Two mixed layers terminate at fault in each block, indicating repetitive seismic faulting on same plane. They are thicker in downthrown block, filling 10–30-cm-deep troughs. Lower mixed layer in downthrown block is also bent and overlain by folded layers. These folds show local downdip transport; dips of axial planes change from toward fault plane near fault (line A) to away from fault on far end of folded strata (line B). Box folds with two axial planes are common at bottom of trough (C). This folding formed because of local slumping of soft layers into trough. Lithologic markers indicate that mixed layers across fault correlate. They formed during two events when fault slipped abruptly and ruptured surface, creating subaqueous scarp. Because of this scarp, subsequent accumulation above mixed layers in downthrown block is thicker than in footwall. Photograph shows area outlined in drawing. Figure 4 gives interpreted sequence of events recorded in outcrop.

Dead Sea have been reported in previous studies (Garfunkel et al., 1981; Reches and Hoexter, 1981; Institute for Petroleum Research and Geophysics, 1983–1995; Ben-Menahem, 1991). We discovered a syndepositional fault zone in the Lisan outcrops, 2 km east of Masada, the Jewish rebel stronghold where strong earthquake damage occurred in the first century B.C. (Karcz et al., 1977); at Masada, disturbed floors, tilted walls, aligned fallen masonry, cracks, and collapsed walls are preserved. Later shocks have been reported in the Dead Sea

area after Masada was abandoned, e.g., in A.D. 362, 746, 1546, and 1834. Accounts of their effects in the Dead Sea include giant waves and appearance of large asphalt blocks that seep out through faults and fissures at the bottom of the lake (Ben-Menahem, 1991). The last damaging earthquake ( $M_L = 6.2$ ) struck the Dead Sea area in 1927 (Fig. 1), causing severe damage and hundreds of casualties in Jericho, Jerusalem, Bethlehem, and other settlements in the region. The identification of disrupted layers as deformations due to earthquakes pro-

vides the tool for expansion of the 4 kyr historical record. In the Masada area, these deformations are associated with repetitive surface ruptures, but the same deformed layers are found also away from observed faults throughout Lisan and post-Lisan outcrops by the Dead Sea. This widespread distribution of earthquake-caused deformations yields a  $\sim 70$  kar paleoseismic record.

### SYNDEPOSITIONAL FAULTS AND MIXED LAYERS

A north-trending fault zone was found near Masada. Most of the fault planes strike north, paralleling the main graben faults and morphological trends. The faults are overlain by undisturbed layers (Figs. 1, 2), indicating that they are syndepositional. Dips are  $40^\circ$  to  $70^\circ$  eastward as well as westward, with normal displacements as much as 2 m. Average strike is  $360^\circ$  (weighted by length;  $\alpha_{95} = 3.4^\circ$ ) with distribution pattern resembling the active graben faults (Fig. 1). Gouges, consisting of fine aragonite and detrital breccia, calcite, and some gypsum, are commonly limited to narrow zones (1–10 cm).

Layers that exhibit unusual thickness, structure, and fabric are associated with the faults. They are composed of massive mixtures of fine-grained matrix and tabular laminated fragments (Figs. 2, 3). Graded bedding is common where fragment-supported texture shows a gradual upward transition to a matrix-supported texture. Fragments are several millimetres to centimetres long. No imbrication, lateral grading, or other transport indicators were found. In many cases, the lower fragments can be restored to their original place in the underlying layers, indicating negligible transport. In contrast to the common  $\sim 1$ -mm-thick laminae of the Lisan, these layers, here referred to as “mixed layers,” are locally up to 1 m thick. The lower contact of many mixed layers is folded (Fig. 3). Each sequence of mixed layer and its folded lower contact is restricted to a single stratigraphic horizon enclosed between undeformed beds. Such sequences can be traced over large distances on the order of hundreds of metres, limited only by the continuity of the outcrop.

The layers are thicker in the downthrown block, partly filling the new relief. Additional thickness near the fault is due to the 20–40-cm-deep troughs that formed by bending of that block. Detailed sections across the faults show thicker accumulation of subsequent sediments above the mixed layers in the downthrown block (Fig. 2).

### DISCUSSION

The mixed layers terminate at faults that ruptured the lake bed, forming subaqueous fault scarps. Thicker accumulation above

the mixed layers in the downthrown block is considered as evidence for a fault scarp. We suggest that the mixed layers formed because of shaking of the top of the sediment simultaneously with slip on the faults. The graded deformation shows that the sediment responded to shaking according to its degree of consolidation with depth. The top of the sediment was fluidized and partly resuspended. Cohesive beds ruptured and brecciated (fluidization). Deeper beds deformed hydroplastically and folded (Lowe, 1975), accommodating local shear between underlying consolidated, undeformed beds, and water-saturated sediment (liquefaction). A mixed layer formed at the water-sediment interface on both sides of the subaqueous scarp together with the fault slip (Fig. 4). Some local mass transport near the

scarp produced thicker mixed layers in the lower block.

Slope failure that involves mass transport is considered an unlikely mechanism because (1) the mixed layers are related to faults, (2) they are flat lying, (3) the extremely friable laminated fragments are expected to be pulverized completely during turbulent transport, (4) the fragments at the bottom can be restored to their original place, and (5) imbrication and lateral grading are absent. Dipping beds are found in the vicinity of faults, and in those places, slope failure shows a distinct behavior: these layers are folded strata that fill the troughs in the downthrown blocks near the faults, show downdip transport, and change thickness within only a few metres of the faults. These folded strata are interpreted as local

slumps on the order of up to several metres, controlled by bottom topography (Fig. 2). Folded Lisan layers have been interpreted as "seismites" (Seilacher, 1984; El-Isa and Mustafa, 1986) although no association with faults was reported. Our observations indicate that such folds are areally limited by local topography. Their formation may have been triggered by earthquakes, but the limited distribution and lack of robustness of these features restrict their use as paleoseismic indicators. Such earthquakes could be significantly weaker than those that triggered the formation of the widespread mixed layers.

Deformed layers of soft sediment akin to the mixed layers are described around the world and attributed to earthquakes (e.g., Davenport and Ringrose, 1987; Doig, 1991; Vittori et al., 1991; Guiraud and Plaziat, 1993, and references therein). The association of such layer deformations with strong earthquakes is also backed by observations of recent events (Sims, 1975; C. R. Allen, 1986). Resuspension of sediments was directly observed in bottoms of lakes less than 10 km from the epicenter of the 1935 Timiskaming, Canada, M 6.3 earthquake. Independently, piston cores recovered a 20-cm-thick chaotic layer, composed of tabular fragments of a previously formed silt layer (Doig, 1991). What makes the mixed layers in the Masada area special is their juxtaposition with surface ruptures (Fig. 2).

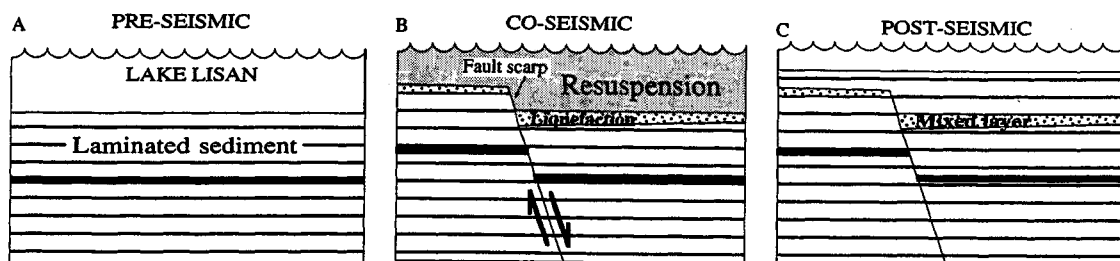
The direct association of the mixed layers with syndepositional fault scarps, their distribution over large areas, and their texture lead us to conclude that each mixed layer formed during an individual earthquake. Its timing is constrained by the first overlying undisturbed lamina (Fig. 4).

Cyclic liquefaction of loose, water-saturated, clastic sediments is commonly attributed to seismic waves that subject the sediment to repeated shaking. Direct observations and experiments indicate that cyclic liquefaction related to earthquakes occurs mainly during those of magnitude 6 and more (Allen, 1982). Liquefaction of sand



Figure 3. Typical mixed layer overlying laminated layers shows gradual upward transition from folded strata, through fragment-supported texture, to matrix-supported texture at top. Underlying folds are asymmetrical and recumbent, and in places they have box shapes. Undisturbed, postseismic layers overlie mixed layer. Such mixed layers abut syndepositional faults (Fig. 2) and are interpreted as earthquake deformations. Each formed at sediment-water interface when top of sediment was fluidized and partly resuspended during an earthquake. Coin is 22 mm diameter.

Figure 4. Interpretation of observed fault-mixed layer association shown in Figure 2. A: Laminated sediments are deposited at bottom of Lake Lisan. B: Fault offsets surface, creating subaqueous scarp. Top of sediment is deformed, liquefied, and resuspended during co-seismic movements. Mixed layer forms on both sides of fault scarp when suspended sediments resettle. Mixed layer in downthrown block is slightly thicker. C: Sedimentation continues; thicker sequence accumulates on downthrown block.



may occur at a magnitude as low as 5 (Audemard and de Santis, 1991) or 4.6 (Sims and Garvin, 1995), but a quantitative analysis (J. R. L. Allen, 1986) based on observations (Kuribayashi and Tatsuoka, 1975; Youd, 1977) indicates that sand liquefaction is more characteristic of greater magnitudes. The clay content in the Lisan (20%–35%) and the grain sizes of a few micrometres (Begin et al., 1974; Arkin and Michaeli, 1986) make it less prone than sand to liquefaction (Allen, 1982). Surface faults are rarely reported from earthquakes of less than magnitude 5.5 (Bonilla et al., 1984; Wells and Coppersmith, 1994), and their existence in the Masada area also indicates the magnitude. The data are insufficient to show whether the faults are throughgoing, the uppermost part of a "flower-structure," or the surface manifestations of lateral spreading due to deeper seismogenic slip events. However, the repetitive faulting and its congruence with active faulting in the Dead Sea area (Fig. 1) support a tectonic origin.

The studied faults do not displace the top of the Lisan Formation. The uppermost ~5 m of the Lisan Formation were deposited after faulting migrated, and the current active fault lies ~3 km east of the Dead Sea shore (Garfunkel et al., 1981). Seismic profiles in the Dead Sea reveal thinning of recent sediments toward fault segments (Ben-Avraham et al., 1993), showing a similar pattern of active syndepositional fault scarps.

The faults near Masada provide high spatial and temporal resolution of a faulting stage, showing repetitive slip events on the order of several tens of centimetres on the same planes within periods on the order of  $10^3$ – $10^4$  yr. The events are typically separated by several hundred years of quiescence.

Mixed layers are found throughout the Lisan Formation and subsequent Dead Sea sediments away from observed faults (Marco et al.). We postulate that they formed by similar seismogenic shaking, and the population of mixed layers in each locality represents the group of strongest events ( $M \geq 5.5$ ) within the time of the Lisan and the Dead Sea. Hence, these lake sediments contain the longest paleoseismic record along the Dead Sea transform (>70 kyr), and possibly the longest in the world.

#### ACKNOWLEDGMENTS

Partly supported by U.S.–Israel Binational Science Foundation grant 92-344/2 (Agnon). We thank Mordechai Stein for constructive discussions and comments, partnership in field work, and review of the manuscript; Hagai Ron, Zvi Garfunkel, Ze'ev Reches, Amos Nur, Daniel Wachs, and Kenneth Hsü for fruitful discussions; Annu Kyöstylä, Meir Abelson, and Revital Kentor for their assistance in field work; and John Sims, Yehoshua Kolodny, Amos Salomon, Hadas

Baruch, and an anonymous referee for helpful reviews.

#### REFERENCES CITED

- Allen, C. R., 1986, Seismological and paleoseismological techniques of research in active tectonics, in Wallace, R. E., ed., *Active tectonics*: Washington, D.C., National Academy Press, p. 148–154.
- Allen, J. R. L., 1982, Sedimentary structures: Their character and physical basis: Amsterdam, Elsevier, 663 p.
- Allen, J. R. L., 1986, Earthquake magnitude-frequency, epicentral distance, and soft-sediment deformation in sedimentary basins: *Sedimentary Geology*, v. 46, p. 67–75.
- Arkin, Y., and Michaeli, L., 1986, The significance of shear strength in the deformation of laminated sediments in the Dead Sea area: *Israel Journal of Earth Sciences*, v. 35, p. 61–72.
- Audemard, F. A., and de Santis, F., 1991, Survey of liquefaction structures induced by recent moderate earthquakes: *Association of Engineering Geologists Bulletin International*, v. 44, p. 5–16.
- Begin, Z. B., Ehrlich, A., and Nathan, Y., 1974, Lake Lisan, the Pleistocene precursor of the Dead Sea: *Israel Geological Survey Bulletin*, v. 63, p. 30.
- Ben-Avraham, Z., Neimi, T. M., Neev, D., Hall, J. K., and Levy, Y., 1993, Distribution of Holocene sediments and neotectonics in the deep north basin of the Dead Sea: *Marine Geology*, v. 113, p. 219–231.
- Ben-Menahem, A., 1991, Four thousand years of seismicity along the Dead Sea rift: *Journal of Geophysical Research*, v. 96, p. 20,195–20,216.
- Bonilla, M. G., Mark, R. K., and Lienkaemper, J. J., 1984, Statistical relations among earthquake magnitude, surface rupture length, and surface fault displacement: *Seismological Society of America Bulletin*, v. 74, p. 2379–2411.
- Davenport, C. A., and Ringrose, P. S., 1987, Deformation of Scottish Quaternary sediment sequence by strong earthquake motions, in Jones, M. E., and Preston, R. M., eds., *Deformation of sediments and sedimentary Rocks*: Geological Society of London Special Publication 29, p. 299–314.
- Doig, R., 1991, Effects of strong seismic shaking in lake sediments, and earthquake recurrence interval, Témiscaming, Quebec: *Canadian Journal of Earth Sciences*, v. 28, p. 1349–1352.
- El-Isa, Z. H., and Mustafa, H., 1986, Earthquake deformations in the Lisan deposits and seismotectonic implications: *Royal Astronomical Society Geophysical Journal*, v. 86, p. 413–424.
- Garfunkel, Z., Zak, I., and Freund, R., 1981, Active faulting along the Dead Sea transform (rift): *Tectonophysics*, v. 80, p. 1–26.
- Guiraud, M., and Plaziat, J. C., 1993, Seismites in the fluvial Bima sandstone: Identification of paleoseisms and discussion of their magnitudes in a Cretaceous synsedimentary strike-slip basin (Upper Benue, Nigeria): *Tectonophysics*, v. 225, p. 493–522.
- Institute for Petroleum Research and Geophysics, 1983–1995, Earthquakes in and around Israel: Hulon, Israel, IRPG Seismological Bulletins.
- Karcz, I., Kafri, U., and Meshel, Z., 1977, Archaeological evidence for Subrecent seismic activity along the Dead Sea–Jordan Rift: *Nature*, v. 269, p. 234–235.
- Katz, A., Kolodny, Y., and Nissenbaum, A., 1977, The geochemical evolution of the Pleistocene Lake Lisan–Dead Sea system: *Geochimica et Cosmochimica Acta*, v. 41, p. 1609–1626.
- Kaufman, A., Yechieli, Y., and Gardosh, M., 1992, Reevaluation of the lake-sediment chronology in the Dead Sea basin, Israel, based on new  $^{230}\text{Th}/^{234}\text{U}$  dates: *Quaternary Research*, v. 38, p. 292–304.
- Kuribayashi, E., and Tatsuoka, F., 1975, Brief review of liquefaction during earthquakes in Japan: *Soils and Foundations*, v. 15, p. 81–92.
- Lowe, D. R., 1975, Water escape structures in coarse-grained sediments: *Sedimentology*, v. 23, p. 285–308.
- Marco, S., Agnon, A., Stein, M., and Ron, H., 1994, A 50,000 year continuous record of earthquakes and surface ruptures in the Lisan Formation, the Dead Sea graben: U.S. Geological Survey Open-File Report 94-568, p. 112–114.
- Marco, S., Stein, M., Agnon, A. and Ron, H., 1995, Long term earthquake clustering: 50,000 year paleoseismic record in the Dead Sea Graben: *Israel Geological Society Annual Meeting, Abstracts*, p. 72.
- Reches, Z., and Hoexter, D. F., 1981, Holocene seismic and tectonic activity in the Dead Sea area: *Tectonophysics*, v. 80, p. 235–254.
- Seilacher, A., 1984, Sedimentary structures tentatively attributed to seismic events: *Marine Geology*, v. 55, p. 1–12.
- Shapira, A., Avni, R., and Nur, A., 1993, A new estimate for the epicenter of the Jericho earthquake of 11 July 1927: *Israel Journal of Earth Science*, v. 42, p. 93–96.
- Sims, J. D., 1975, Determining earthquake recurrence intervals from deformational structures in young lacustrine sediments: *Tectonophysics*, v. 29, p. 144–152.
- Sims, J. D., and Garvin, C. D., 1995, Recurrent liquefaction induced by the 1989 Loma Prieta earthquake and 1990 and 1991 aftershocks: Implications for paleoseismicity studies: *Seismological Society of America Bulletin*, v. 85, p. 51–65.
- ten Brink, U. S., and Ben-Avraham, Z., 1989, The anatomy of a pull-apart basin: Reflection observations of the Dead Sea basin: *Tectonics*, v. 8, p. 333–350.
- van Eck, T., and Hofstetter, A., 1990, Fault geometry and spatial clustering of microearthquakes along the Dead Sea–Jordan rift fault zone: *Tectonophysics*, v. 180, p. 15–27.
- Vittori, E., Labini, S. S., and Serva, L., 1991, Palaeoseismology: Review of the state-of-the-art: *Tectonophysics*, v. 193, p. 9–32.
- Wells, D. L., and Coppersmith, K. J., 1994, New empirical relationships among magnitudes, rupture length, rupture width, rupture area, and surface displacement: *Seismological Society of America Bulletin*, v. 84, p. 974–1002.
- Youd, T. L., 1977, Discussion of "Brief review of liquefaction during earthquakes in Japan" by E. Kuribayashi and T. Tatsuoka: *Soils and Foundations*, v. 17, p. 82–85.

Manuscript received December 8, 1994

Revised manuscript received March 30, 1995

Manuscript accepted April 24, 1995

# Prehistoric earthquake deformations near Masada, Dead Sea graben

Shmuel Marco Institute of Earth Sciences, Hebrew University, Jerusalem 91904, Israel, and Geological Survey of Israel, 30 Malkhe Israel, Jerusalem 95501, Israel

Amotz Agnon Institute of Earth Sciences, Hebrew University, Jerusalem 91904, Israel

## ABSTRACT

Earthquake-induced fluidizations and suspensions of lake sediments, associated with syndepositional faults, form a paleoseismic record in the Dead Sea graben. The association of fluidized beds with surface faulting supports the recognition of mixed layers as reliable earthquake indicators and provides a tool for the study of very long term (>70 ka) seismicity along the Dead Sea transform. The faults compose a fault zone that offsets laminated sediments of the late Pleistocene Lake Lisan. They exhibit displacements of as much as 2 m. Layers of massive mixtures of laminated fragments are interpreted as disturbed beds, each formed by an earthquake. The undisturbed laminated layers between these mixed layers represent the interseismic interval. A typical vertical slip of about 0.5 m per event is separated by several hundred years of quiescence. The fault zone lies within the Dead Sea graben, 2 km east of Masada, where archaeology and historical accounts indicate repeated strong earthquake damage. The distribution of strikes in the fault zone resembles that of the faults exposed in and around the graben, including the seismogenic ones. The excellent exposures over hundreds of metres allow an unprecedented temporal and spatial resolution of slip events on faults.

## INTRODUCTION

Paleoseismic records in active regions are valuable in estimating past activity and associated seismic hazard. An ideal record consists of reliable, clear, and datable earthquake indicators that span a long time. We show that the laminated sediments of Lake

Lisan (paleo-Dead Sea) provide an excellent opportunity to study the paleoseismicity along the Dead Sea transform.

The Lisan Formation was deposited continuously along a 220-km-long tectonic depression that is part of the Dead Sea transform (Fig. 1). U-series ages range from 72 to

18 ka; the sedimentation rate has averaged 0.8–0.9 mm/yr (Kaufman et al., 1992; Marco et al., 1994). Most of the Lisan Formation in the study area is composed of alternating laminae of aragonite and detritus; the latter consists of fine-grained calcite, dolomite, quartz, and clay. Because of the absence of bioturbation in Lake Lisan, fine and clearly visible ~1-mm-thick laminae were preserved. The paired laminae resemble present deposits of the Dead Sea; they are interpreted as annual varves. Winter floods supplied detritus and carbonate, and evaporation during summer deposited aragonite (Begin et al., 1974; Katz et al., 1977). The Lisan deposits postdate the major landscaping of the current topography. In places, they are overlain by the Dead Sea highstand deposits that exhibit similar features. The retreat of the modern Dead Sea enables ongoing incision of canyons into the Lisan, creating vertical exposures of more than 40 m.

Post-Lisan faulting, historical earthquakes, and current seismic activity near the

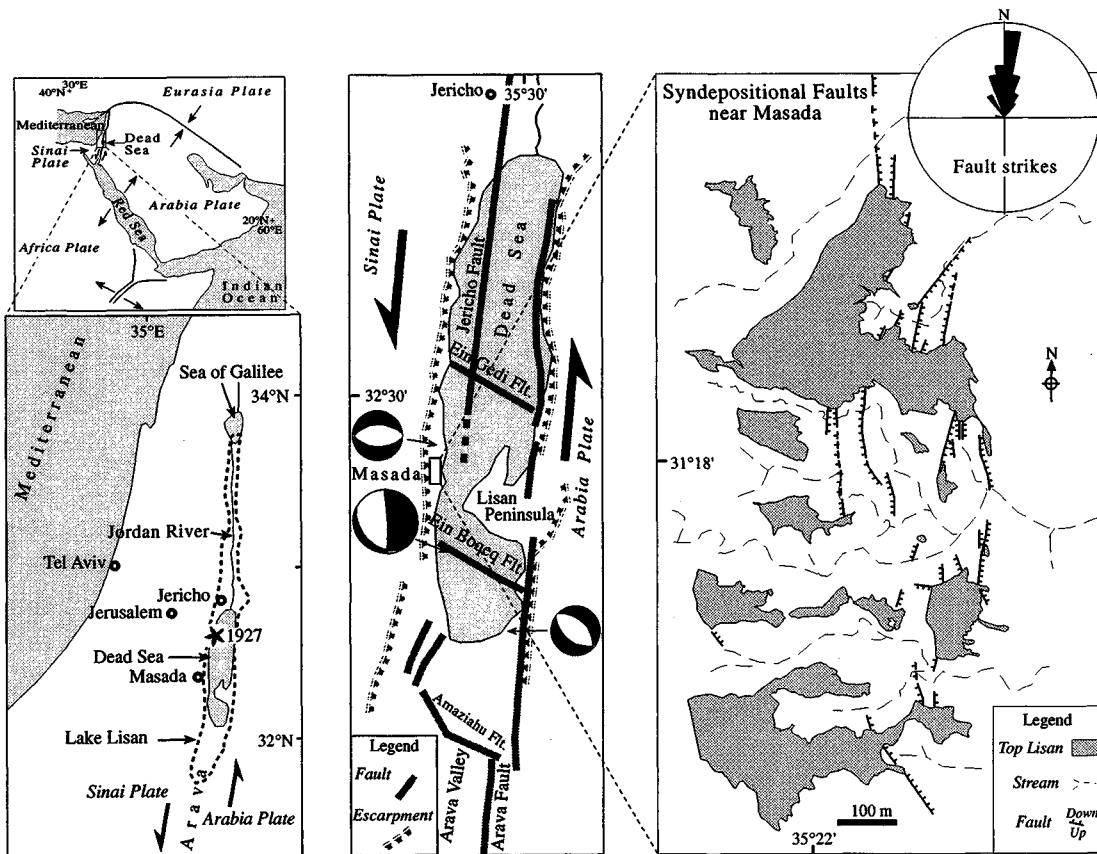
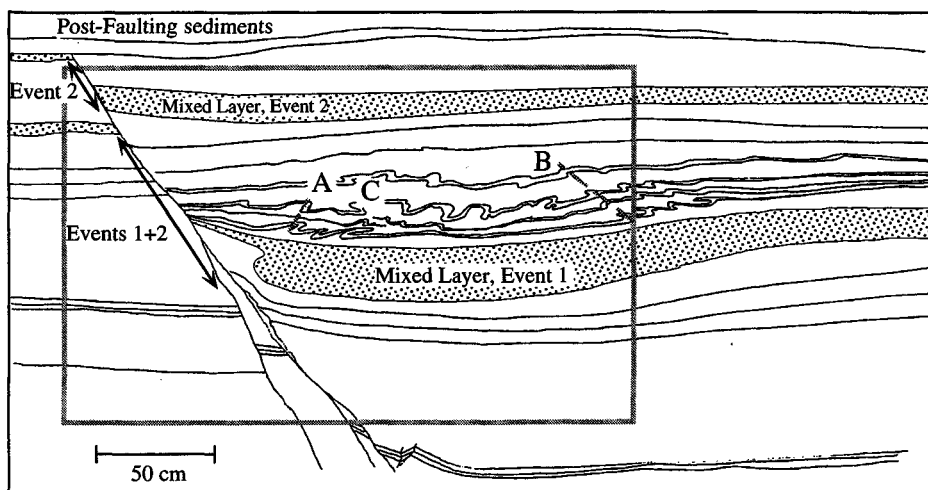


Figure 1. Right: Syndepositional fault zone near Masada. General north trend parallels Dead Sea transform in area and principal morphotectonic features to east and west of fault zone. Most fault planes similarly strike north, and a few strike northeast or southeast. Dips are 40°–70° eastward as well as westward. Rose diagram shows strike distribution weighted by fault length; largest petal is 28%. Upper left: Plate-tectonic setting of Middle East. Lower left: Extent of Lake Lisan. Star denotes epicenter of 1927 M 6.2 damaging earthquake (Shapira et al., 1993). Center: Active faults in Dead Sea region (Garfunkel et al., 1981; ten Brink and Ben-Avraham, 1989). In addition to left-lateral motion on north-striking faults, focal mechanisms of M<sub>L</sub> 2–4 earthquakes (van Eck and Hofstetter, 1990) show normal faulting on planes parallel to syndepositional faults near Masada.



**Figure 2.** Syndepositional normal fault in Lisan Formation near Masada unconformably overlain by undisturbed layers. Two mixed layers terminate at fault in each block, indicating repetitive seismic faulting on same plane. They are thicker in downthrown block, filling 10–30-cm-deep troughs. Lower mixed layer in downthrown block is also bent and overlain by folded layers. These folds show local downdip transport; dips of axial planes change from toward fault plane near fault (line A) to away from fault on far end of folded strata (line B). Box folds with two axial planes are common at bottom of trough (C). This folding formed because of local slumping of soft layers into trough. Lithologic markers indicate that mixed layers across fault correlate. They formed during two events when fault slipped abruptly and ruptured surface, creating subaqueous scarp. Because of this scarp, subsequent accumulation above mixed layers in downthrown block is thicker than in footwall. Photograph shows area outlined in drawing. Figure 4 gives interpreted sequence of events recorded in outcrop.

Dead Sea have been reported in previous studies (Garfunkel et al., 1981; Reches and Hoexter, 1981; Institute for Petroleum Research and Geophysics, 1983–1995; Ben-Menahem, 1991). We discovered a syndepositional fault zone in the Lisan outcrops, 2 km east of Masada, the Jewish rebel stronghold where strong earthquake damage occurred in the first century B.C. (Karcz et al., 1977); at Masada, disturbed floors, tilted walls, aligned fallen masonry, cracks, and collapsed walls are preserved. Later shocks have been reported in the Dead Sea

area after Masada was abandoned, e.g., in A.D. 362, 746, 1546, and 1834. Accounts of their effects in the Dead Sea include giant waves and appearance of large asphalt blocks that seep out through faults and fissures at the bottom of the lake (Ben-Menahem, 1991). The last damaging earthquake ( $M_L = 6.2$ ) struck the Dead Sea area in 1927 (Fig. 1), causing severe damage and hundreds of casualties in Jericho, Jerusalem, Bethlehem, and other settlements in the region. The identification of disrupted layers as deformations due to earthquakes pro-

vides the tool for expansion of the 4 kyr historical record. In the Masada area, these deformations are associated with repetitive surface ruptures, but the same deformed layers are found also away from observed faults throughout Lisan and post-Lisan outcrops by the Dead Sea. This widespread distribution of earthquake-caused deformations yields a ~70 kyr paleoseismic record.

#### SYNDEPOSITIONAL FAULTS AND MIXED LAYERS

A north-trending fault zone was found near Masada. Most of the fault planes strike north, paralleling the main graben faults and morphological trends. The faults are overlain by undisturbed layers (Figs. 1, 2), indicating that they are syndepositional. Dips are  $40^\circ$  to  $70^\circ$  eastward as well as westward, with normal displacements as much as 2 m. Average strike is  $360^\circ$  (weighted by length;  $\alpha_{95} = 3.4^\circ$ ) with distribution pattern resembling the active graben faults (Fig. 1). Gouges, consisting of fine aragonite and detrital breccia, calcite, and some gypsum, are commonly limited to narrow zones (1–10 cm).

Layers that exhibit unusual thickness, structure, and fabric are associated with the faults. They are composed of massive mixtures of fine-grained matrix and tabular laminated fragments (Figs. 2, 3). Graded bedding is common where fragment-supported texture shows a gradual upward transition to a matrix-supported texture. Fragments are several millimetres to centimetres long. No imbrication, lateral grading, or other transport indicators were found. In many cases, the lower fragments can be restored to their original place in the underlying layers, indicating negligible transport. In contrast to the common ~1-mm-thick laminae of the Lisan, these layers, here referred to as “mixed layers,” are locally up to 1 m thick. The lower contact of many mixed layers is folded (Fig. 3). Each sequence of mixed layer and its folded lower contact is restricted to a single stratigraphic horizon enclosed between undeformed beds. Such sequences can be traced over large distances on the order of hundreds of metres, limited only by the continuity of the outcrop.

The layers are thicker in the downthrown block, partly filling the new relief. Additional thickness near the fault is due to the 20–40-cm-deep troughs that formed by bending of that block. Detailed sections across the faults show thicker accumulation of subsequent sediments above the mixed layers in the downthrown block (Fig. 2).

#### DISCUSSION

The mixed layers terminate at faults that ruptured the lake bed, forming subaqueous fault scarps. Thicker accumulation above

the mixed layers in the downthrown block is considered as evidence for a fault scarp. We suggest that the mixed layers formed because of shaking of the top of the sediment simultaneously with slip on the faults. The graded deformation shows that the sediment responded to shaking according to its degree of consolidation with depth. The top of the sediment was fluidized and partly resuspended. Cohesive beds ruptured and brecciated (fluidization). Deeper beds deformed hydroplastically and folded (Lowe, 1975), accommodating local shear between underlying consolidated, undeformed beds, and water-saturated sediment (liquefaction). A mixed layer formed at the water-sediment interface on both sides of the subaqueous scarp together with the fault slip (Fig. 4). Some local mass transport near the

scarp produced thicker mixed layers in the lower block.

Slope failure that involves mass transport is considered an unlikely mechanism because (1) the mixed layers are related to faults, (2) they are flat lying, (3) the extremely friable laminated fragments are expected to be pulverized completely during turbulent transport, (4) the fragments at the bottom can be restored to their original place, and (5) imbrication and lateral grading are absent. Dipping beds are found in the vicinity of faults, and in those places, slope failure shows a distinct behavior: these layers are folded strata that fill the troughs in the downthrown blocks near the faults, show downdip transport, and change thickness within only a few metres of the faults. These folded strata are interpreted as local

slumps on the order of up to several metres, controlled by bottom topography (Fig. 2). Folded Lisan layers have been interpreted as "seismites" (Seilacher, 1984; El-Isa and Mustafa, 1986) although no association with faults was reported. Our observations indicate that such folds are areally limited by local topography. Their formation may have been triggered by earthquakes, but the limited distribution and lack of robustness of these features restrict their use as paleoseismic indicators. Such earthquakes could be significantly weaker than those that triggered the formation of the widespread mixed layers.

Deformed layers of soft sediment akin to the mixed layers are described around the world and attributed to earthquakes (e.g., Davenport and Ringrose, 1987; Doig, 1991; Vittori et al., 1991; Guiraud and Plaziat, 1993, and references therein). The association of such layer deformations with strong earthquakes is also backed by observations of recent events (Sims, 1975; C. R. Allen, 1986). Resuspension of sediments was directly observed in bottoms of lakes less than 10 km from the epicenter of the 1935 Timiskaming, Canada, M 6.3 earthquake. Independently, piston cores recovered a 20-cm-thick chaotic layer, composed of tabular fragments of a previously formed silt layer (Doig, 1991). What makes the mixed layers in the Masada area special is their juxtaposition with surface ruptures (Fig. 4).

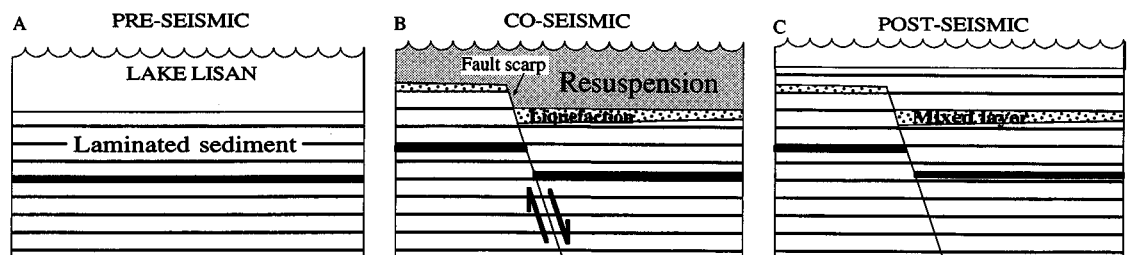
The direct association of the mixed layers with syndepositional fault scarps, their distribution over large areas, and their texture lead us to conclude that each mixed layer formed during an individual earthquake. Its timing is constrained by the first overlying undisturbed lamina (Fig. 4).

Cyclic liquefaction of loose, water-saturated, clastic sediments is commonly attributed to seismic waves that subject the sediment to repeated shaking. Direct observations and experiments indicate that cyclic liquefaction related to earthquakes occurs mainly during those of magnitude 6 and more (Allen, 1982). Liquefaction of sand



**Figure 3.** Typical mixed layer overlying laminated layers shows gradual upward transition from folded strata, through fragment-supported texture, to matrix-supported texture at top. Underlying folds are asymmetrical and recumbent, and in places they have box shapes. Undisturbed, postseismic layers overlie mixed layer. Such mixed layers abut syndepositional faults (Fig. 2) and are interpreted as earthquake deformations. Each formed at sediment-water interface when top of sediment was fluidized and partly resuspended during an earthquake. Coin is 22 mm diameter.

**Figure 4.** Interpretation of observed fault-mixed layer association shown in Figure 2. A: Laminated sediments are deposited at bottom of Lake Lisan. B: Fault offsets surface, creating subaqueous scarp. Top of sediment is deformed, liquefied, and resuspended during co-seismic movements. Mixed layer forms on both sides of fault scarp when suspended sediments resettle. Mixed layer in downthrown block is slightly thicker. C: Sedimentation continues; thicker sequence accumulates on downthrown block.



may occur at a magnitude as low as 5 (Audemard and de Santis, 1991) or 4.6 (Sims and Garvin, 1995), but a quantitative analysis (J. R. L. Allen, 1986) based on observations (Kuribayashi and Tatsuoka, 1975; Youd, 1977) indicates that sand liquefaction is more characteristic of greater magnitudes. The clay content in the Lisan (20%–35%) and the grain sizes of a few micrometres (Begin et al., 1974; Arkin and Michaeli, 1986) make it less prone than sand to liquefaction (Allen, 1982). Surface faults are rarely reported from earthquakes of less than magnitude 5.5 (Bonilla et al., 1984; Wells and Coppersmith, 1994), and their existence in the Masada area also indicates the magnitude. The data are insufficient to show whether the faults are throughgoing, the uppermost part of a “flower-structure,” or the surface manifestations of lateral spreading due to deeper seismogenic slip events. However, the repetitive faulting and its congruence with active faulting in the Dead Sea area (Fig. 1) support a tectonic origin.

The studied faults do not displace the top of the Lisan Formation. The uppermost ~5 m of the Lisan Formation were deposited after faulting migrated, and the current active fault lies ~3 km east of the Dead Sea shore (Garfunkel et al., 1981). Seismic profiles in the Dead Sea reveal thinning of recent sediments toward fault segments (Ben-Avraham et al., 1993), showing a similar pattern of active syndepositional fault scarps.

The faults near Masada provide high spatial and temporal resolution of a faulting stage, showing repetitive slip events on the order of several tens of centimetres on the same planes within periods on the order of  $10^3$ – $10^4$  yr. The events are typically separated by several hundred years of quiescence.

Mixed layers are found throughout the Lisan Formation and subsequent Dead Sea sediments away from observed faults (Marco et al.). We postulate that they formed by similar seismogenic shaking, and the population of mixed layers in each locality represents the group of strongest events ( $M \geq 5.5$ ) within the time of the Lisan and the Dead Sea. Hence, these lake sediments contain the longest paleoseismic record along the Dead Sea transform (>70 kyr), and possibly the longest in the world.

#### ACKNOWLEDGMENTS

Partly supported by U.S.-Israel Binational Science Foundation grant 92-344/2 (Agnon). We thank Mordechai Stein for constructive discussions and comments, partnership in field work, and review of the manuscript; Hagai Ron, Zvi Garfunkel, Ze'ev Reches, Amos Nur, Daniel Wachs, and Kenneth Hsü for fruitful discussions; Annu Kyöstylä, Meir Abelson, and Revital Kentor for their assistance in field work; and John Sims, Yehoshua Kolodny, Amos Salamon, Hadas

Baruch, and an anonymous referee for helpful reviews.

#### REFERENCES CITED

- Allen, C. R., 1986, Seismological and paleoseismological techniques of research in active tectonics, in Wallace, R. E., ed., *Active tectonics*: Washington, D.C., National Academy Press, p. 148–154.
- Allen, J. R. L., 1982, Sedimentary structures: Their character and physical basis: Amsterdam, Elsevier, 663 p.
- Allen, J. R. L., 1986, Earthquake magnitude-frequency, epicentral distance, and soft-sediment deformation in sedimentary basins: *Sedimentary Geology*, v. 46, p. 67–75.
- Arkin, Y., and Michaeli, L., 1986, The significance of shear strength in the deformation of laminated sediments in the Dead Sea area: *Israel Journal of Earth Sciences*, v. 35, p. 61–72.
- Audemard, F. A., and de Santis, F., 1991, Survey of liquefaction structures induced by recent moderate earthquakes: *Association of Engineering Geologists Bulletin International*, v. 44, p. 5–16.
- Begin, Z. B., Ehrlich, A., and Nathan, Y., 1974, Lake Lisan, the Pleistocene precursor of the Dead Sea: *Israel Geological Survey Bulletin*, v. 63, p. 30.
- Ben-Avraham, Z., Neimi, T. M., Neev, D., Hall, J. K., and Levy, Y., 1993, Distribution of Holocene sediments and neotectonics in the deep north basin of the Dead Sea: *Marine Geology*, v. 113, p. 219–231.
- Ben-Menahem, A., 1991, Four thousand years of seismicity along the Dead Sea rift: *Journal of Geophysical Research*, v. 96, p. 20,195–20,216.
- Bonilla, M. G., Mark, R. K., and Lienkaemper, J. J., 1984, Statistical relations among earthquake magnitude, surface rupture length, and surface fault displacement: *Seismological Society of America Bulletin*, v. 74, p. 2379–2411.
- Davenport, C. A., and Ringrose, P. S., 1987, Deformation of Scottish Quaternary sediment sequence by strong earthquake motions, in Jones, M. E., and Preston, R. M., eds., *Deformation of sediments and sedimentary Rocks*: Geological Society of London Special Publication 29, p. 299–314.
- Doig, R., 1991, Effects of strong seismic shaking in lake sediments, and earthquake recurrence interval, Témiscaming, Quebec: *Canadian Journal of Earth Sciences*, v. 28, p. 1349–1352.
- El-Isa, Z. H., and Mustafa, H., 1986, Earthquake deformations in the Lisan deposits and seismotectonic implications: *Royal Astronomical Society Geophysical Journal*, v. 86, p. 413–424.
- Garfunkel, Z., Zak, I., and Freund, R., 1981, Active faulting along the Dead Sea transform (rift): *Tectonophysics*, v. 80, p. 1–26.
- Guiraud, M., and Plaziat, J. C., 1993, Seismites in the fluvial Bima sandstone: Identification of paleoseisms and discussion of their magnitudes in a Cretaceous syndepositional strike-slip basin (Upper Benue, Nigeria): *Tectonophysics*, v. 225, p. 493–522.
- Institute for Petroleum Research and Geophysics, 1983–1995, Earthquakes in and around Israel: Hulon, Israel, IRPG Seismological Bulletins.
- Karcz, I., Kafri, U., and Meshel, Z., 1977, Archaeological evidence for Subrecent seismic activity along the Dead Sea–Jordan Rift: *Nature*, v. 269, p. 234–235.
- Katz, A., Kolodny, Y., and Nissenbaum, A., 1977, The geochemical evolution of the Pleistocene Lake Lisan–Dead Sea system: *Geochimica et Cosmochimica Acta*, v. 41, p. 1609–1626.
- Kaufman, A., Yechieli, Y., and Gardosh, M., 1992, Reevaluation of the lake-sediment chronology in the Dead Sea basin, Israel, based on new  $^{230}\text{Th}/^{234}\text{U}$  dates: *Quaternary Research*, v. 38, p. 292–304.
- Kuribayashi, E., and Tatsuoka, F., 1975, Brief review of liquefaction during earthquakes in Japan: *Soils and Foundations*, v. 15, p. 81–92.
- Lowe, D. R., 1975, Water escape structures in coarse-grained sediments: *Sedimentology*, v. 23, p. 285–308.
- Marco, S., Agnon, A., Stein, M., and Ron, H., 1994, A 50,000 year continuous record of earthquakes and surface ruptures in the Lisan Formation, the Dead Sea graben: U.S. Geological Survey Open-File Report 94-568, p. 112–114.
- Marco, S., Stein, M., Agnon, A. and Ron, H., 1995, Long term earthquake clustering: 50,000 year paleoseismic record in the Dead Sea Graben: *Israel Geological Society Annual Meeting, Abstracts*, p. 72.
- Reches, Z., and Hoexter, D. F., 1981, Holocene seismic and tectonic activity in the Dead Sea area: *Tectonophysics*, v. 80, p. 235–254.
- Seilacher, A., 1984, Sedimentary structures tentatively attributed to seismic events: *Marine Geology*, v. 55, p. 1–12.
- Shapira, A., Avni, R., and Nur, A., 1993, A new estimate for the epicenter of the Jericho earthquake of 11 July 1927: *Israel Journal of Earth Science*, v. 42, p. 93–96.
- Sims, J. D., 1975, Determining earthquake recurrence intervals from deformational structures in young lacustrine sediments: *Tectonophysics*, v. 29, p. 144–152.
- Sims, J. D., and Garvin, C. D., 1995, Recurrent liquefaction induced by the 1989 Loma Prieta earthquake and 1990 and 1991 aftershocks: Implications for paleoseismicity studies: *Seismological Society of America Bulletin*, v. 85, p. 51–65.
- ten Brink, U. S., and Ben-Avraham, Z., 1989, The anatomy of a pull-apart basin: Reflection observations of the Dead Sea basin: *Tectonics*, v. 8, p. 333–350.
- van Eck, T., and Hofstetter, A., 1990, Fault geometry and spatial clustering of microearthquakes along the Dead Sea–Jordan rift fault zone: *Tectonophysics*, v. 180, p. 15–27.
- Vittori, E., Labini, S. S., and Serva, L., 1991, Palaeoseismology: Review of the state-of-the-art: *Tectonophysics*, v. 193, p. 9–32.
- Wells, D. L., and Coppersmith, K. J., 1994, New empirical relationships among magnitudes, rupture length, rupture width, rupture area, and surface displacement: *Seismological Society of America Bulletin*, v. 84, p. 974–1002.
- Youd, T. L., 1977, Discussion of “Brief review of liquefaction during earthquakes in Japan” by E. Kuribayashi and T. Tatsuoka: *Soils and Foundations*, v. 17, p. 82–85.

Manuscript received December 8, 1994

Revised manuscript received March 30, 1995

Manuscript accepted April 24, 1995

## High-resolution geological record of historic earthquakes in the Dead Sea basin

Revital Ken-Tor, Amotz Agnon, Yehouda Enzel, and Mordechai Stein

Institute of Earth Sciences, The Hebrew University, Jerusalem

Shmuel Marco<sup>1</sup>

Geological Survey of Israel, Jerusalem, and Department of Geophysics, Tel Aviv University, Tel Aviv

Jorg F. W. Negendank

GeoForschungsZentrum Potsdam, Potsdam

**Abstract** A 2000 year paleoseismic record of the Dead Sea area was recovered from a lacustrine sedimentary section. The section is being exposed at the Ze'elim Terrace on the shores of the Dead Sea due to the fast retreat of the lake. The section consists of laminated detrital and chemical (mainly aragonite) sediments that were deposited in the Holocene paleo-Dead Sea. Eight layers in the section show deformed sedimentary structures and are identified as seismites. Their chronology was determined by radiocarbon dating on organic remains. The seismite ages are well correlated with the historically documented earthquakes of 64 and 31 B.C. and 33, 363, 1212, 1293, 1834 and 1927 A.D.. The few historically documented earthquakes that have no correlatives in the Ze'elim seismite record occurred in times of sedimentary hiatuses at this site (e.g., 749 A.D.). Based on modern analogues and the association of similar disturbed layers with syndepositional faults, the Ze'elim Terrace seismites indicate  $M > 5.5$  earthquakes. The average recurrence interval is estimated as ~100-300 years and represents slip events on different faults in the Dead Sea area. The Ze'elim section provides a unique opportunity to correlate two independent and extensive data sets, the historical and sedimentary records. This study opens the way for better understanding of spatial and temporal distribution of earthquakes along the Dead Sea Transform and elsewhere.

### 1. Introduction

Paleoseismic records provide essential data for seismic hazard assessment, imposing important constraints on the temporal and spatial distribution of strong and harmful earthquakes. Information on pre-instrumental paleoseismic events is derived from historical and geological records. The historical information is mainly based on eyewitness reports and their preservation, the objectivity of the reporters, and the accessibility of the reports to historians. The quality of the geological information depends on the availability of suitable sedimentary sequences and the possibility of obtaining absolute ages on the paleoseismic events.

The Dead Sea is located along one of the major strike-slip fault systems in the world, the Dead Sea Transform (DST), which has been active since the Neogene [Garfunkel, 1981; Garfunkel and Ben-Avraham, 1996] (Figure 1). The DST is part of the 6000 km long Syrian-African rift system, which was a main route of travel for prehistorical mankind on its migration out of Africa. and since then, the locus of various his-

torical communities. Thus, the DST and its surroundings contain numerous archeological remains that record human settlement since early prehistoric time, throughout the Bronze and Iron ages and the historical period. Some of the archeological sites were disturbed by earthquakes and, together with historical accounts of felt earthquakes, they provide a unique opportunity to monitor past seismic activity in the region [Ben-Menahem, 1991].

During the Pleistocene and Holocene, laminated evaporitic and detrital sediments were deposited at the bottom of a series of lakes that existed along the DST. The deposits contain suitable material for dating by U-series and radiocarbon [Schramm *et al.*, 2000]. The well-exposed sedimentary record in the region represents a potentially rich source of paleoseismic information that has not been fully exploited. An excellent example of this potential is given by the Lisan Formation, which consists of ~ 50 kyr laminated sedimentary sequence that contains deformed units representing individual, datable seismic events [Marco and Agnon, 1995; Marco *et al.*, 1996]. The present study focuses on the paleoseismic record of the last 2000 years in the Dead Sea basin. During this time the level of the Dead Sea has been low (at ~ 400 m below sea level) and subjected to small lake level fluctuations. Continuous retreat of the Dead Sea during the past 40 years (~ 80 cm yr<sup>-1</sup>) has exposed the Holocene sediments, allowing the study of their structure and composition. In this study, the late Holo-

<sup>1</sup> Also at Geological Survey of Israel, Jerusalem, Israel.

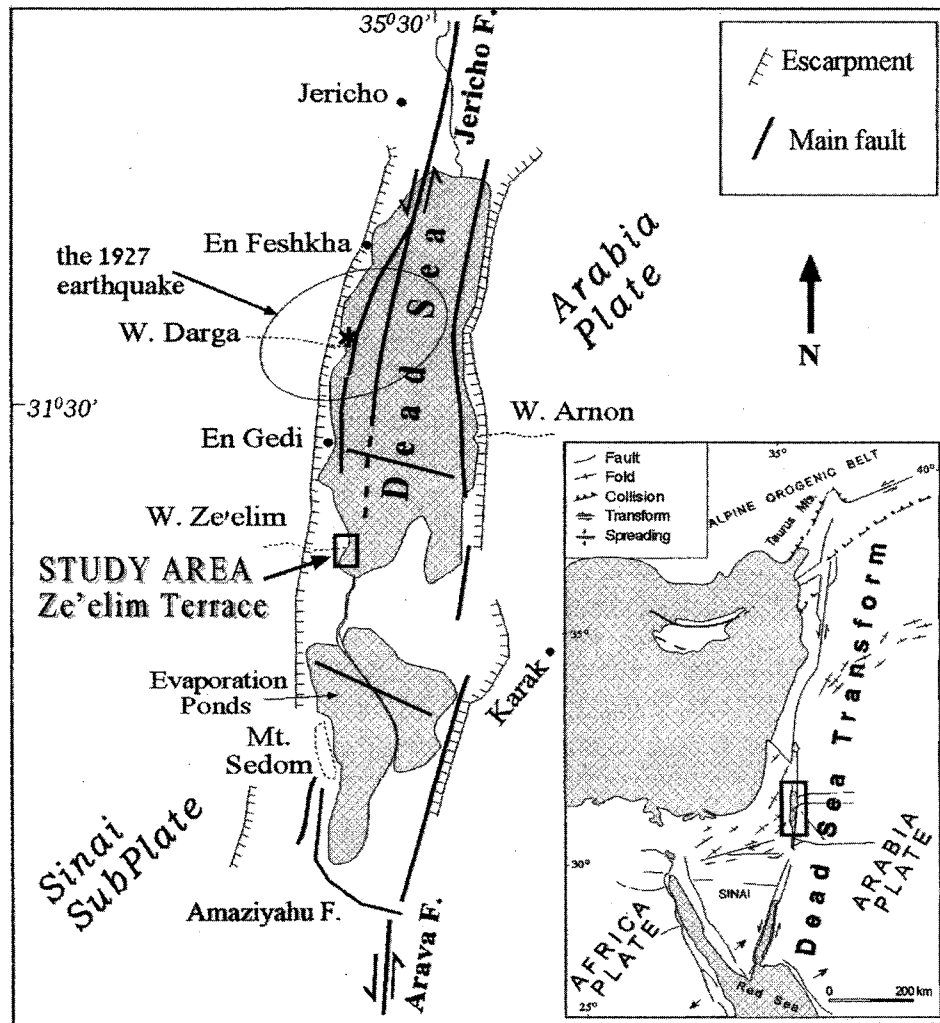


**Figure 1.** Location Map showing major faults in the Dead Sea region [Garfunkel and Ben-Avraham, 1996; Garfunkel et al., 1981]. Also marked are the epicenter of the Jericho 1927 earthquake and its uncertainty ellipse [Shapira et al., 1993]. Inset shows the general plate tectonic setting of the Dead Sea Transform.

cene sedimentary section exposed at the Ze'elim Terrace (Figure 1) is described. Several of the layers in this sequence contain features that are interpreted as seismically induced structures (seismites). The aim of this work is to document this paleoseismic record and to test its chronology against the historical earthquake record of the Dead Sea area.

## 2. The Ze'elim Formation

After the retreat of Lake Lisan at 17-13 kyr, the lake stabilized (for most of the time) at elevation of ~ 400 mbsl. [Frumkin et al., 1991; Neev and Emery, 1995; Kadan, 1997]. Sediments deposited in this post-Lisan water body (or paleo-Dead Sea) compose the Ze'elim Formation [Ken-Tor et al., 1998; Migowski et al., 1999; Yechieli, 1993]. The Ze'elim Formation records the sedimentological, limnological, and tectonic history of the lake during the Holocene. It is exposed along the periphery of the Dead Sea and was recovered in several boreholes along the western shore of the lake [Migowski et al., 1999]. The Ze'elim Formation consists of different lacustrine to fluvial sediments that reflect the lake-level fluctuations in

the semiarid environment of the Dead Sea area. The thickness of the Holocene deposits reaches about 20-30 m at the western shore of the lake's northern basin [Kadan, 1997; Migowski et al., 1999; Yechieli et al., 1993], and about 80 m in the southern basin [Neev and Emery, 1995].

The Ze'elim Terrace (Figure 1) is incised by several gullies, up to a few meters deep and up to a few tens of meters wide (Plate 1a). Fieldwork was conducted in two gullies where approximately 7 m of the upper Ze'elim Formation are exposed. Figure 2 provides a composite section of the outcrops exposed in the two gullies. The depositional environment exposed in the northern gully is mainly lacustrine, while in the southern gully the depositional environments are shore and nearshore.

The section was divided into several lithological units. The lacustrine sediments consist of alternating aragonite and detrital laminae (~1-2 mm thick) and thicker clastic layers (>10cm). The aragonite precipitated chemically from the water column as was described for the Lisan Formation (cf. Begin et al., 1974; Stein et al., 1997). The detrital layers consist of clay- and silt-size grains of Cretaceous rocks exposed in the catchment area and therefore represent flood input that entered

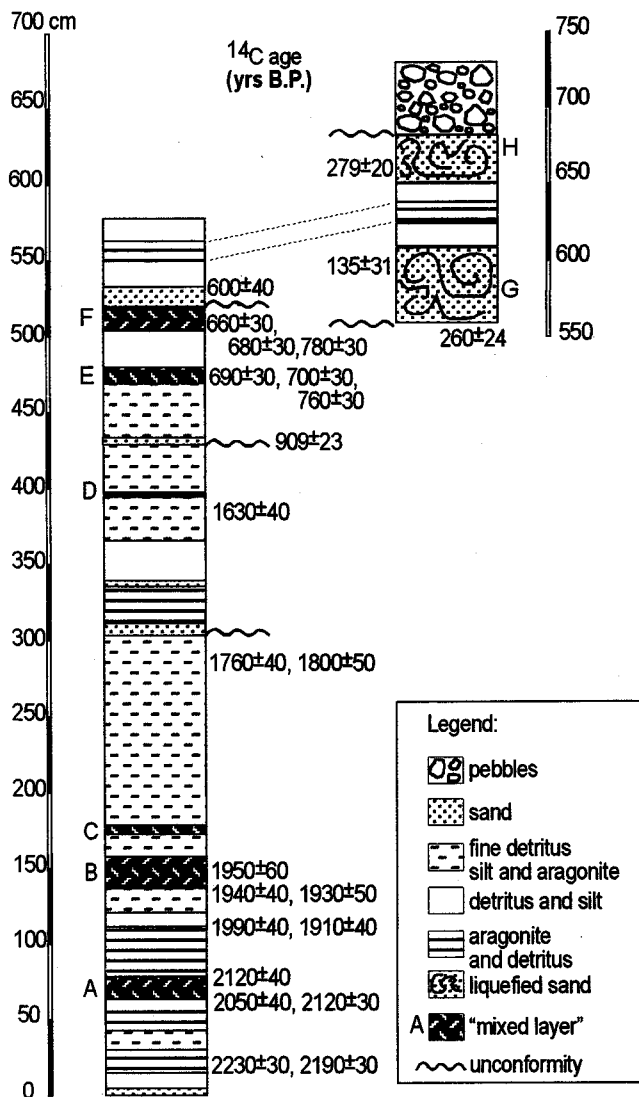


**Figure 2.** The lithology and chronology of a composite section exposed in Ze'elim Plain. The section is described from two outcrops exposed in different gullies 300 m apart. The correlation between the outcrops is based on the sedimentary sequence, laminae counting, and  $^{14}\text{C}$  dates. Ages presented in  $^{14}\text{C}$  years B.P. Deformed units (mixed layers and liquefied sands) are marked by capital letters.

the lake during rainy seasons. Well-sorted carbonate silty sand occurs in ripple marks or forms massive beds that were deposited in the nearshore environment. Aragonite crusts covering coarse carbonate sand or lacustrine clay and silt indicate that the deposits were exposed above lake-level at the shore environment. The presence of alluvial sediments (pebbles) indicates relatively low lake level and shifting of the shoreline to the east. The section is disturbed by several unconformities, representing periods of lowering of the lake-level and erosion.

### 3. Chronology of the Ze'elim Section

The chronology of the Ze'elim composite section is established by 24 radiocarbon ages on vegetation debris (Table 1). The detrital sediments from which the samples were recovered

are rich in leaves, stalks, small branches, and seeds that were flushed into the lake with the seasonal floods and buried within the detrital units. The transport time of the analyzed material is probably very short [Ely *et al.*, 1992]. Samples collected in recent fluvial channels in the Dead Sea area yield very high percent of modern carbon (PMC) values, indicating short residence time (< 100 years) of the organic material in the channels [Yecheili, 1993].

In most cases, the radiocarbon ages are stratigraphically consistent (Figure 3A). The ages range from 390 B.C. to 1960 A.D.. Radiocarbon analyses of samples from the same stratigraphic horizons yield very similar ages (Table 1). The chronology is discussed further in the context of the ages of the seismic events.

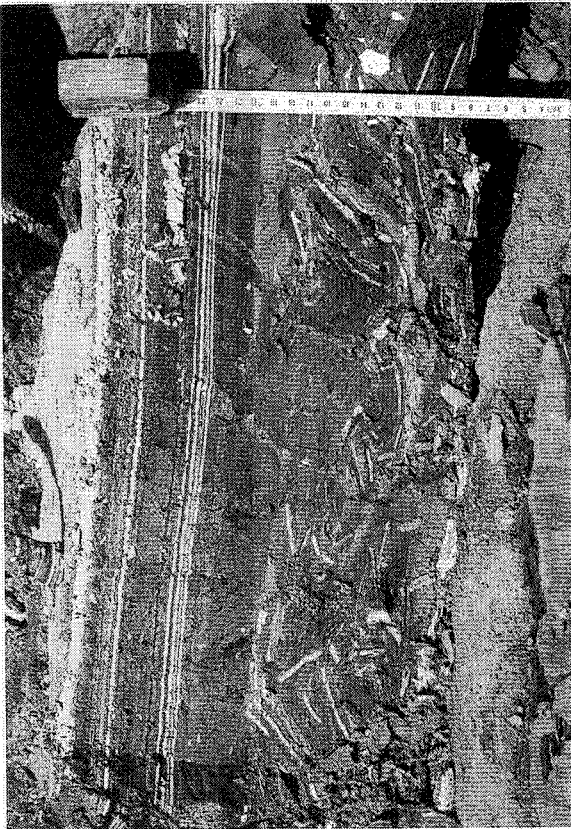
The sedimentation rates vary along the section, ranging from 3 to 13  $\text{mm yr}^{-1}$ . In most of the section the sedimentation rate is significantly higher than the average rate in the late Pleistocene Lisan Formation ( $\sim 0.8 \text{ mm yr}^{-1}$  [Schramm *et al.*, 2000]). The higher rate in Ze'elim section reflects the proximity of the section to the Ze'elim Wadi fan-delta. Nevertheless, the Ze'elim section also contains several depositional hiatuses, which lower the average sedimentation rate (Figure 3B).

### 4. "Mixed layers": Soft Sediment Deformation Structures

The typical sequence of alternating aragonite and detritus laminae and thicker clastic units in the Ze'elim Terrace is interrupted by units that show evidence for soft sediment deformation (Figure 2). These deformed units typically consist of mixtures of fine-grained dark clay and silt, with tabular fragments of aragonite laminae (millimeters to centimeters long) (Plate 1b). The units are a few centimeters to about 20 cm thick, with sharp and flat upper contacts. Below and above each deformed unit the section is laminated and undisturbed. The lateral distribution of the deformed units is not uniform; several of them extend over a large distance and can be traced and correlated among exposures in different gullies and different facies, whereas some have limited distribution.

The origin of the deformed layers is intriguing in light of the flat topography of the Ze'elim Terrace. There is no obvious reason and no field evidence for gravitational slides. Furthermore, the aragonite laminae fragments within the disturbed units are scattered randomly in the dark detritus and show no lateral grading, imbrication or other transport indicators and do not point to any oriented movement as slides or floods over the lake floor. More significantly, the disturbed units extend across sedimentary facies (lacustrine to shore facies) and show no evidence for turbidity currents or any other lateral flow.

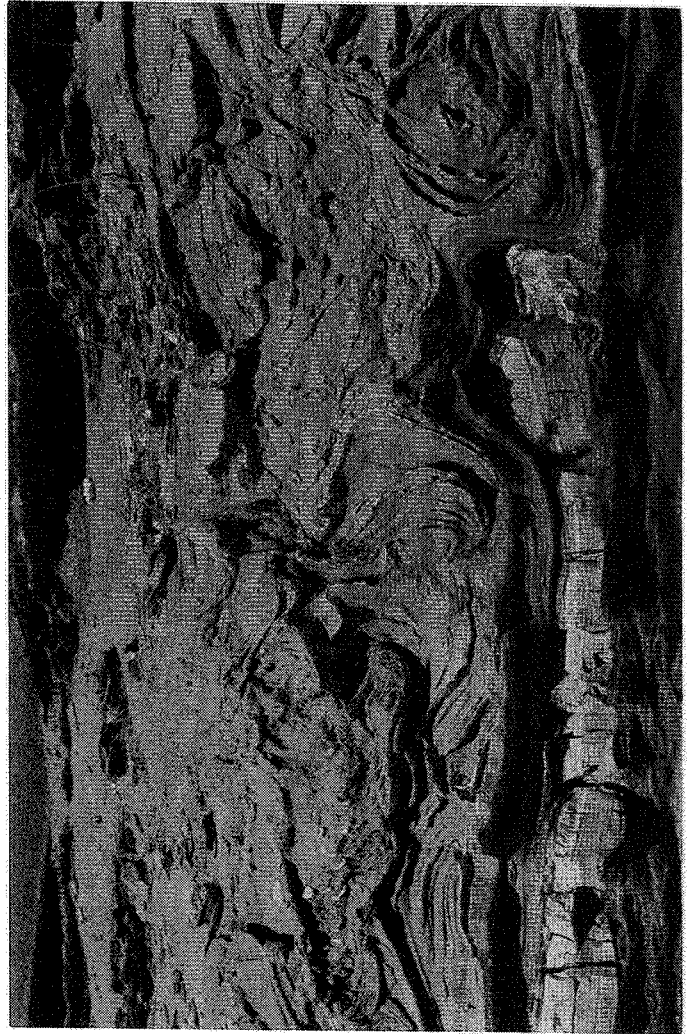
Similar layers of fine detritus and tabular aragonite fragments in the Dead Sea basin sediments have been described in the Lisan Formation [Marco and Agnon, 1995; Marco *et al.*, 1996]. The disturbed units (termed "mixed layers") were interpreted as seismites largely because of their association with syndepositional surface fault ruptures. It was suggested that each mixed layer represents an originally flat laminated aragonite and detritus unit, which, during an earthquake, was fluidized, brecciated, suspended, and then resettled in its present structure at the water-sediment interface. The flat upper surface of each mixed layer and the undisturbed postseismic layers above them (Plate 1b) point to deformation on the surface of the lake floor during the earthquake events [Marco and Ag-



b



a



c

**Table 1.** AMS Results of Radiocarbon Dating

Laboratory Sample	Height in Section, cm	Dated Material	Radiocarbon Years B.P.	Calibrated Date ( $2\sigma$ ) <sup>a</sup>	Most Probable Calibrated Ages
KIA8260 <sup>b</sup>	650 <sup>c</sup>	macro residue, alkali residue	279 ± 20	1520-1670 A.D.	20th century
KIA8261 <sup>b</sup>	600 <sup>c</sup>	wood bark, alkali residue	135 ± 31	1670-1960 A.D.	19th century
KIA8259	550 <sup>c</sup>	Wood, alkali residue	260 ± 24	1520-1800 A.D.	1520-1800 A.D.
KIA3213	478.5-532.5	wood, alkali residue	600 ± 40	1290-1420 A.D.	1290-1420 A.D.
KIA3214A <sup>b</sup>	519	wood twig, alkali residue	780 ± 30	1210-1290 A.D.	1270-1400 A.D.
KIA3215 <sup>b</sup>	519	twigs, alkali residue	660 ± 30	1280-1400 A.D.	
KIA3216 <sup>b</sup>	519	plant remains, seed, alkali residue	680 ± 30	1270-1400 A.D.	
KIA3217 <sup>b</sup>	469.5	wood, alkali residue	690 ± 30	1270-1390 A.D.	1220-1390 A.D.
KIA3218 <sup>b</sup>	469.5	wood, alkali residue	700 ± 30	1260-1390 A.D.	
KIA3219 <sup>b</sup>	469.5	wood, alkali residue	760 ± 30	1220-1295 A.D.	
KIA8258	430 <sup>c</sup>	wood, alkali residue	909 ± 23	1030-1210 A.D.	1030-1210 A.D.
KIA3220	381.5	wood, alkali residue	1630 ± 40	340-540 A.D.	340-540 A.D.
KIA3221	282.5	stick, alkali residue	1760 ± 40	130-390 A.D.	130-390 A.D.
KIA3222	282.5	stem, alkali residue	1800 ± 50	80-390 A.D.	
KIA3223 <sup>b</sup>	146	plant, stem, alkali residue	1950 ± 60	100 B.C. to 230 A.D.	50 B.C. to 230 A.D.
KIA3224	132.5	wood, alkali residue	1940 ± 40	50 B.C. to 140 A.D.	50 B.C. to 180 A.D.
KIA3225	132.5	wood, alkali residue	1930 ± 50	50 B.C. to 220 A.D.	
KIA3227A	107	diverse plant mater., alkali resid.	1990 ± 40	50 B.C. to 80 A.D.	50 B.C. to 80 A.D.
KIA3227B	107	diverse plant material, humic acid	1910 ± 40	0-230 A.D.	
KIA3228 <sup>b</sup>	73.5	diverse plant mater., alkali resid.	2120 ± 40	360-40 B.C.	200-40 B.C.
KIA3232	51	root or twig, stem, alkali residue <sup>d</sup>	2050 ± 40	170 B.C. to 50 A.D.	200 B.C. to 10 A.D.
KIA3233	51	wood, alkali residue	2120 ± 30	350-40 B.C.	
KIA3234	14.5	stem and root, alkali residue <sup>d</sup>	2230 ± 30	390-200 B.C.	
KIA3235	14.5	stem, alkali residue	2190 ± 30	380-160 B.C.	380-180 B.C.

<sup>a</sup> Calibrated ages ( $2\sigma$ ) according to *Stuiver et al.* [1998]. The samples are listed according to their stratigraphic height, top to bottom.

<sup>b</sup> Samples collected from the deformed units.

<sup>c</sup> Samples collected from the southern section (see composite section, Figure 2).

<sup>d</sup> Root debris (not in situ root).

non, 1995, Figure 4]. The deformation occurred prior to the deposition above. Irregular surfaces of the mixed layers are observed locally, where they overlie syndepositional fault ruptures. In this places subaqueous scarps were created during the seismic event [Marco and Agnon, 1995]. Similar soft sediment deformation structures have been documented in several other localities worldwide and also interpreted as seismites [cf. Allen, 1986; Davenport and Ringrose, 1987; Hempton and Dewey, 1983; Sims, 1973, 1975]. For example, Doig [1991] describes a chaotic zone of organic-rich lake sediment mixed with partly tabular fragments of a previously laminated silt layer that was disturbed during the 1935 (M6.3) Témiscaming (Quebec) earthquake.

## 5. Distribution of Deformation in Different Depositional Environments

The sediments exposed at the Ze'elim Plain were deposited in a transition zone between two depositional environments of a lacustrine basin: the shore and near-shore environment and the lake water body. This setting is ideal for the purpose of analyzing the effects of simultaneous ground shaking on sediments with different properties (e.g., aragonite-detrital laminae versus sandy units) because it is possible to trace continuously the changes in deformation character along with the facies variations. Where the lacustrine lithology changes to silt and sorted sand of the shore environment, load-cast and flame

**Plate 1.** (a) The Late Holocene outcrop exposed at the Ze'elim Plain, viewed from the lake shore to the west. The western escarpment of the Dead Sea Graben is seen in the backside. The Ze'elim Plain was covered by the Dead Sea 15-20 years ago. A drastic retreat in the lake level ( $\sim 80 \text{ cm y}^{-1}$ ) incised deep gullies and exposed the sediments of the upper Ze'elim Formation. The present thickness of the exposed section reaches about 7 m. (b) Mixed layer B (see also Figure 2) composed of aragonite fragments suspended in fine dark detritus. The fragments are few millimeters to few centimeters long and do not show any preferred orientation. The overlying and underlying (not seen in the figure) laminated deposits are undisturbed. This layer is correlated with the 31 B.C. earthquake (see text). (c) Liquefied carbonate sands, fine detritus, and aragonite laminae of the shore environment. This deformed unit ( $\sim 0.5 \text{ m}$  thick) illustrates the simultaneous deformation of deposits from different depositional environments in the same stratigraphic horizon, which was at the surface at that time.

structures are visible (Plate 1c). The thickness of the deformed unit changes within a short distance. It is clearly visible that the character of deformation is related to grain size and the thickness of the unit. When the sand units become too thin, the deformation disappears.

The change in the deformation pattern is illustrated here by the behavior of a prominent mixed layer (B in Figure 2). This mixed layer can be traced over the entire studied area, across the facies changes. Yet it exhibits different structures according to the type of the sediments.

The observation of simultaneous deformation in different sedimentary facies of the same stratigraphic horizon in Ze'elim outcrops, supports the interpretation of the mixed lay-

ers as seismites. No other process could have simultaneously affected the various depositional environments of the same stratigraphic horizon. Together with the juxtaposition of the mixed layers over surface ruptures (as observed in the Lisan Formation), the transformation of disturbance through various sedimentary facies strongly supports the interpretation of the mixed layers as seismites.

## 6. Dating and Correlation of the Seismites With Historic Earthquake

The ages of the deformed layers were constrained by  $^{14}\text{C}$  dates derived from the layers themselves and by extrapolating

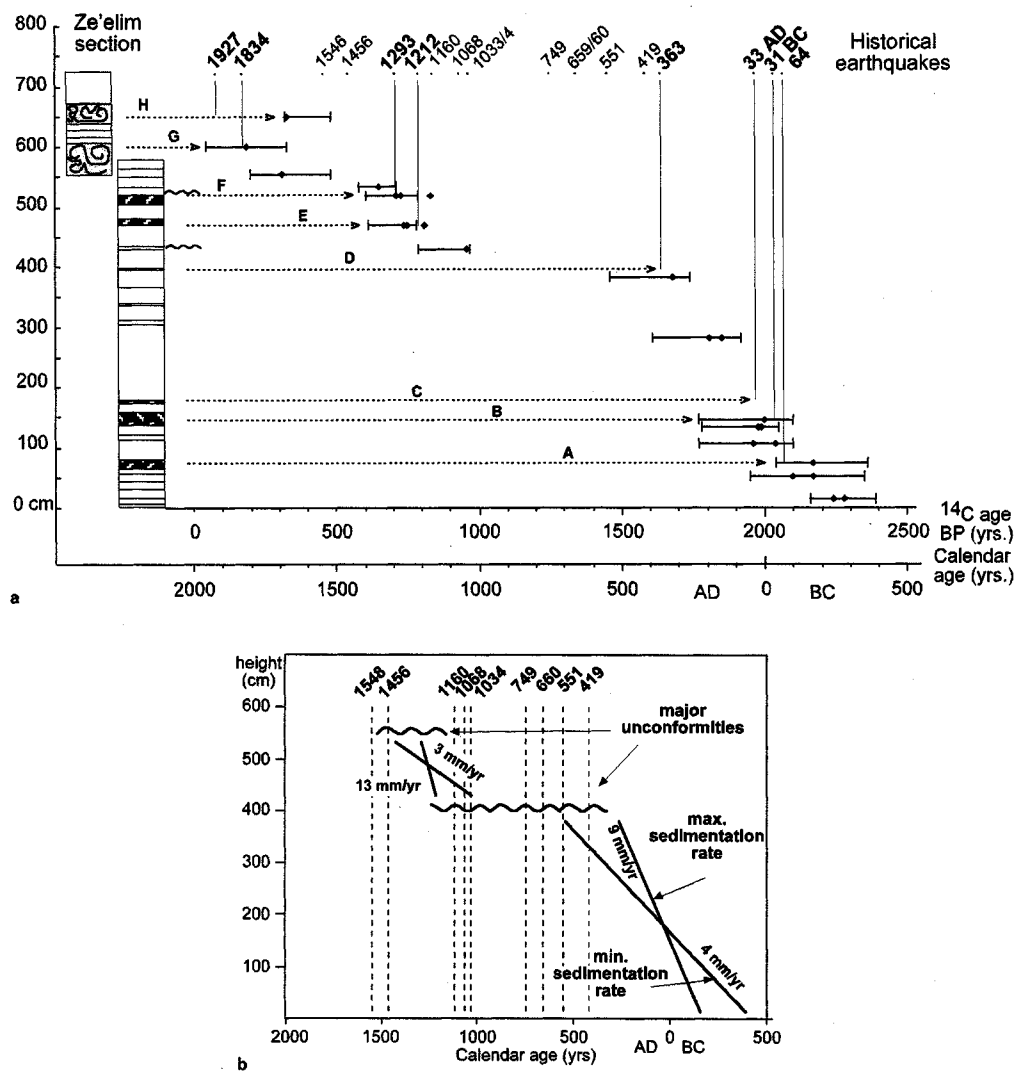


**Figure 3.** (a) Chronology of the deformed units (seismites) in the Ze'elim section. Solid dots represent  $^{14}\text{C}$  ages in years B.P.. Error bars represent the ranges in the calibrated ages ( $2\sigma$ ) of all samples in each stratigraphic horizon. Vertical thin lines represent historical earthquakes in the Dead Sea area, which were correlated to the deformed units in the Ze'elim section. Horizontal dashed arrows are drawn from the deformed units (listed in capital letters) to the correlative earthquakes. (b) Sedimentation rates calculated for the lower part of the composite section. The longest calibrated range was used for calculating the minimum sedimentation rate, and the shortest range for calculating the maximum sedimentation rate. Two clear unconformities are evident: The upper one is dated to 1290-1420 A.D., and the lower one to 1030-1210 A.D.. The lower unconformity is marked by a sharp decrease in the sedimentation rate. Vertical dashed lines represent earthquakes that lie within the sedimentological hiatuses. Sedimentation rate of the upper part in the section was not calculated because datable samples were insufficient.

**Table 2.** The  $^{14}\text{C}$  Chronology of the Deformed Layers (Seismites)

Deformed Layer <sup>a</sup>	Sample Laboratory Number	Calendar Age Years ( $2\sigma$ )	Most Probable Calibrated Ages
A	KIA3228	360-40 B.C.	200 -40 B.C.
B	KIA3223	100 B.C. to 230 A.D.	50 B.C. to 230 A.D.
C	-	64 B.C. to 311 A.D. <sup>b</sup>	5 -50 A.D.
D	-	358-580 A.D. <sup>b</sup>	358-580 A.D.
E	KIA3219, KIA3218, KIA3217	1220-1390 A.D.	1220 -1390 A.D.
F	KIA3214A, KIA3215, KIA3216	1270-1400 A.D.	1270 -1400 A.D.
G	KIA8261	1670-1960 A.D.	19th century
H	KIA8260	1520-1670 A.D.	20th century

<sup>a</sup> Listed by their stratigraphic height, bottom to top.

<sup>b</sup> Age calculated according to sedimentation rate, interpolated from adjacent dated layers.

between ages of layers directly beneath and above a particular mixed layer (Table 2). The radiocarbon ages of the mixed layers were calibrated to calendar years according to *Stuiver et al.* [1998]. The calibrated ages lie in ranges that are defined by the  $2\sigma$  envelope error of the measured data. For example, the measured radiocarbon age of event A ( $2120\pm 40$  years B.P., Table 1) is calibrated to the range of 360 to 40 years B.C.. Applying the superposition principle and rate of sedimentation further narrowed these ranges. Samples, which are stratigraphically lower in the section, thus older, reduce the calendar range of the samples above. This procedure allows us to resolve the calendar ages of samples that yielded analytical data that are statistically indistinguishable. The use of sedimentation rates allows determining ages of mixed layers that were not directly dated by radiocarbon because of lack of organic debris. The sedimentation rate is sensitive to depositional hiatuses in the section. Thus, different rates are used for different parts of the section (see varying slopes in Figure 3b).

The radiocarbon sample collected from a mixed layer is dating the deposition within the layer before it was disturbed. Hence the seismic event that caused the deformation is younger. The time elapsed between the deposition and the deformation by the earthquake was short relatively to the uncertainty in the dating. Two lines of evidence support this assumption:

1. Deformation of the mixed layer occurred at the sediment-water interface. This is indicated by graded bedding and by the juxtaposition of mixed layers with syndepositional faults in the Lisan Formation. Thicker accumulation above the mixed layer on the downthrown block is considered as evidence for a fault scarp. Some local mass transport near the scarp produced thicker mixed layers in the lower block [*Marco and Agnon, 1995*].

2. In the Ze'elim section, two of the mixed layers, A and B, are separated by only about 75 cm and approximately 200  $^{14}\text{C}$  years (Figure 2). Thus, the time elapsed between the deposition and disturbance of unit A must have been shorter than 200 years.

Liquefaction is often attributed to subsurface deformation. In Ze'elin section liquefaction seems to have occurred at the surface. This surface deformation is consistent with the absence of sand volcanoes and dikes.

A final assessment of the mixed layer ages and their identification as seismites is achieved by correlation with the chronology of the historical earthquakes. The concept we used here is to assess whether all individual pieces of information (the structures, the ages and the correlation to known chronology) fit an internally consistent framework.

## 6.1. Comparison With the Historical Earthquake Record

The historical earthquake record of the last four millennia in the Middle East [*Ben-Menahem, 1991*] represents one of the longest seismic records on Earth. The dated paleoseismic record recovered from the mixed layers in the Ze'elim Terrace correlates with the last and best documented 2000 years of this record (see description of the relevant historical earthquakes in Table 3). Several reported historical earthquakes are not identified in the Ze'elim record but can be correlated with depositional hiatuses or periods of erosion. Conversely, it is possible to correlate all deformed units with particular historic earthquakes.

The correlation between the Ze'elim seismic record and the historical record is based mainly on reports from three sites in the Dead Sea region: Jericho, Karak, and the Darga fan delta (Figure 4). Jericho is located to the northwest of the Dead Sea adjacent to one of the major faults, the Jericho Fault (Figure 1) [*Reches and hoexter, 1981*]. The site was settled in the Neolithic period and has been continuously populated during the time represented by the Ze'elim section. Karak is located on the eastern escarpment of the Dead Sea Graben, 1400 m above the Dead Sea shore. Its prominence peaked during the Crusaders period, and it has been populated continuously during the last millennium. We also compare our data to the Darga fan delta (Figure 1), where a geological earthquake record was recently described [*Enzel et al., 2000*]. The historical and geologic reports on earthquakes around the Dead Sea area are summarized in Figures 4 and 5. The following events are identified in the Ze'elim section:

**6.1.1. Event A.** Event A was dated based on a mixed layer sample collected 73.5 cm above the bottom of the section. The age of the sample is  $2120\pm 40$  radiocarbon years B.P. (Table 1), with a calibration range of 360-40 B.C.. Below this mixed layer, at 14.5 cm, two samples were dated to  $2190\pm 30$  and  $2230\pm 30$  years B.P. (with calibration ranges of 380-160 B.C. and 390-200 B.C., respectively). At 51 cm, two other samples were dated to  $2120\pm 30$  and  $2050\pm 40$  years B.P. (350-40 B.C. and 170 B.C.-50 A.D., respectively). Taken together, the four samples constrain the age of event A within the calendar range of 200 B.C.-40 B.C..

Mixed layer A, which is the oldest in the section, can be correlated to the historically documented 64 B.C. earthquake, which was felt strongly in Jerusalem and damaged the city walls and the Second Temple [*Amiran et al., 1994*]. A deformed unit in the Darga fan delta was also dated to this time range [*Enzel et al., 2000*]. The appearance of deformed units in both the Ze'elim Terrace and the Darga fan delta during the 64 B.C. earthquake may indicate that the epicenter was located

**Table 3.** Description of Earthquakes in the Dead Sea Region According to Historical Reports

Date	Location and Description	References
64 B.C.	In Jerusalem the Temple and city walls were damaged. In Syria it was felt as far as Antioch.	1,7
31 B.C.	Reports were from Israel. There was great destruction in the Dead Sea area (e.g. Herod's winter palace in Jericho, Qumran and Massada). Severe damage occurred in the Galilee, and Judea. In Jerusalem the earthquake damaged the Second Temple. According to Josephus, 30,000 people were killed. Epicentral intensity was possibly MMS X.	1,5,7,8
33 A.D.	Reports were from Judea region. The Temple in Jerusalem was damaged.	1,7
363 A.D.	Reports were from Baniyas in the north through Petra in the south and from the coastal littoral through the Jordan Valley and beyond. In Jerusalem the Temple area was damaged. In Syria several castles were damaged. Karak was destroyed. Seiche was reported in the Dead Sea.	1,3,4,5,7,8
419 A.D.	In the reports, Jerusalem is specifically mentioned. Many towns and villages were destroyed (e.g., Aphek/Antipatris). The shock was moderate to severe.	1,4,7,8
551 A.D.	Reports were from northeast Egypt (?), Israel, Arabia, Phoenicia, Syria, and north Mesopotamia. Damage was reported along the Lebanon coast and in villages in the Galilee. Damage occurred in Jerusalem, Jerash, Mount. Nebo. The el-Lejjun fortress east of Karak was destroyed. Petra was destroyed and never rebuilt. Tsunami occurred on the coast of Lebanon.	1,4,7
659/660 A.D.	There are different suggested epicenter locations: offshore from Lebanon or in the Jordan Valley. Reports were from Jordan Valley and Rehov in Beth Shean basin. In Jericho it was felt strongly. The monasteries of St. John the Baptist (on the Jordan river, east of Jericho) and St. Euthymius were destroyed.	4,7,8
749 A.D.	Reports were from Egypt, Mesopotamia, Syria, Arabia, and Israel. Damage occurred to 600 settlements, and there were many casualties on both sides of the Jordan, from Tiberias to Arad. Hisham Palace near Jericho and buildings in all major cities and monasteries were destroyed. A Seiche was reported in Lake Galilee and the Dead Sea. Tsunami occurred on Mediterranean coast. Epicentral intensity possibly MMS X. Local magnitude was estimated to 7.3.	4,5,6,7,8
1033/1034 A.D.	Reports were from Syria, along the Jordan Valley, as far as Gaza and Ashkelon and probably in the Negev and Egypt. Heavy damage and casualties occurred in Tiberias. The earthquake affected the Galilee, Akko, Jaffa, Nablus, Ramle, Jerusalem, Hebron, and Jericho. Tsunami occurred on the Mediterranean coast of Israel.	2,5,6,7
1068 A.D.	Epicentral intensity possibly MMS X. Suggested epicenter near the Lake of Galilee. Reports were from northwest Arabia. The city of Elat was completely ruined, and its inhabitants perished. In Tabuk, new springs appeared. The earthquake was felt at Wadi al-Qura, Khaibar, and al-Marwa and as far as Medina, Yanbu, and Badr in the south. In the Baniyas, 100 people died under the debris. Ramla was destroyed, and 15,000 people died (seems exaggerated). In Jerusalem the roof of the Dome of the rock was displaced. Yavne and Ashdod were affected. Tsunami washed Israel coast. The epicentral area of this earthquake must be sought in the sparsely inhabited region between Elat and Taima in Northern Hejaz.	2,6,7
1160 A.D.	Reports were from Israel alone. Slight damage occurred in Bethlehem and Jerusalem. The Monastery of Mar Elias (Jerusalem) was seriously damaged and the Monastery of St. John on the Jordan River was destroyed	1,7
1212 A.D.	Reports were from south Israel and Egypt. It was strongly felt in Cairo and Fustat, and destroyed a number of houses. At al-Shaubak and Karak (VIII MMS) towers and houses were destroyed, killing a number of women and children. Strong in Elat (VIII-IX MMS). In Sinai Peninsula the shock caused severe damage to the monastery of St. Catherine. The earthquake was located in the gulf of Aqaba or south of the Dead Sea.	6,7
1293 A.D.	Most of the reports come from south and central Israel. The earthquake damaged Gaza (VII MMS) Ramla (VII MMS), Ludd (VI MMS), Qaqun, and Karak (VIII MMS), where three fortress towers destroyed. The earthquake ruined many places on the coast of Israel. The epicenter was probably in the Dead Sea Rift.	2,6,7
1456-1459 A.D.	Reports were from southern Israel and Jerusalem. It was felt weakly in Cairo. In Karak, destruction and casualties are reported.	1,6,7
1546 AD	Damage and victims were reported from Safed, Tiberias, Ramla, Jerusalem, Hebron, Gaza, Salt, and Karak. In Nablus hundreds of victims were buried under the ruins. The earthquake was felt as far as Damascus. The flow of the Jordan River was stopped for 2 days by a landslide near Damia. Tsunami washed the Mediterranean coast from Jaffa to Gaza. Seiche occurred in the Dead Sea. Maximum epicentral intensity was MMS IX.	1,5,6,7
1834 A.D.	Damage reports were from Jerusalem, Bethlehem, Nablus, Gaza, and Karak. It was felt strongly in Tiberias, Akko, and Ashkelon. Large blocks of asphalt floated on the Dead Sea. The shallow	1,5,7

Table 3. (continued)

Date	Location and Description	References
	water road connecting the Lisan with En-Gedi disappeared, and the Dead Sea became impassable by foot.	
1927 AD	Reports of great damage were in Judea and Samaria in Israel. The flow of the Jordan River stopped for 22 hours due to landslides near Damia. The earthquake was felt in Syria and Lebanon. This is the first major earthquake in the area to be recorded instrumentally. $M=6.25$ , maximum epicentral intensity was MMS IX in the Jordan Valley. Revised epicenter was located near Darga fan-delta on the shores of the Dead Sea. Sites far from the epicenter such as Nablus, Ramla, and Lod also experienced relatively high local intensity (MMS VIII). On the other hand, the towns closer to the epicenter, i.e., Jericho and Jerusalem, experienced lower intensity (MMS VII).	9,10,11,12

The information is collected from historical catalogues. The catalogues summarize information from different historical sources that were studied and analyzed during the last century. Our assessment is based on the information that is written in the catalogues only. References are 1, Willis [1928]; 2, Arieh [1977]; 3, Russell [1980]; 4, Russell [1985]; 5, [Ben-Menahem [1991]; 6, Ambraseys et al. [1994]; 7, Amiran et al. [1994]; 8, Guidoboni et al., [1994]; 9, Ben-Menahem et al. [1976]; 10, Vered and Striem [1976]; 11, Shapira et al. [1993]; 12, Avni [1999]. All references are based on historic sources that are described therein.

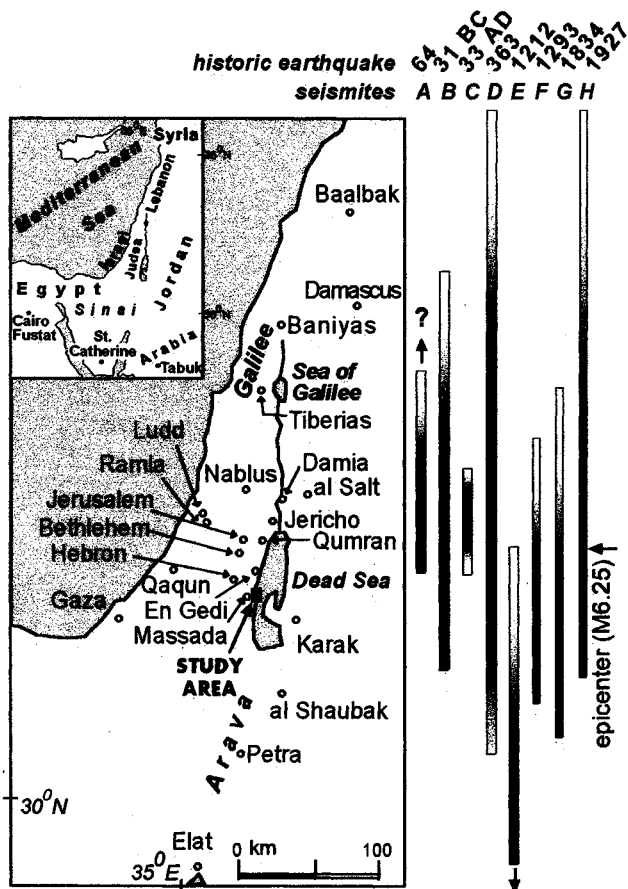


Figure 4. Location map of sites that were affected by earthquakes generated in the Dead Sea area (see Table 3 for historical information and references). On the right side, the area affected by the earthquakes according to the historic reports and the new evidence from this study. Estimated epicenter locations along the Dead Sea fault system are indicated by the gradual change into darker shading. The 1927 A.D. earthquake is likely better represented by the historical data relatively to older events mainly because it is a recent event.

in the Dead Sea area (Figure 5). The lack of independent reports from other places in the area probably reflects the event's antiquity and moderate intensity.

6.1.2. Event B. The time elapsed between events A and B was bracketed by four radiocarbon dates:  $1910 \pm 40$  and  $1990 \pm 40$  years B.P. (0 to 230 A.D., 50 B.C. to 80 A.D.) for samples at 107 cm, and  $1930 \pm 50$  and  $1940 \pm 40$  years B.P. (50 B.C. to 220 A.D. and 50 B.C. to 140 A.D., respectively) for samples at 132.5 cm. Based on the age of a sample collected from within the mixed layer itself at 146 cm event B was dated to  $1950 \pm 60$  years BP (100 B.C.-230 A.D.), a range which overlaps with that of the samples between events A and B. Nevertheless, the age range of event B can be reduced to 50 B.C. to 230 A.D. according to its stratigraphical location above event A. Moreover, the association of event A with the 64 B.C. earthquake implies that event B is younger and may be correlated with an earthquake that took place in the early spring of 31 B.C..

The 31 B.C. earthquake is described by Josephus Flavius in the "Jewish Wars" (Book I, Ch. XIX, 370-380) and in "Jewish Antiquities" (Book XV, Chapter. V, pp. 121-147). The earthquake occurred during the battle of Actium between Caesar and Anthony in the seventh year of King Herod's reign. According to Flavius, the earthquake caused great destruction and many casualties, killing as many as 30,000 people. The Second Temple in Jerusalem, Herod's winter palace at Jericho, and structures in Massada and Qumran were damaged [Amiran et al., 1994; Ben-Menahem, 1991; Guidoboni et al., 1994]. The earthquake was strongly felt in Judea and the Galilee (Figure 4).

The mixed layer of event B can be traced along all the outcrops in the study area and can also be identified in the Darga fan delta [Enzel et al., 2000]. On the Jericho Fault, a surface rupture that has also been related to the 31 B.C. earthquake [Reches and Hoexter, 1981] is located near the city of Jericho, about 60 km north of the Ze'elim Terrace (Figure 1). Local intensity is inferred to have reached MMS X in several places [Amiran et al., 1994]. Considering the geological evidence and trusting the extensive historical records, despite their antiquity, it can be concluded that the 31 B.C. event was a strong earthquake with an epicenter located on the main Jericho Fault, not far from the Ze'elim Terrace.

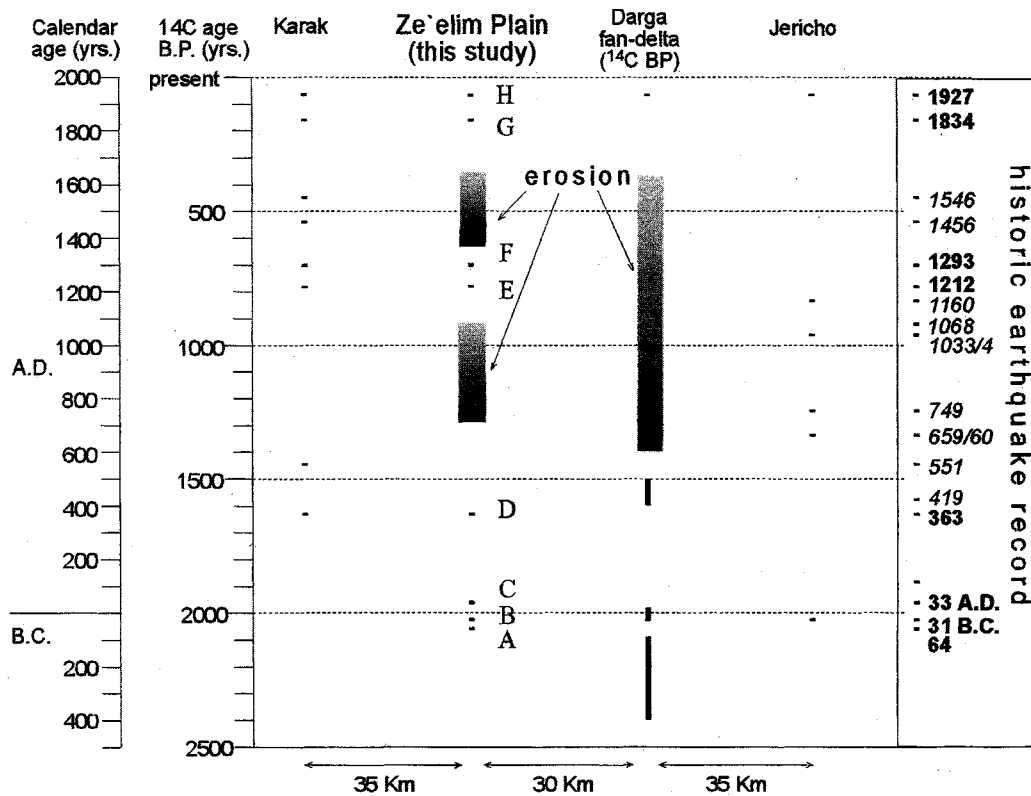


**Figure 5.** The historical record of earthquakes that have been reported to affect the Dead Sea area during the Late Holocene. The Ze'elim Terrace (this study) and the Darga fan delta [Enzel *et al.*, 2000] are geological records. The Karak and Jericho records are composed of the historical reports of damage from these sites. At the right column the complete historic earthquakes record is presented (Table 3). The criterion of choosing an earthquake to be presented in the historical record is that there are distinct reports of damage in the Dead Sea area or Jerusalem (which was occupied during the entire historical record presented). Bold indicates historical earthquakes recovered from the Ze'elim Terrace. Italics indicates earthquakes that are reported in the historical record but do not appear in the Ze'elim section (see text). Capital letters indicate the corresponding deformed unit in Ze'elim Terrace.

The prominent thickness and regional distribution of mixed layer B further argue that it can be identified with the 31 B.C. earthquake. We will subsequently use this mixed layer as a chronological "anchor point", which is used in the assessment of the ages of other mixed layers.

**6.1.3. Event C.** Mixed layer C is a few cm thick and discontinuous. It is located at 178.5 cm, 32.5 cm above the sample that dates the previous event (at 146 cm). Since no organic debris was found in unit C, the event was dated according to the sedimentation rate at this part of the section ( $4\text{--}9\text{ mmy}^{-1}$ , Figure 3b) to a calendar range of 64 B.C. to 311 A.D.. This range can be further reduced to 5-50 A.D. by using the 31 B.C. earthquake (event B) as a chronological anchor point in the section. Mixed layer C is correlated with the earthquake of 33 A.D. that damaged the Second Temple in Jerusalem [Amiran *et al.*, 1994; Willis, 1928]. The earthquake was not reported elsewhere in the Dead Sea area. The lack of documentation and the limited evidence for geological disturbance suggest a small magnitude earthquake in the Dead Sea area (Figure 4).

**6.1.4. Event D.** Mixed layer D contains no organic debris for radiocarbon dating, therefore the age of this event was estimated from the sedimentation rate in the underlying interval.

The samples below and above mixed layer D were dated to  $1630\pm 40$  years B.P. (340-540 A.D.) and  $909\pm 23$  years B.P. (1030-1210 A.D.), respectively. The older sample was located at 381.5 cm and the younger at 430 cm from the bottom, yielding a sedimentation rate of  $0.5\text{--}1\text{ mm y}^{-1}$ . This rate probably represents a minimum value because the younger sample was collected above a depositional unconformity. The unconformity is characterized by coarse sand and aragonite crusts that indicate lowering of the lake level, which is usually accompanied by erosion of the surface. The erosion is probably the reason for the low sedimentation rate (e.g. an order of magnitude lower than the one in the previously studied interval). Therefore, for the interval including layer D we assign the mean sedimentation rate that characterizes the lower part of the section ( $4\text{--}9\text{ mm y}^{-1}$ , Figure 3b). This rate would yield a calibrated age for event D in the range of 358-580 A.D.. A similar result is achieved when the 31 B.C. earthquake (top of unit B) is taken as a chronological anchor point in the section. Mixed layer D was probably deformed by the 363 A.D. earthquake. Documentary evidence concerning this earthquake is preserved in a letter originally composed and circulated in Cyril's name (the Bishop of Jerusalem) during the early years of the 5th century [Russell, 1980]. The destruction caused by

this earthquake stretched from Baniyas in northern Israel through Petra and Elat in the south and from the Mediterranean coast through the Jordan Valley and eastward [Russell, 1985]. Damage in Karak and a seiche in the Dead Sea in response to the earthquake are reported [Amiran *et al.*, 1994]. In the Darga fan delta, a liquefied unit [Enzel *et al.*, 2000] is probably associated with the same event.

**6.1.5. Events E and F.** The timing of event E is inferred from the ages of three samples from this mixed layer:  $760 \pm 30$ ,  $700 \pm 30$ , and  $690 \pm 30$  years B.P.. Event F is dated by three samples from the next mixed layer to  $780 \pm 30$ ,  $680 \pm 30$ , and  $660 \pm 30$  years B.P.. The 780 years B.P. sample (within unit F) is out of stratigraphic order and probably represents reworked material; thus it is excluded from the analysis. The calibrated ranges for E and F are 1220-1390 A.D. and 1270-1400 A.D., respectively. Statistically, these dates are indistinguishable, but their stratigraphic order suggests a correlation to the earthquakes of 1212 and 1293 A.D.. The two mixed layers are separated by a 20-30 cm thick uniform detrital unit that represents approximately 20-100 years of deposition, based on the sedimentation rate in this part of the section ( $3-13 \text{ mm y}^{-1}$ , Figure 3b). The calculated age difference between the two mixed layers is similar to the historical age interval between the two earthquakes.

The 1212 A.D. earthquake was strongly felt in Egypt, particularly in Cairo and Fustat. At al-Shaubak and Karak, towers and houses were destroyed, and casualties were reported. In the Sinai Peninsula, the shock caused severe damage to the monastery of St. Catherine [Ambraseys *et al.*, 1994]. Based on the distribution of damage, it was suggested that the earthquake's epicenter must have been located south of the Dead Sea [Ambraseys *et al.*, 1994] (Figure 4).

The epicenter of the 1293 A.D. earthquake was probably located in the Dead Sea basin near Karak, [Arieh, 1977]. This earthquake affected the region of Gaza, Ramla, Ludd, Qaqun and Karak, where towers and many houses were destroyed [Ambraseys *et al.*, 1994]. The 1293 A.D. as well as 1212 A.D. earthquakes were not reported from Jericho suggesting that their epicenters may be located south to the Dead Sea basin (Figure 4).

**6.1.6. Events G and H.** These events are recorded as liquefied sand layers in the uppermost part of the Ze'elim section (Figure 2). Thus, they may record the youngest reported earthquakes in the region, probably from the last two centuries. The most pronounced and well-documented earthquakes of that period are those of 1834 and 1927.

Events G and H are constrained by radiocarbon ages from three samples, which are arranged in the following stratigraphic order from bottom to top:  $260 \pm 24$ ,  $135 \pm 31$  and  $279 \pm 20$  years B.P.. These correspond to calibrated ranges of 1520-1800 A.D., 1670-1960 A.D. and 1520-1670 A.D., respectively (Figure 3a). In addition, the liquefied layers G and H are separated by a few centimeters of lacustrine sediments (laminated aragonite and detritus), which mark a rise in lake level and may be related to the relatively high stand of the Dead Sea at the end of the 19th century [Klein, 1961]. It appears that the lower and middle layers are older than the 1890's lake level rise and the upper layer (H) is younger. The range of ages of the middle and lower layers is consistent with this interpretation, while that of the upper layer is out of the stratigraphic order and inconsistent with the 1890's high-stand. The discrepancy could reflect reworking of the or-

ganic debris, which occurs in the shore environment. If the lacustrine layer corresponds to the 1890's high-stand, then the upper liquefied layer H can be correlated with the 1927 earthquake and layer G with the previous 1834 event. The identification of mixed layer H with the 1927 earthquake indicates that water depth was  $\sim 10$  m above the deformed sediment (the Dead Sea elevation during 1927 was 392 mbsl [Klein, 1982] and the deformed unit is at about 402 mbsl).

Accounts of damage from the 1834 A.D. earthquake are reported from Jerusalem, where several churches and minarets and the city wall were damaged. At Bethlehem, several monasteries were damaged and many people were killed [Amiran *et al.*, 1994]. Nablus and Gaza were also damaged. Large blocks of asphalt appeared on the Dead Sea [Ben-Menahem, 1991]. This earthquake damaged Karak, but it is neither visible in the Darga fan delta section nor reported to have damaged Jericho (Figure 5). Therefore, the epicenter was likely south of the Dead Sea basin (Figure 4).

The 1927 earthquake is the only relatively large ( $M=6.25$ ) earthquake in Israel to be recorded instrumentally [Ben-Menahem *et al.*, 1976]. Its epicenter was reinterpreted recently to have been located just north of the Darga fan-delta (Figure 1) [Shapira *et al.*, 1993]. Evaluations of the effects of this earthquake yield a maximum intensity MMS IX along the Jordan River, from the Allenby Bridge (south east of Jericho) southward to the north coast of the Dead Sea [Avni, 1999]. The 1927 earthquake was correlated with the youngest deformed layer in Darga fan-delta [Enzel *et al.*, 2000].

## 6.2. Reported Historic Earthquakes That Are Not Visible in the Geological Record

Several earthquakes from the Dead Sea area that are reported in the historical catalogues have no correlative deformed units in the Ze'elim record (Figures 3b and 5). The absence of these earthquakes from the Ze'elim record may be due to a remote epicenter and/or small magnitude ( $<5.5$ ), which was not sufficient to induce a disturbance in the Dead Sea area. Another obvious reason is the incompleteness of the geological record in the Ze'elim Terrace. During times of climatic change, the lake level dropped and the Ze'elim Terrace was exposed, resulting in depositional hiatuses.

Two major unconformities are identified in the section (Figures 3b and 5). To constrain the ages of the hiatuses we determined three ranges of calibrated ages for each unconformity. The first range is obtained from the closest samples below an unconformity; the second range represents samples obviously related to the unconformity (samples recovered from sand and aragonite crust); the third range is of samples collected from layers above the unconformity. The older unconformity has yielded the respective ranges of 340-540 A.D., 1030-1210 A.D. and 1220-1390 A.D. (Table 1). The younger unconformity has yielded the ranges 1270-1400 A.D., 1290-1420 A.D., and, 1520-1800 A.D. (Table 1). The age ranges presented in Figure 3 are the samples obviously related to the unconformities (i.e. the second age range).

Nine earthquakes reported in historical documentation from the Dead Sea area do not appear in the Ze'elim seismite record and they all fall in the unconformities and depositional hiatuses discovered in the section (Figure 3b). This is consistent with the interpretation of the mixed layers as earthquake induced structures in the Ze'elim record. If a strong earthquake that was reported broadly in the Dead Sea area would be

missing from a complete sedimentary record, it would have been difficult to explain the interpretation of the mixed layers as seismites.

The 419, 551, 659/660, 749, 1033/1034, 1068, 1160 A.D. dates are correlative to the first major unconformity and the 1458 and 1546 A.D. earthquakes are correlative to the younger unconformity (description of the earthquakes in Table 3). It is impossible to determine according to the Ze'elim record whether these events were generated in the Dead Sea area. Probably, few of the events were too remote or of moderate magnitude. However, the 749 A.D. earthquake caused regional damage along the Dead Sea Transform, destroyed the Hisham Palace in Jericho, and was identified as a fault rupture on the Jericho Fault [Ambraseys *et al.*, 1994; Amiran *et al.*, 1994; Ben-Menahem, 1991; Guidoboni *et al.*, 1994; Reches and Hoexter, 1981]. This earthquake probably did affect the Ze'elim area, but the evidence was lost. We predict that this event will be identified in cores taken from deeper parts of the lake, where erosion due to lowering of the lake level is less frequent.

## 7. Recurrence Intervals of Earthquakes in the Dead Sea Area

The outcrops in the Ze'elim Terrace represent almost the entire last two millennia in the geological history of the Dead Sea region. Combined with the historical record, the evidence from these sediments provides constraints on the temporal and spatial distribution of earthquakes in the region.

In the Ze'elim Terrace eight deformed units have been identified as seismites. These are correlated to historical earthquakes that occurred in 64 and 31 B.C. and in 33, 363, 1212, 1293, 1834, and 1927 A.D.. Other historical earthquakes probably occurred during the two periods of depositional hiatuses. Overall, the deformed units and the historical record indicate that a minimum of 8 to a maximum of 17 earthquakes affected the Dead Sea area within a period of about 2000 years, implying a recurrence interval of about 100-300 years. Based on reported earthquake damage Ben-Menahem [1991] estimated that the recurrence time of strong earthquakes (e.g.,  $M=7.3$ ) in the southern half of the Dead Sea Transform is about 1500 years. The significantly shorter recurrence interval estimated from the Ze'elim record probably reflects its sensitivity to a broader range of earthquake magnitudes. The threshold intensity of these earthquakes is largely an unresolved question. We estimate it, however, as  $M>5.5$  at epicentral distances smaller than 100 km, a figure that can accommodate the observation of liquefaction and fluidization in the deformed units of the Ze'elim section. Liquefaction of sand may occur during earthquakes of magnitudes as low as 5 [Audemard and Santis, 1991], in most cases liquefaction and fluidization of sediments are associated with earthquakes of magnitude 6 and greater [Allen, 1982]. Liquefaction of sediments occurs within the first tens of kilometers from the epicenter [Ambraseys, 1988; Obermeier, 1996]. At distances exceeding 100 km,  $M_S = 7$  appears to be a minimum threshold for causing liquefaction. Based on this information and the previous estimates from the mixed layers in the Lisan Formation record [Marco *et al.*, 1996], it is reasonable to suppose that the mixed layers observed in the Ze'elim outcrops document the seismicity in the Dead Sea area. The earthquake magnitudes were probably of  $M>5.5$  and the epicenters of the

earthquakes that caused them lie within several tens of km from their occurrence.

Reches and Hoexter [1981] estimated a recurrence interval of about 1000 years, based on ruptures on the Jericho Fault (Figure 1). The sediments in the Ze'elim Terrace record more earthquakes for two reasons: (1) Earthquakes that do not rupture the surface may still generate mixed layers. Moreover, even earthquakes that rupture the surface require significant slip for showing in coarse sediments as those trenched by Reches and Hoexter [1981]. For example, the maizoseismic zone of the 1927 earthquake indicates rupture on the Jericho Fault [Avni, 1999], yet this rupture is not expressed in the trenches of Reches and Hoexter [1981]. (2) The sediments in Ze'elim terrace were disturbed by ruptures on various faults in the Dead Sea area, and not only by ruptures on the Jericho Fault. The Ze'elim sediments record a regional and not a fault specific recurrence interval, hence the recurrence interval calculated in this work cannot be compared with recurrence intervals calculated according to specific fault ruptures.

Liquefied layers identified in the Darga fan-delta sequence indicate a recurrence interval of approximately 600 years for earthquakes with  $M>5.5$  [Enzel *et al.*, 2000]. The reconstruction of the Darga fan delta paleoseismic record is similar to that of Ze'elim, although the sediments in Ze'elim are of a more lacustrine nature. The fine laminae and the less and smaller depositional hiatuses and unconformities in the Ze'elim section make the paleoseismic record more sensitive. This may explain why more historical earthquakes are represented in the Ze'elim section and the recurrence period is somewhat shorter.

The temporal distribution of earthquakes was recovered from the ~50000 years paleoseismic record of the late Pleistocene Lisan Formation (in outcrops located a few kilometers west of our study area) [Marco *et al.*, 1996]. The Lisan paleoseismic record indicates that the events cluster at periods of ~10,000 years, separated by quieter periods of similar length. Within the clusters the rate of activity reported by Marco *et al.* [1996] is 8 earthquakes in 5000 years (recurrence interval of 400 years). Comparing the Ze'elim record with the long-term Lisan record suggests that the Dead Sea area has been in an active seismic cycle during the past 2000 years.

## 8. Location of Epicenters of Paleearthquakes

The epicenters of the earthquakes that deformed the sediments in Ze'elim Terrace were probably within the Dead Sea basin, not more than a few tens of kilometers from the study area. A surface rupture and an epicenter are more precisely known for only two events recorded in the Ze'elim Terrace, the 31 B.C. event and the 1927 A.D. event, respectively. Both events were generated on the Jericho Fault [Reches and Hoexter, 1981; Shapira *et al.*, 1993]. The 31 B.C. earthquake created a distinct mixed layer in the Ze'elim sequence, about 65 km from where the fault rupture was identified in a paleoseismic trench east of Jericho [Reches and Hoexter, 1981]. In the Darga fan-delta, the event is marked by very large slump structures located above the Jericho Fault [Enzel *et al.*, 2000].

The location of the epicenters of other historical earthquakes can be approximately estimated from the historic reports on the distribution of damage. It should be noted, however, that in older historical periods, time acted as a "high

pass" magnitude filter, and strong and harmful earthquakes were selectively preserved in the written documents [Ben-Menahem, 1991]. Thus, a reasonable assumption is that if an earthquake is reported widely in ancient historical records (e.g., 31 B.C. earthquake), it was a high intensity earthquake. The reports on a small magnitude earthquake that did not severely affect the population probably faded away along with other unimportant historical events.

The reports of the 64 B.C. and 33 A.D. earthquakes are very limited. Compared to the 31 B.C. earthquake, these seem moderate and localized. Nevertheless, since most of the reports come from Jerusalem, a reasonable estimation is that the earthquakes occurred on the Jericho Fault (Figures 1 and 4). The 363 A.D. earthquake was probably a stronger earthquake because reports are more extensive, even though they originate only from Israel and western Jordan. However, the deformed unit that was correlated to this event is only a few centimeters thick, implying that the epicenter was probably not as close to the Ze'elim Terrace.

During and after the Crusader period, reports on earthquakes become more frequent [Ambraseys *et al.*, 1994] and they are preserved better than the older historical reports. From the distribution of the historical reports, it seems that the 1212, 1293, 1456, 1546, and 1834 A.D. earthquakes were generated by one of the southern faults of the Dead Sea Graben (Figure 4). Extensive damage from the 1212 A.D. and 1546 A.D. events, reported outside of Israel and Jordan, argues for magnitudes larger than for the 1293, 1456, and 1834 A.D. events. The 1834 A.D. event is a relatively recent event and was reported only in southern Israel, indicating that it produced moderate ground shaking in the Dead Sea area but strong enough to liquefy the sediments in Ze'elim Terrace. The Arava Fault, located on the eastern side of the graben (Figure 1), can be the source for earthquakes located south of the Dead Sea [Klinger *et al.*, 2000].

Although the centers of earthquake damage can be approximately located, it is difficult to assign an earthquake to a particular fault segment. The Jericho and Arava segments of the DST (Figure 1) are expected to be the source of the strongest shocks because they are the largest and most continuous faults in the area [Garfunkel *et al.*, 1981]. However, the entire Dead Sea area is undergoing active deformation [Garfunkel and Ben-Avraham, 1996]. As evidence of this, intra-basin faults under the Dead Sea are active and displace the lake floor [Ben-Avraham *et al.*, 1993]. In the Darga fan delta 30 km north of Ze'elim, surface ruptures have been related to late Holocene earthquake events [Enzel *et al.*, 2000]. Post-Lisan deformation is also observed a few km to the west of the study area, on the Ze'elim Terrace, and south of the study area, along the western shores of the southern basin of the Dead Sea [Agnon, 1982; Bartov, 1999]. It is likely that some of these ruptures act in the postseismic (aftershocks) or preseismic (foreshocks) periods of a large earthquake, hence they do not affect the paleoseismic record. While these and many other questions regarding the seismic activity in the Dead Sea region remain open, our correlation between historical earthquake records and the deformed units in the Ze'elim section provides a new approach in the assessment of paleoearthquakes.

## 9. Conclusions

The Ze'elim Formation provides an opportunity to reconstruct the paleoseismic record of the last two millennia in the

Dead Sea area and to explore the temporal pattern of earthquakes in this part of the Dead Sea Transform. The following conclusions sum up our study:

1. The paleoseismic record of the Dead Sea during the past two millennia was reconstructed based on the identification of deformed layers as seismites.

2. The ground shaking accompanying earthquakes simultaneously affected layers that extended from the lacustrine environment (characterized by laminated aragonite and detritus) to the shore environment (characterized by sand). This induced the formation of mixed layers in the former and liquefied sand in the latter. Lake-level is estimated to have been less than few meters above the sediment surface during times of earthquakes.

3. Eight layers identified as seismites were dated by radiocarbon at Ze'elim Terrace. These seismites are well correlated with the historical record of earthquakes from the area (64 and 31 B.C. and 33, 363, 1212, 1293, 1834, and 1927 A.D.). Other well-documented earthquakes that affected the Dead Sea area do not show up on the Ze'elim sequence. This could be related to destruction of the relevant layers during times of low lake level and erosion. Indeed, all missing earthquakes are correlated with depositional hiatuses in the section.

4. The regional recurrence interval of earthquakes according to the record recovered from the Ze'elim sedimentary section is about 300 years, but when all earthquakes reported in historical records are considered, the recurrence interval is even shorter, about 100 years.

5. The correlation of historical earthquake with dated seismites provides a new approach in the assessment of paleoseismicity. It provides independent geologic documentation of the historical reports and their approximate location and magnitude. By these means, it may be inferred that the epicenters of the 64, 31 B.C. and 33 and 363 A.D. earthquakes were probably located north of the Dead Sea and along the Jericho Fault, while those of the 1212, 1293, 1456, 1548, 1834 A.D. earthquakes were located to the south of the Dead Sea.

**Acknowledgments.** We wish to thank Nicolas Waldmann, Yuval Bartov, Claudia Migowski, and GSI technicians for their assistance in the fieldwork. The manuscript benefited from the review of Bill Lettis. This research was supported by the German - Israel Foundation for Research and Development (GIF grant #137/95), the Israel-United States Bi National Science Foundation (BSF grant #97-00286), Israel Science Fund (ISF, Grant # 694/95), the Dead Sea Minerva Center and the Ministry of National Infrastructure.

## References

- Agnon, A., Post Lisan faulting at the Dead Sea graben border, in *Annual Meeting 1982*, p. 1, Israel Geological Society, Elat, 1982.
- Allen, J.R.L., *Developments in Sedimentology*, 663 pp., Elsevier Sci., New York, 1982.
- Allen, J.R.L., Earthquake magnitude-frequency, epicentral distance, and soft-sediments deformation in sedimentary basins, *Sediment. Geol.*, 46, 67-75, 1986.
- Ambraseys, N. N. Engineering seismology; earthquake engineering and structural dynamics, *J. Int. Assoc. Earthquake Eng.*, 17,1-105, 1988.
- Ambraseys, N.N., C.P. Melville, and R.D. Adams, *The Seismicity of Egypt, Arabia and the Red Sea: A Historical Review*, 181 pp., Cambridge Univ. Press, New York, 1994.
- Amiran, D.H.K., E. Ariei, and T. Turcotte, Earthquake in Israel and adjacent areas: macroseismic observation since 100 B.C.E., *Israel Explor. J.*, 44, 260-305, 1994.
- Ariei, E., An evaluation of six significant historical earthquakes, 24 pp., Seismol. Sec., Geol. Sur. of Israel, Jerusalem, 1977.

- Audemard, F.A., and F. Santis, Survey of liquefaction structures induced by recent moderate earthquakes, *Assoc. Eng. Geol. Bull. Int.*, 44, 5-16, 1991.
- Avni, R., The 1927 Jericho earthquake, comprehensive macroseismic analysis based on contemporary sources, Ph.D. thesis, Ben-Gurion Univ. of the Negev, Beer-Sheva, Israel, 1999.
- Bartov, Y., The geology of the lisan Formation in Massada and the lisan Peninsula (in Hebrew, abstract in English), The Hebrew University of Jerusalem, Jerusalem, 1999.
- Begin, Z.B., A. Ehrlich, and Y. Nathan, Lake-Lisan- The Pleistocene precursor of the Dead Sea, *Geol. Sur. Israel Bull.*, 63, 30, 1974.
- Ben-Avraham, Z., T.M. Niemi, D. Neev, J.K. Hall, and Y. Levy, Distribution of Holocene sediments and neotectonics in the deep north basin of the Dead Sea, *Mar. Geol.*, 113, 219-231, 1993.
- Ben-Menahem, A., Four thousand years of seismicity along the Dead Sea Rift, *J. Geophys. Res.*, 96, 20, 195-20,216, 1991.
- Ben-Menahem, A., A. Nur, and M. Vered, Tectonics, seismicity and structure of the afro- Eurasian junction - the breaking of an incoherent plate, *Phys. Earth Planet. Inter.*, 12, 1-50, 1976.
- Davenport, C.A., and P.S. Ringrose, Deformation of Scottish Quaternary sediments sequence by strong earthquakes motions, in *Deformation of Sediments and Sedimentary Rocks*, edited by M.E. Jones and R.M. Preston, *Geol. Soc. Spec. Publ.*, 29, 299-314, 1987.
- Doig, R., Effects of strong seismic shaking in lake sediments, and earthquake recurrence interval, Temiscaming, Quebec, *Can. Earth Sci.*, 28, 1349-1352, 1991.
- Ely, L.L., R.H. Webb, and Y. Enzel, Accuracy of post-bomb  $^{137}\text{Cs}$  and  $^{14}\text{C}$  in dating fluvial deposits, *Quat. Res.*, 38, 196-204, 1992.
- Enzel, Y., G. Kadan, and Y. Eyal, Holocene earthquakes in the Dead Sea graben from a fan-delta sequence, *Quat. Res.*, 73/74 137-144, 2000.
- Frumkin, A., M. Magaritz, I. Carmi, and I. Zak, The Holocene climatic record of the salt caves of Mount Sedom, Israel, *Holocene*, 1, 191-200, 1991.
- Garfunkel, Z., Internal structure of the Dead Sea Leaky Transform (rift) in relation to plate kinematics, *Tectonophysics*, 80, 81-108, 1981.
- Garfunkel, Z., and Z. Ben-Avraham, The structure of the Dead Sea basin, *Tectonophysics*, 266, 155-176, 1996.
- Garfunkel, Z., I. Zak, and R. Freund, Active faulting in the Dead Sea rift, *Tectonophysics*, 80, 1-26, 1981.
- Guidoboni, E., A. Comastri, and G. Traina, *Catalogue of Ancient Earthquakes in the Mediterranean Area up to the 10th Century*, 504 pp., Inst. Naz. Geofis., Rome, 1994.
- Hempton, M.R., and J.F. Dewey, Earthquake-induced deformational structures in young lacustrine sediments, East Anatolian Fault, southeast Turkey, *Tectonophysics*, 98, T7-T14, 1983.
- Kadan, G., Evidence for Dead Sea lake-level fluctuations and recent tectonism from the Holocene fan-delta of Nahal Darga, Israel (in Hebrew, abstract in English), M.Sci. thesis, Ben-Gurion Univ. of the Negev, Beer-Sheva, Israel, 1997.
- Kaufman, A., U-series dating of Dead Sea carbonates, *Geochim. Cosmochim. Acta*, 35, 1269-1281, 1971.
- Kaufman, A., Y. Yecheili, and M. Gardosh, Reevaluation of lake-sediment chronology in the Dead Sea basin, Israel, based on new  $^{230}\text{Th}/\text{U}$  dates, *Quat. Res.*, 38, 292-304, 1992.
- Ken-Tor, R., M. Stein, S. Marco, Y. Enzel, and A. Agnon, Late Holocene earthquakes recorded by lake sediments, Ze'elim Plain, Dead Sea, in *Israel Geological Society Annual Meeting, 1998*, edited by R. Weinberger et al., p. 53, Mitzpe Ramon, Israel, 1998.
- Klein, C., On the fluctuations of the level of the Dead Sea since the beginning of the 19th century, 83 pp., Hydrol. Serv., Minist. of Agric., Jerusalem, 1961.
- Klein, C., Morphological evidence of lake level changes, western shore of the Dead Sea, *Isr. J. Earth Sci.*, 31, 67-94, 1982.
- Klinger, Y., J.P. Avouac, L. Dorbath, N. Abou Karaki, and N. Tisserat, Seismic behavior of the Dead Sea fault along Araba Valley, *Geophys. J. Int.*, 142, 769-782, 2000.
- Marco, S., and A. Agnon, Prehistoric earthquake deformations near Masada, Dead Sea graben, *Geology*, 23 (8), 695-698, 1995.
- Marco, S., M. Stein, A. Agnon, and H. Ron, Long-term earthquake clustering: A 50,000-year paleoseismic record in the Dead Sea Graben, *J. Geophys. Res.*, 101, 6179-6191, 1996.
- Migowski, C., R. Ken-Tor, J.F.W. Negendank, M. Stein, and J. Mingram, Post-Lisan record documented in sediment sequences from the western shore area and the central basin of the Dead Sea, paper presented at Terra Nostra 98/6: 3rd ELDP Workshop, sponsor, Ptolemais, Greece, 1999.
- Neev, D., and K.O. Emery, *The Destruction of Sodom, Gomorrah, and Jericho: Geological, Climatological, and Archaeological Background*, 175 pp., Oxford Univ. Press, New York, 1995.
- Obermeier, S., Using liquefaction induced features for paleoseismic analysis, in *Paleoseismology*, edited by J. McCaipin, *Int. Geophys. Ser.*, 62, 331-396, 1996.
- Reches, Z., and D.F. Hoexter, Holocene seismic and tectonic activity in the Dead Sea area, *Tectonophysics*, 80, 235-254, 1981.
- Russell, K.W., The earthquake of May 19, A.D. 363, *Bull. Am. Sch. Orient. Res.*, 238, 47-64, 1980.
- Russell, K.W., The earthquake chronology of Palestine and northwest Arabia from the 2nd through the mid-8th century A.D., *Bull. Am. Sch. Orient. Res.*, 260, 37-59, 1985.
- Schramm, A., M. Stein, and S.L. Goldstein, Calibration of the 14C timescale to 50 kyr by  $^{234}\text{U}$ - $^{230}\text{Th}$  dating of sediments from Lake Lisan (the paleo-Dead Sea), *Earth Planet. Sci. Lett.*, 175, 27-40, 2000.
- Shapira, A., R. Avni, and A. Nur, A new estimate for the epicenter of the Jericho earthquake of 11 July 1927, *Israel J. Earth Sci.*, 42, 93-96, 1993.
- Sims, J.D., Earthquake-induced structures in sediments of Van Norman Lake, San Fernando, California, *Science*, 182, 161-163, 1973.
- Sims, J.D., determining earthquake recurrence intervals from deformational structures in young lacustrine sediments, *Tectonophysics*, 29, 141-152, 1975.
- Stein, M., A. Starinsky, A. Katz, S.L. Goldstein, M. Machlus and A. Schramm, Strontium isotopic, chemical and sedimentological evidence for the evolution of Lake Lisan and the Dead Sea, *Geochim. Cosmochim. Acta*, 61, 3975-3992, 1997.
- Stuiver, M., P.J. Reimer, E. Bard, J.W. Beck, G.S. Burr, K.A. Hughen, B. Kromer, G. McCormac, J. van-der-Plicht, and M. Spurk, INTCAL98 radiocarbon age calibration, 24,000-0 cal BP, *Radiocarbon*, 40, 1041-1083, 1998.
- Vered, M., and H.L. Striem, A macroseismic study of the July 11, 1927 earthquake, *Isr. At. Energy Comm. Licensing Div. Rep. IA-LD-1-107*, 18 pp., 1976.
- Wells, D.L., and K.J. Coppersmith, New empirical relationship among magnitudes, rupture length, rupture width, rupture area, and surface displacement, *Bull. Seismol. Soc. Am.*, 84, 974-1002, 1994.
- Willis, B., Earthquakes in the Holy Land, *Bull. Seismol. Soc. Am.*, 18, 73-103, 1928.
- Yecheili, Y., The effects of water levels change in closed lakes (Dead Sea) on the surrounding groundwater and country rocks, Ph.D. thesis, Weizman Inst., Rehovot, Israel, 1993.
- Yecheili, Y., M. Magaritz, Y. Levy, U. Weber, U. Kafri, W. Woelfli, and G. Bonani, Late Quaternary geological history of the Dead Sea area, Israel, *Quat. Res.*, 39, 59-67, 1993.

A. Agnon, Y. Enzel, R. Ken-Tor, and M. Stein, Institute of Earth Sciences, the Hebrew University, Givat Ram, Jerusalem 91904, Israel. (amotz@cc.huji.ac.il; yenzel@vms.huji.ac.il; revival@vms.huji.ac.il; motis@vms.huji.ac.il)

S. Marco, Raymond and Beverly Sackler Faculty of Exact Sciences, Department of Geophysics and Planetary Sciences, Tel Aviv University, Ramat Aviv, Tel Aviv 69978, Israel.

J.F.W. Negendank, Geoforschungszentrum Potsdam, Telegrafenberg, D-14473 Potsdam, Germany.

(Received January 25, 2000; revised August 11, 2000; accepted August 18, 2000.)